

ZINC OXIDE BASED THIN FILMS FOR SENSOR APPLICATION

Thesis

Submitted in partial fulfilment of the requirements for the degree of

DOCTOR OF PHILOSOPHY

By

BHARATH S.P.



DEPARTMENT OF PHYSICS

NATIONAL INSTITUTE OF TECHNOLOGY KARNATAKA,

SURATHKAL, MANGALORE - 575025

FEBRUARY, 2020

ZINC OXIDE BASED THIN FILMS FOR SENSOR APPLICATION

Thesis

Submitted in partial fulfilment of the requirements for the degree of

DOCTOR OF PHILOSOPHY

by

BHARATH S.P.



DEPARTMENT OF PHYSICS

NATIONAL INSTITUTE OF TECHNOLOGY KARNATAKA,

SURATHKAL, MANGALORE - 575025

FEBRUARY, 2020

DECLARATION

by the Ph.D. Research Scholar

I hereby *declare* that the Research Thesis entitled “**Zinc Oxide based Thin Films for Sensor Application**” Which is being submitted to the National Institute of Technology Karnataka, Surathkal in partial fulfilment of the requirements for the award of the Degree of **Doctor of Philosophy** in **Physics** is a *bonafide report of the research work carried out by me*. The material contained in this Research Thesis has not been submitted to any University or Institution for the award of any degree.

Mr. Bharath S.P.

(Reg. No.: PH14F05)

Department of Physics

Place: NITK-Surathkal

Date:

CERTIFICATE

This is to *certify* that the Research Thesis entitled “**Zinc Oxide based Thin Films for Sensor Application**” submitted by **Bharath SP** (Register Number: **PH14F05**) as the record of the research work carried out by him, is *accepted as the Research Thesis submission* in partial fulfilment of the requirements for the award of degree of Doctor of Philosophy.

Prof. Kasturi V. Bangera
Research Guide

Chairman – DRPC

ACKNOWLEDGEMENTS

Completion of this doctoral research work is possible with the support of several people. I would like to express my sincere gratitude to all of them. First of all, I am extremely grateful to my research guide, Prof. (Mrs.) Kasturi V. Bangera, for her valuable guidance, scholarly inputs and consistent encouragement I received throughout the research work. This accomplishment is possible only because of the unconditional support provided by her.

I would like to express my gratitude to Prof. G. K. Shivakumar for his valuable suggestions and advice towards my research work.

I sincerely thank the members of RPAC Dr. Kartick Tarafdar and Dr. A. V. Hegde for their valuable suggestions and excellent advice in pursuing this research work.

I am grateful to the Head of Department for supporting me to attend various conferences and workshops, which in turn helped me to understand the current research work.

I heartily thank my fellow lab mates Dr. Shashidara A., Dr. Veena E., Dr. Santhosh T. C. M., Mrs. Sowjanya V., Mr. Biswajit B., Ms. Subhasmita Ray for their cooperation and best wishes. I also thank MSc students Ms. Manasa, Mrs. Preethi, Ms. Navya, Ms. Amaya for their best wishes.

I am greatly indebted to companionship of circle of friends outside the lab and institute, who have continuously supported me in many aspects throughout these years. I owe a lot to CA Manjunath U. S., Mr. Raghavendra K. S., CA Ram Mohan, Mr. Prashanth Bayar for being there for me when I was in need of support. I thank Mr. Dhanush Shanbhag, Dr. Raghavendra Hebbar, Mr. Achyutha, Mr. Makesh, Mr. Mahendra, Mr. Brijesh, Mr. Karthik Hegde, Ms. Bindu, Ms. Amudha. I appreciate their friendly encouragement and making my experience a lot better.

I owe special thanks to my parents Latha and Prakash S. R., wife Varshini G. V., sister S. P. Nanditha. A special thanks to family members, Manu, Vidyashankar and Rajeshwari, for their care and support along the way.

There are many more whom I must remember with gratitude. Their names, though I might have failed to mention here, shall never be forgotten.

Mr. Bharath S.P.

ABSTRACT

The present work deals with the preparation of ZnO thin films doped with Cd [$\text{Cd}_x\text{Zn}_{1-x}\text{O}$ (0-20 at. %)], In [$\text{In}_x\text{Zn}_{1-x}\text{O}$ (0-5 at. %)], Al [$\text{Al}_x\text{Zn}_{1-x}\text{O}$ (0-5 at. %)] and mixed oxides with copper [$\text{Cu}_{1-x}\text{Zn}_x\text{O}$ ($0 \leq x \leq 1$)], tin [$\text{Zn}_x\text{Sn}_{1-x}\text{O}$ ($0 \leq x \leq 1$)] on glass substrates using spray pyrolysis technique. The structural, morphological, compositional and optical properties were studied to understand the effect of different doping and its concentration with intension of using prepared thin films for gas sensor application. The XRD analysis revealed that doped ZnO thin films were having hexagonal wurtzite structure with preferred orientation along (002) direction. Slight shift in the (002) peak was also observed and it was dependent on doping concentration and radii of dopant. The SEM studies confirmed the formation of homogeneous and uniform thin films with granular morphology and surface features were reliant on doping concentration. The resistivity of undoped films were very high and it was decreasing with addition of dopant. Optimal doping concentration was found to be 10 at. % for cadmium and 3 at. % for indium and aluminium with >80% optical transmittance in visible region. The gas sensing properties were investigated at optimal temperature of 350⁰C for various volatile organic compounds like acetone, ethanol and methanol. The ZnO thin films with 10 at. % cadmium doping showed highest sensitivity of 50% for 1 ppm ethanol.

XRD studies on prepared $\text{Cu}_{1-x}\text{Zn}_x\text{O}$ and $\text{Zn}_x\text{Sn}_{1-x}\text{O}$ thin films confirmed formation of composite and amorphous thin films respectively. Formation of $\text{Cu}_{1-x}\text{Zn}_x\text{O}$ composite thin film improves sensing property, but formation of amorphous phase in $\text{Zn}_x\text{Sn}_{1-x}\text{O}$ thin films do not contribute towards any improvement in sensitivity. Maximum electrical conductivity was achieved for $\text{Cu}_{0.75}\text{Zn}_{0.25}\text{O}$ composite thin films, which also showed highest sensing property for VOCs. $\text{Cu}_{0.75}\text{Zn}_{0.25}\text{O}$ thin films were selective towards ethanol and were capable of detecting 1 ppm of ethanol at operating temperature of 290⁰C.

Studies gave better insight into behaviour of metal oxides thin films towards sensor application, which will help in improvement of device applicability. Further

research is required to improve selectivity, stability and miniaturization of sensor material for hand held gas sensor and electronic nose application.

CONTENTS

CHAPTER 1 Introduction

1.1 General introduction	1
1.2 Metal oxides	3
1.3 Gas sensors	4
1.4 Literature survey	6
1.5 Scope of work	12
1.6 Objectives	13
1.7 Thesis outline	13

CHAPTER 2 Experimental techniques

2.1 Thin film preparation	15
2.2 Characterization of thin films	
2.2.1 Thickness measurement	17
2.2.2 X-ray powder diffraction	17
2.2.3 Scanning electron microscope	18
2.2.4 Optical studies	20
2.2.5 Electrical studies	20
2.2.6 Gas sensor studies	21

CHAPTER 3 Preparation and characterization of doped ZnO thin films

3.1 Introduction	23
3.2 Effect of Cd doping on the properties of ZnO thin films	
3.2.1 Experimental details	24
3.2.2 X-ray diffraction	24
3.2.3 Morphological and compositional analysis	27
3.2.4 Optical properties	28
3.2.5 Electrical properties	29
3.3 Effect of annealing on Cd _x Zn _{1-x} O thin films	
3.3.1 X-ray diffraction	30
3.3.2 Morphological and compositional analysis	32
3.3.3 Optical properties	33

3.3.4 Electrical properties	33
3.4 Effect of In doping on the properties of ZnO thin films	
3.4.1 Experimental details	34
3.4.2 X-ray analysis	34
3.4.3 Surface morphological and compositional analysis	36
3.4.4 Optical analysis	37
3.4.5 Electrical studies	38
3.5 Effect of Al doping on the properties of ZnO thin films	
3.5.1 Experimental details	39
3.5.2 X-ray analysis	39
3.5.3 Surface morphological and compositional analysis	41
3.5.4 Optical properties	42
3.5.5 Electrical properties	43
CHAPTER 4 Gas sensing properties of doped ZnO thin films	
4.1 Introduction	45
4.2 Gas sensing studies of cadmium doped ZnO thin films	45
4.3 Gas sensing studies of indium doped ZnO thin films	51
4.4 Gas sensing studies of aluminium doped ZnO thin films	55
CHAPTER 5 Synthesis, characterization and gas sensing properties of mixed metal oxide thin films	
5.1 Introduction	58
5.2 Synthesis and characterization of $\text{Cu}_{1-x}\text{Zn}_x\text{O}$ composite thin films for sensor application	
5.2.1 Experimental details	59
5.2.2 X-ray analysis	60
5.2.3 Morphological and compositional analysis	61
5.2.4 Optical properties	62
5.2.5 Electrical properties	63
5.2.6 Gas sensing properties	64
5.3 Synthesis and characterization of $\text{Zn}_{1-x}\text{Sn}_x\text{O}$ composite thin films for sensor application	

5.3.1 Experimental details	71
5.3.2 X-ray analysis	71
5.3.3 Surface morphology and compositional analysis	73
5.3.4 Optical properties	74
5.3.5 Electrical properties	75
5.3.6 Gas sensing characteristics	75
CHAPTER 6 Development of data acquisition and gas sensor system	
6.1 Introduction	78
6.2 Development of sensor assembly and data acquisition system	
6.2.1 Sensor array	79
6.2.2 Measuring circuit	79
6.2.3 Data acquisition system	80
6.3 Development of gas sensor system	84
CHAPTER 7 Summary and conclusions	
7.1 Introduction	86
7.2 Conclusions	
7.2.1 Preparation and characterization of doped ZnO thin films	86
7.2.2 Gas sensing applications of doped ZnO thin films	86
7.2.3 Synthesis, characterization and gas sensing properties of mixed oxides	87
7.2.4 Development of data acquisition system and gas sensor system	87
7.3 Scope for the future work	88

REFERENCES

PUBLICATIONS

CURRICULUM VITAE

LIST OF FIGURES

Figure 1.1: Different Crystal structures of ZnO (a) Rocksalt, (b) Zinc blende (c) Wurtzite	4
Figure 2.1: (a) Schematic representation and (b) photo graph of spray pyrolysis equipment	16
Figure 2.2: (a) Schematic representation of XRD, (b) Photograph of Rigaku-miniflex600	18
Figure 2.3: Photograph of FE-SEM model Zeiss-Sigma	19
Figure 2.4: Schematic diagram of contact used for electrical measurement	20
Figure 2.5: Schematic diagram of hot probe method	21
Figure 2.6: Schematic representation of gas sensing set up	22
Figure 3.1: XRD patterns of $Cd_xZn_{1-x}O$ thin films (a) 0%, (b) 5 at. %, (c) 10 at. %, (d) 20 at. %	25
Figure 3.2: Shift in the (002) peak position of $Cd_xZn_{1-x}O$	26
Figure 3.3: FE-SEM images of $Cd_xZn_{1-x}O$ (a) 0%, (b) 5 at. %, (c) 10 at. % and (d) 20 at. %	27
Figure 3.4: EDAX spectra (inset: mapping) of $Cd_xZn_{1-x}O$ thin films for different Cd concentration (a) 0%, (b) 5 at. %, (c) 10 at. % and (d) 20 at. %	28
Figure 3.5: (a) Transmittance spectra, (b) Tauc's plots of $Cd_xZn_{1-x}O$ thin film and (c) appearance of deposited $Cd_xZn_{1-x}O$ thin films	29
Figure 3.6: I-V characteristic curve of $Cd_xZn_{1-x}O$ thin films	30
Figure 3.7: XRD patterns of annealed $Cd_xZn_{1-x}O$ thin films (a) 0%, (b) 5 at. %, (c) 10 at. %, (d) 20 at. %	31

Figure 3.8: FE-SEM images of annealed $\text{Cd}_x\text{Zn}_{1-x}\text{O}$ (a) 0%, (b) 5at.%, (c) 10at.%(d) 20at.%	32
Figure 3.9: (a) Transmittance spectra and (b) Tauc's plots of annealed $\text{Cd}_x\text{Zn}_{1-x}\text{O}$ thin films	33
Figure 3.10: XRD patterns of $\text{In}_x\text{Zn}_{1-x}\text{O}$ thin films (a) 0 at. %, (b) 1 at. %, (c) 3 at. %, (d) 5 at. %	35
Figure 3.11: FE-SEM image of $\text{In}_x\text{Zn}_{1-x}\text{O}$ thin films (a) 0 at.%, (b) 1 at.%, (c) 3 at.% and (d) 5 at.%	36
Figure 3.12: (a) Transmittance spectra and (b) Tauc's plots of indium doped ZnO thin films	37
Figure 3.13: I-V characteristics of $\text{In}_x\text{Zn}_{1-x}\text{O}$ thin films	38
Figure 3.14: XRD patterns $\text{Al}_x\text{Zn}_{1-x}\text{O}$ thin films (a) ZnO, (b) $\text{Al}_{0.005}\text{Zn}_{0.995}\text{O}$, (c) $\text{Al}_{0.01}\text{Zn}_{0.99}\text{O}$, (d) $\text{Al}_{0.015}\text{Zn}_{0.985}\text{O}$, (e) $\text{Al}_{0.03}\text{Zn}_{0.97}\text{O}$, (f) $\text{Al}_{0.05}\text{Zn}_{0.95}\text{O}$	40
Figure 3.15: FE-SEM images of $\text{Al}_x\text{Zn}_{1-x}\text{O}$ thin films (a) ZnO, (b) $\text{Al}_{0.005}\text{Zn}_{0.995}\text{O}$, (c) $\text{Al}_{0.01}\text{Zn}_{0.99}\text{O}$, (d) $\text{Al}_{0.015}\text{Zn}_{0.985}\text{O}$, (e) $\text{Al}_{0.03}\text{Zn}_{0.97}\text{O}$, (f) $\text{Al}_{0.05}\text{Zn}_{0.95}\text{O}$	42
Figure 3.16: (a) Transmittance spectra, (b) Tauc's plots of $\text{Al}_x\text{Zn}_{1-x}\text{O}$ thin films	42
Figure 3.17: I-V characteristics of $\text{Al}_x\text{Zn}_{1-x}\text{O}$ thin films	43
Figure 4.1: Resistance transient response of $\text{Cd}_{0.1}\text{Zn}_{0.9}\text{O}$ thin film (a) Acetone, (b) Methanol and (c) Ethanol	46
Figure 4.2: Resistance transient response of $\text{Cd}_{0.2}\text{Zn}_{0.8}\text{O}$ thin film (a) Acetone, (b) Methanol and (c) Ethanol	47
Figure 4.3: Resistance transient response for 5ppm, 2.5ppm and 1ppm of ethanol for (a) $\text{Cd}_{0.10}\text{Zn}_{0.90}\text{O}$ and (b) $\text{Cd}_{0.20}\text{Zn}_{0.80}\text{O}$ thin film and (c) reproducibility for 5ppm of ethanol for $\text{Cd}_{0.10}\text{Zn}_{0.90}\text{O}$ thin film	48
Figure 4.4: Response of $\text{Cd}_{0.1}\text{Zn}_{0.9}\text{O}$ thin films (a) Acetone, (b) Methanol and (c) Ethanol	49

Figure 4.5: Response of $\text{Cd}_{0.2}\text{Zn}_{0.8}\text{O}$ thin films (a) Acetone, (b) Methanol and (c) Ethanol	50
Figure 4.6: Comparison of sensitivity for different ppm of vapours (a) $\text{Cd}_{0.1}\text{Zn}_{0.9}\text{O}$, (b) $\text{Cd}_{0.2}\text{Zn}_{0.8}\text{O}$	50
Figure 4.7: Response and recovery time of $\text{Cd}_{0.1}\text{Zn}_{0.9}\text{O}$ thin film for (a) 5ppm, (b) 2.5ppm and (c) 1ppm of ethanol	51
Figure 4.8: Resistance variation curves of (a) $\text{In}_{0.01}\text{Zn}_{0.99}\text{O}$, (b) $\text{In}_{0.05}\text{Zn}_{0.95}\text{O}$, (c) $\text{In}_{0.03}\text{Zn}_{0.97}\text{O}$	52
Figure 4.9: Resistance variation curves of $\text{In}_{0.03}\text{Zn}_{0.97}\text{O}$ thin films for (a) Acetone, (b) Methanol and (c) reproducibility of 250ppm of ethanol	53
Figure 4.10: (a) Sensitivity curve for $\text{In}_{0.03}\text{Zn}_{0.97}\text{O}$ thin films, (b) Comparison of sensitivity of 250 ppm of Acetone, Ethanol and Methanol	54
Figure 4.11: Response and recovery time of $\text{In}_{0.03}\text{Zn}_{0.97}\text{O}$ thin film for 250ppm of ethanol	54
Figure 4.12: Resistance transient of $\text{Al}_{0.03}\text{Zn}_{0.97}\text{O}$ thin films for (a) ethanol, (b) Acetone and (c) Methanol	56
Figure 4.13: Sensitivity of $\text{Al}_{0.03}\text{Zn}_{0.97}\text{O}$ thin films (a) Ethanol, (b) Acetone	56
Figure 5.1: XRD patterns of $\text{Cu}_{1-x}\text{Zn}_x\text{O}$ thin films (a) CuO , (b) $\text{Cu}_{0.75}\text{Zn}_{0.25}\text{O}$ and (c) $\text{Cu}_{0.50}\text{Zn}_{0.50}\text{O}$, (d) $\text{Cu}_{0.25}\text{Zn}_{0.75}\text{O}$	60
Figure 5.2: Surface morphology of $\text{Cu}_{1-x}\text{Zn}_x\text{O}$ thin films (a) CuO , (b) $\text{Cu}_{0.75}\text{Zn}_{0.25}\text{O}$ and (c) $\text{Cu}_{0.50}\text{Zn}_{0.50}\text{O}$, (d) $\text{Cu}_{0.25}\text{Zn}_{0.75}\text{O}$	61
Figure 5.3: EDX spectra of $\text{Cu}_{1-x}\text{Zn}_x\text{O}$ thin films (a) CuO , (b) $\text{Cu}_{0.75}\text{Zn}_{0.25}\text{O}$ and (c) $\text{Cu}_{0.50}\text{Zn}_{0.50}\text{O}$, (d) $\text{Cu}_{0.25}\text{Zn}_{0.75}\text{O}$	62
Figure 5.4: (a) Transmission spectra of $\text{Cu}_{1-x}\text{Zn}_x\text{O}$ thin films, (b) Tauc's plot of $\text{Cu}_{1-x}\text{Zn}_x\text{O}$ thin films	63

Figure 5.5: I-V characteristics of $\text{Cu}_{1-x}\text{Zn}_x\text{O}$ thin films	63
Figure 5.6: Resistance response of CuO for acetone, Ethanol and Methanol at different operating temperature (a) 270°C (b) 290°C (c) 310°C	64
Figure 5.7: Resistance transient response of $\text{Cu}_{0.50}\text{Zn}_{0.50}\text{O}$ composite thin Films for 100ppm of acetone, ethanol and methanol at different operating temperature (a) 270°C (b) 290°C (c) 310°C (d) 330°C	65
Figure 5.8: Resistance transient response of $\text{Cu}_{0.50}\text{Zn}_{0.50}\text{O}$ composite thin films at operating temperature of 310°C (a) acetone, (b) ethanol, (c) Methanol	66
Figure 5.9: Resistance transient response of $\text{Cu}_{0.50}\text{Zn}_{0.50}\text{O}$ thin films for 1-10 ppm of ethanol	67
Figure 5.10: Resistance response of $\text{Cu}_{0.75}\text{Zn}_{0.25}\text{O}$ thin films at operating temperature 270°C (a) acetone, (b) ethanol, (c) Methanol	68
Figure 5.11: Resistance response of $\text{Cu}_{0.75}\text{Zn}_{0.25}\text{O}$ thin films at operating temperature 290°C (a) acetone, (b) ethanol, (c) Methanol	68
Figure 5.12: Resistance response of $\text{Cu}_{0.75}\text{Zn}_{0.25}\text{O}$ thin films at operating temperature 310°C (a) acetone, (b) ethanol, (c) Methanol	69
Figure 5.13: (a) Resistance transient response for 10-1 ppm of ethanol (b) Reproducibility curve of $\text{Cu}_{0.75}\text{Zn}_{0.25}\text{O}$ thin films for 10ppm of ethanol	69
Figure 5.14: Comparison of sensitivity of $\text{Cu}_{1-x}\text{Zn}_x\text{O}$ for 500 ppm of ethanol	70
Figure 5.15: XRD patterns of $\text{Zn}_{1-x}\text{Sn}_x\text{O}$ thin films (a) ZnO, (b) $\text{Zn}_{0.75}\text{Sn}_{0.25}\text{O}$, (c) $\text{Zn}_{0.50}\text{Sn}_{0.50}\text{O}$, (d) $\text{Zn}_{0.25}\text{Sn}_{0.75}\text{O}$, (e) SnO_2	72
Figure 5.16: FE-SEM images of $\text{Zn}_{1-x}\text{Sn}_x\text{O}$ thin films (a) ZnO, (b) $\text{Zn}_{0.75}\text{Sn}_{0.25}\text{O}$, (c) $\text{Zn}_{0.50}\text{Sn}_{0.50}\text{O}$, (d) $\text{Zn}_{0.25}\text{Sn}_{0.75}\text{O}$, (e) SnO_2	73

Figure 5.17: Optical transmittance spectra of $Zn_{1-x}Sn_xO$ thin films	74
Figure 5.18: I-V characteristics of $Zn_{1-x}Sn_xO$ thin films	75
Figure 5.19: (a) Resistance response of $Zn_{0.50}Sn_{0.50}O$ thin films for ethanol, (b) reproducibility curve for 1000ppm of ethanol for $Zn_{0.50}Sn_{0.50}O$ thin films	76
Figure 5.20: Resistance transient response of $Zn_{0.50}Sn_{0.50}O$ thin films for (a)Acetone, (b) Methanol	77
Figure 5.21: (a) Responsivity curve of $Zn_{0.50}Sn_{0.50}O$ thin films for ethanol, (a)Comparison of sensitivity for different gas vapours	77
Figure 6.1: Comparison of mammalian and artificial olfactory system	78
Figure 6.2: Gas sensing measurement circuit	79
Figure 6.3: (a) Arduino mega, (b) LED display used in data acquisition system	80
Figure 6.4: Block diagram of data acquisition system	81
Figure 6.5: (a) Developed DAS, (b) Computer connected DAS and (c)Resistance value	81
Figure 6.6: Resistance transient response of $Cu_{0.75}Zn_{0.25}O$ for (a) ethanol, (b) acetone and (c) methanol at 290^0 C	82
Figure 6.7: Calibration curve for (a) ethanol, (b) acetone and (c) methanol	83
Figure 6.8: (a) Selection window, (b) Display showing concentration in ppm	84

LIST OF TABLES

Table 1.1: Physical and chemical properties of metal oxide	4
Table 1.2: Summary of gas sensor materials	7
Table 3.1: Structural parameters of $\text{Cd}_x\text{Zn}_{1-x}\text{O}$ estimated from XRD	26
Table 3.2: Electrical data of $\text{Cd}_x\text{Zn}_{1-x}\text{O}$ thin films	30
Table 3.3: Structural parameters of annealed $\text{Cd}_x\text{Zn}_{1-x}\text{O}$ estimated from XRD	31
Table 3.4: Compositional information $\text{Cd}_x\text{Zn}_{1-x}\text{O}$ thin film	32
Table 3.5: Electrical data of $\text{Cd}_x\text{Zn}_{1-x}\text{O}$ thin films	33
Table 3.6: Estimated structural parameters of $\text{In}_x\text{Zn}_{1-x}\text{O}$ thin films	35
Table 3.7: Compositional information $\text{In}_x\text{Zn}_{1-x}\text{O}$ thin films	37
Table 3.8: Estimated electrical properties of $\text{In}_x\text{Zn}_{1-x}\text{O}$ thin films	38
Table 3.9: Estimated structural parameters of $\text{Al}_x\text{Zn}_{1-x}\text{O}$ thin films	40
Table 3.10: Compositional information $\text{Al}_x\text{Zn}_{1-x}\text{O}$ thin films	41
Table 3.11: Electrical data of $\text{Al}_x\text{Zn}_{1-x}\text{O}$ thin films	43
Table 4.1: Comparison of sensitivity of $\text{Cd}_{0.2}\text{Zn}_{0.8}\text{O}$ and $\text{Cd}_{0.1}\text{Zn}_{0.9}\text{O}$ thin films	51
Table 4.2: Response and recovery time of $\text{Cd}_{0.1}\text{Zn}_{0.9}\text{O}$ thin film for ethanol	51
Table 4.3: Comparison of sensitivity of $\text{In}_x\text{Zn}_{1-x}\text{O}$ thin films	54
Table 4.4: Response and recovery time of $\text{In}_x\text{Zn}_{1-x}\text{O}$ thin film for ethanol	55
Table 4.5: Comparison of sensitivity of $\text{Al}_x\text{Zn}_{1-x}\text{O}$ thin films	57
Table 4.6: Response and recovery time of $\text{Al}_x\text{Zn}_{1-x}\text{O}$ for ethanol and acetone	57
Table 5.1: Electrical data of $\text{Cu}_{1-x}\text{Zn}_x\text{O}$ thin films	64

Table 5.2: Responsivity of $\text{Cu}_{0.75}\text{Zn}_{0.25}\text{O}$ thin films	70
Table 5.3: Response and recovery time of $\text{Cu}_{0.75}\text{Zn}_{0.25}\text{O}$ thin film for acetone, ethanol and methanol	71
Table 5.4: Compositional information of $\text{Zn}_{1-x}\text{Sn}_x\text{O}$ thin film	74
Table 5.5: Electrical data of $\text{Zn}_{1-x}\text{Sn}_x\text{O}$ thin films	75
Table 6.1: Responsivity of $\text{Cu}_{0.75}\text{Zn}_{0.25}\text{O}$ for ethanol, acetone and methanol	83
Table 6.2: Estimated concentration of ethanol using developed gas sensor	84
Table 6.3: Estimated concentration of acetone using developed gas sensor	85
Table 6.4: Estimated concentration of methanol using developed gas sensor	85
Table 7.1: List of different criteria to choose transparent conducting material	87
Table 7.2: List of different criteria to choose different gas sensor	88

NOMENCLATURE

ABBREVIATIONS

Zn	Zinc
O	Oxygen
ZnO	Zinc Oxide
Cd	Cadmium
In	Indium
Al	Aluminium
Cu	Copper
Sn	Tin
In ₂ O ₃	Indium Oxide
SnO ₂	Tin Oxide
CuO	Copper Oxide
Al ₂ O ₃	Aluminium Oxide
CdO	Cadmium Oxide
Zn ₂ SnO ₃	Zinc Stannate
TCO	Transparent Conducting Oxide
PVD	Physical Vapour Deposition
MBE	Molecular Beam Epitaxy
TFT	Thin Film Transistor
XRD	X-Ray Diffractometer

FE-SEM	Field Emission Scanning Electron Microscope
EDAX	Energy Dispersive Analysis of X-rays
UV	Ultra Violet
VIS	Visible
VOC	Volatile Organic Compounds
I-V	Current – Voltage
n-	n-type
p-	p-type

SYMBOLS AND UNITS

eV	Electron Volt
μm	Micrometer
nm	Nanometer
hr	Hour
D	Crystallite Size
a and c	lattice constants
d	Interplanar Distance
2θ	Bragg angle
ρ	Resistivity
R	Resistance
T	Temperature
E_g	Bandgap

at. %	Atomic percent
$h\nu$	Photon energy
h	Planck's constant
Å	Angstrom
$^{\circ}\text{C}$	Degree Celsius
A	Ampere
cm	Centimetre
Ω	Ohms
λ	Wavelength
V	Volt
ν	Frequency

CHAPTER 1

INTRODUCTION

1.1 GENERAL INTRODUCTION

The Modern era in which we live in, is in quest of materials that would satisfy the thirst of the ever blooming technology. Tremendous ideas have been realized to improve human lifestyle, but the advancement in science and technology is always inadequate to achieve vision and ambition of mankind. The field of material science and engineering community's ability to conceive the novel materials with extraordinary combination of chemical, physical and mechanical properties is creating many new opportunities and possibilities, which can be very helpful for modern society. The technology and understanding of materials with less than 1-micron thickness have made remarkable advances in the last decade, primarily because of the industrial demand for reliable thin-film microelectronic devices to fulfil the urgent needs of the modern era. This progress has brought maturity and much scientific confidence in using of thin films for basic and applied research in addition to major contributions to a variety of new and scientifically based technologies.

A thin film is a layer of material ranging from fractions of a nanometres to several micrometres in thickness. The physical properties of solid bulk materials are almost independent of their thickness. However, drastic reduction in the thickness may change the properties of the solid materials. When the thickness is much smaller than a micrometre, the properties of the material may depend on its thickness. Such materials whose properties change as a function of their thickness are called thin films. Unique phenomena related to thin films are consequence of their small thickness, large surface to volume ratio, and distinctive physical structure, planar geometry and size.

Thin films of noble metals have been used for decorating glass and ceramics for over a thousand years. However, the methods used at that time were very crude and involved thinning down of a bulk material by mechanical means, for example

beating of gold leafs to get thin gold films. The thickness of the films produced were about five millionth of an inch. The application of these films were also very much limited, mainly for decorative purposes. The more practical uses of thin films were realized in latter half of 19th century when attractive optical uses of thin films were observed. The first use of thin films for optical purposes can be traced back to 1912. Pohl and Pringsheim published about production of mirrors in which they vaporized metals like Ag and Al out of a MgO crucible in high vacuum. After that almost all metals were examined for their usability in mirror production especially Cr, Ni, Pt, Rh, Pd, Sn, Au etc. greater industrial importance was achieved only for Rh, Ag and Al. However, of all metals, only Al and Ag succeeded in the long run. The utilization of thin films for electronic device applications began in the latter half of the last century. The compactness and seamless integration capability of thin films boosted the rapid growth of microelectronics. The use of thin films in electronic circuit designing resulted in the miniaturization of electronic devices. Integrated chips containing hundreds of circuits and thousands of circuit elements were realized. The rapid progress in the technology prompted Gordon E. Moore to propose his famous Moore's law which predicted that the number of transistors in an IC would double in every 18months. Epitaxial growth, size-limited electron and phonon transport processes in metals, insulators and semiconductors, quantum mechanical tunnelling through normal and superconducting metal-insulator junctions, micro magnetics and plasma resonance absorption are some of the noteworthy contributions of thin film phenomenon to solid state physics. The technical interest which stimulated these studies have also rewarded in the form of useful inventions such as variety of active and passive microminiaturized components and devices, solar cells, radiation sources and detectors, magnetic memory devices, bolometer, sensors and anti-reflection coatings.

Development of new technologies is always accompanying with availability and accessibility of suitable materials and ability of manipulation to yield desired properties. Progress in understanding relation between processing, properties, structure and performance of material is also important to stepwise progression of a technology. In present era, many of sophisticated electronic devices are dependent on

elemental (IV group elements) and compound (III-V, II-VI, IV-VI etc.) semiconductors. Among different semiconductors, Si, Ge and compound semiconductor GaAs are most used materials in device applications. This is because of understanding and ability to control properties of those materials, gained from the extensive studies carried out. On the other hand, numerous attempts have been carried out to understand properties of metal oxide semiconductors because of ease of their production, stability and wide variety of application.

1.2 METAL OXIDES

Semiconductor metal oxides exhibit a wide variety of physico-chemical and electrical characteristics. The electrical behaviour of metal oxides ranges from insulators (Al_2O_3 , MgO , SiO_2) through wide band gap (SnO_2 , ZnO , WO_3 , Cr_2O_3) and narrow band gap semiconductors (Fe_2O_3) to metal-like semiconductors (*e.g.* V_2O_3 , ReO_3 , CuO) and super conductors (LaAlO_3 , SrTiO_3 , MgO). Some important properties of different metal oxides are tabulated in table 1.1. Many of the metal oxides are very important semiconductor material with different electrical properties which can be exploited in many different areas such as catalysis, superconductors, water treatment, personal care and beauty products and energy application. Particularly, metal oxide in thin film form found a huge application in the field of sensors, light emitting diodes and as transparent conductor in displays and solar cells. In relation to chemical sensing applications, metal oxides are potential candidates for gas sensor, bio and electrochemical sensor because of ability to change its electrical conductivity with change in surrounding atmosphere.

Among different metal oxides zinc oxide (ZnO) is important material, which has stable hexagonal structure at ambient conditions. ZnO also exhibits other two structures called rocksalt and zinc blende. The rocksalt structure may be exhibited at relatively higher pressure and zinc blende structure can be stabilized only by growing it on cubic structure substrate. In wurtzite structure each anion is surrounded by cations at corners of the tetrahedral, and vice versa. The figure 1.1 shows the crystal structure of ZnO . ZnO is naturally an n-type semiconductor because of the deviation from stoichiometry due to the presence of intrinsic defects such as Zn interstitials and

oxygen vacancies. Table 1.1 lists the important properties of ZnO. Different morphological ZnO thin film can be synthesized from chemical method. ZnO nanostructures have fascinating properties like large specific surface area, good biocompatibility, high electron mobility and piezoelectricity. Due to these versatile characteristics, ZnO nanostructures can be used to construct gas sensors, chemical sensors, biosensors, pH sensors and other sensors.

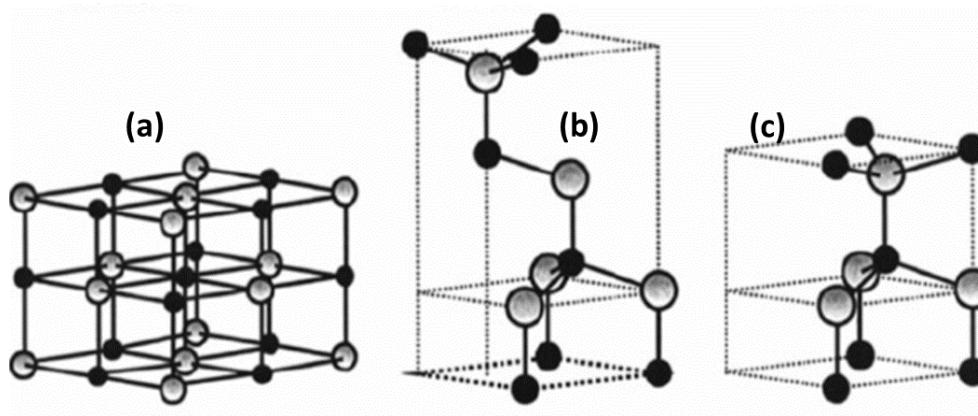


Figure 1.1: Different Crystal structures of Zinc Oxide (a) Rocksalt, (b) Zinc blende (c) Wurtzite

Table 1.1: Physical and chemical properties of metal oxide

Chemical Formula	ZnO	SnO ₂	CuO
Stable structure	Wurtzite	Rutile	Monoclinic
Lattice parameter	a=3.2535Å, c=5.2151Å	a = 4.737 Å, c = 3.185 Å	a = 4.6837, b = 3.4226, c = 5.1288
Molar mass and Density	81.408 and 5.606g/cm ³	150.708 and 6.85 g/cm ³	79.545 and 6.315 g/cm ³
Melting point	1975 ⁰ C	1,630 °C	1,326 °C
Band gap	~3.37eV	~3.7eV	~1.2 eV
Conductivity type	n-Type	n-Type	p-Type

1.3 GAS SENSORS

Gas sensors is fined as “a device which provides an electrical output in response to the change in partial pressure of a gas”. They consist of two parts: the

sensing element and the transducer. The sensing element changes its chemical properties in response to changes in the ambient concentration of a gas. The transducer transforms the chemical signal into an easily measurable electrical one. In addition to the conductivity change of gas-sensing material, the detection of this reaction can be performed by measuring the changes in capacitance, work function, mass, optical characteristics or reaction energy released by the gas/solid interaction. Various materials synthesized in the form of porous ceramics are deposited in the form of thick or thin films, are used as active layers in such gas-sensing devices. The readout of the measured value is performed via electrodes, diode arrangements, transistors, surface wave components, thickness-mode transducers or optical arrangements. However, in spite of variety of approaches to gas sensor design the basic operation principles of all gas sensors mentioned above are similar for all the devices. As a rule, chemical processes, which detect the gas by means of selective chemical reaction with a reagent, mainly utilize solid-state chemical detection principles.

There is a great interest in implementing sensing devices in order to improve environmental and safety control of gas. There is also a great need of this type of sensors to carry out the optimization of combustion reactions in the emerging transport industry, domestic as well as industrial applications. For example, hydrogen sensors are needed in the rocket propulsion industry as hydrogen propellant leaks pose significant safety risks. In addition, the automotive industry routinely monitors the air to fuel ratio in vehicles with oxygen sensors that utilize an electrochemical cell containing ZrO_2 , which conducts oxygen ions at high temperatures. The automotive industry also has interest in NO_x sensors because nitrogen oxides form when fuel burns at high temperatures. Nitrogen oxides are dangerous as they can travel great distances from their emission source and result in ozone, smog, and particulate matter far from the actual source of pollution. CO_2 sensors are examples of devices that have found multiple uses; they are needed for indoor air quality operations as well as for incubators in food storage and processing. Hydrocarbon sensors are needed for aeronautic and automotive exhaust monitoring, leak detection, and fire detection. Hydrocarbons are also a precursor to ground level ozone, and some types of

hydrocarbons are known to be toxic. There are many needs for accurate and reliable sensors in the environment.

1.4 LITERATURE SURVEY

Since the early 1920s, numerous investigations have been undertaken to demonstrate the influence of the gas atmosphere on conductivity, free carrier mobility, work function and surface potential of semiconductor materials. Upon these results a new phenomenon of the reversible changes of the semiconductor conductivity in response to changes in gas concentration has been introduced. In the early 1950s, Brattain and Bardeen, two scientists working at Bell Laboratories, gave the first demonstration that some semiconductor materials such as Ge modify their resistance, depending on the surrounding atmosphere (Brattain and Bardeent 1952). Chemiresistive gas sensors were introduced for the first time nearly fifty years ago. At the beginning of the 1960s, Seiyama, using ZnO thin film as a sensing layer, was able to demonstrate that gas sensing is possible with simple electrical devices. He used a simple chemoresistive device based on ZnO thin films operating at the temperature of 485 °C. The response of the detection system to propane was about 100 times higher compared to the thermal conductivity detector used at that time (Seiyama et al. 1962).

Later, Heiland additionally described that metal oxides such as ZnO modify their semiconducting properties with a change in the partial pressure of oxygen or other gases in the surrounding atmosphere (Heiland et al. 1954). After Seiyama's work, Shaver in 1967 described effects achievable with oxide semiconductors modified by the addition of noble metals (e.g., Pt, Pd, Ir, Rh) (Shaver et al 1967). Since that time, the sensitivity and selectivity of semiconductor sensing devices have been enhanced significantly, and the search of new formulations for sensing materials has been intensified. At the beginning of the 1970s, Taguchi fabricated and patented the first chemoresistive gas sensor device for practical applications using tin dioxide (SnO₂) as the sensitive material (Caldwell et al. 1971). Indeed, after investigating many metal oxides, he found that SnO₂ has many advantageous properties such as higher sensitivity, low operating temperature, and a thermal stable structure. Its first generation of thick film sensors was based on a mixture of tin chloride (SnCl₄) and

stearic acid that was painted on the substrate and fired at 700 °C in air. Firing burned off the organic component, leaving behind a porous SnO₂ layer. In order to increase the sensitivity, selectivity and stability, Taguchi used Pd as a metal catalyst. These devices commercialized by Figaro Inc., was as alarms to prevent accidents and fire in domestic residences by monitoring the presence of hazardous levels of explosive gases. Intense efforts in this direction resulted in widespread application of semiconductor gas sensors.

In the late 1980s, the field of semiconductor gas sensors underwent a significant expansion and became one of the most active research areas within the sensor community. The demand for high performance gas sensors with high sensitivity and selectivity, faster response, together with low power consumption and high device reliability, generated intensive efforts in order to develop new sensing materials. Results of a study on semiconductor metal oxides used as sensing materials for chemiresistive gas sensors, including both the n-type and p-type oxides, are summarized in the figure 2.1 (Neri 2015).

Table 1.2: Summary of gas sensor materials

Material type			
n-type		p-type	
Material name	Sensor study(%)	Material name	Sensor study(%)
SnO ₂	37.39	CuO	42
ZnO	20.83	NiO	35
TiO ₂	12.81	Co ₃ O ₄	12
WO ₃	8.65	Cr ₂ O ₃	10
In ₂ O ₃	6.64	Mn ₂ O ₄	1
Fe ₂ O ₃	4.27	--	

In 1999, Trivikrama Rao et al, prepared calcined powders of pure and doped ZnO. Pure-ZnO, Pd-ZnO, Fe-ZnO and Ru-ZnO thick film sensor elements have been prepared and tested for specific sensitivity to ammonia gas in air at room temperature. Among all, Pd-ZnO showed high sensitivity to ammonia in the range 50–90 ppm in air and showed a response time of ~4 s at 30 ppm of ammonia gas (Rao and Tarakarama Rao 1999).

In 2006, Gong et al produced Cu-doped ZnO (CZO) film on a glass substrate by co-sputtering using ZnO and Cu targets. These films possessed a columnar structure consisting of small crystals with an average grain size of around 5 nm. The CO-sensing properties of the film were tested at operating temperatures of 150, 300, 350 and 400⁰C. It was found that sensor exhibited the highest sensitivity to CO at 350⁰C. An obvious change in resistance of the film was also observed when the sensor was exposed to 6 ppm CO at 150⁰C (Gong et al. 2006).

In 2008, Jing et al successfully synthesized porous ZnO nanoplates through a simple microwave process. Novel gas sensor based on these porous nanoplates exhibits high response to chlorobenzene at relatively low operating temperatures, from 150 to 250⁰C, and also strong response to ethanol at relatively high operating temperatures, from 250 to 450⁰C. They can have potential application in chlorobenzene and ethanol detection at different operating temperatures(Jing and Zhan 2008).

In 2008, Ferro et al prepared nitrogen dioxide (NO₂) sensors based on sprayed ZnO thin films. The effect of the film thickness and the In-doping on the sensor performance (sensor response and resistance) is analysed. By adding 3 wt.% of indium nitrate to the spraying solution it is possible to enhance the film–gas response to 5 ppm of NO₂ at 275 °C. At the same time the film resistance is sensibly reduced. (Ferro et al. 2008).

In 2009, Zhang et al synthesized three-dimensional porous ZnO architectures by a template-free, economical hydrothermal method. The calcination of the precursor produced hierarchically 3D porous ZnO architectures composed of interconnected ZnO nanosheets with high porosity resulting from the thermal decomposition of the precursor. Gas sensing tests showed that these hierarchically porous ZnO architectures were highly promising for gas sensor applications, as the gas diffusion and mass transportation in sensing materials were significantly enhanced by their unique structures (Zhang et al. 2009).

In 2010, Forleo et al prepared ZnO nano crystals by wet chemical method. Gas sensor fabricated by drop casting the synthesized ZnO nanocrystals on alumina substrate. Studies shows the selectivity towards nitrogen oxide at 200⁰C, while at temperature above 350⁰C high responses are obtained for acetone and methanol (Forleo et al. 2010).

In 2011, Han et al prepared Sn-, Ni-, Fe- and Al-doped ZnO and pure ZnO by coprecipitation method. Their formaldehyde gas sensing properties are evaluated and the results show that Sn dopant can increase the response of ZnO by more than 2 folds, while other dopants increase little response or even decrease response. Further, CdO is used to activate ZnO based formaldehyde sensing material. It is demonstrated that CdO activated Sn-doped ZnO has the highest formaldehyde gas response, with a linear sensitivity of ~10/ppm at lowered work temperature of 200⁰C than 400⁰C of pure ZnO, and high selectivity over toluene, CO and NH₃ (Han et al. 2011).

Again in 2011, Fan et al synthesized two dimensional ZnO nanosheets with dimensions of several microns in length and tens of nanometers in thickness by hydrothermal process. Gas sensing properties were measured between 180 and 360⁰C. Sensing studies confirms the as-synthesized ZnO nano sheets are of good selectivity. It shows high response for acetone at lower temperature and gasoline at high temperature (Fan and Jia 2011).

In 2013 Rambu et al obtained the Ni doped ZnO by spin coating. A characterization shows the formation of polycrystalline films. The sensitivity of Ni:ZnO films, at three different gasses (ammonia, liquefied petroleum gas and ethanol) was investigated. Obtained results indicate that films are most sensitive to ammonia, the operating temperature was found to be 190⁰C and the response time was 35s. The gas sensitivity was found to depend on the Ni concentration in ZnO films (Rambu et al. 2013).

In 2014, Qin et al, using low temperature hydrothermal reaction synthesized hexagonal disk prismoid, prism and pyramid of ZnO. At a working temperature of 330 °C, the ZnO disk with the most exposed (0001) plane showed the highest gas

response toward ethanol, which was nearly 2, 3, and 6 times higher than those of the prismoid, prism and pyramid structures, respectively. This superior gas sensing performance strongly depends on the predominantly exposed polar facets (0001), which can provide more active sites for oxygen adsorption and subsequent reaction with the detected gas than other polar facets. (Qin et al. 2014).

In 2014, Khasim et al, reported the fabrication of heterostructures based on conducting orthochloropolyaniline–zinc-oxide nanocomposites by in situ polymerization using sodium dodecylbenzene sulphonic acid. The synthesized nanocomposites were used to fabricate the sensor device on a glass substrate with aluminium-top electrodes. It is observed that 50 wt% of nanocomposites show high sensitivity of 93% at 400 ppm with a rapid response and small recovery time of 56.76 and 37.59 s, respectively. A selectivity study was carried out by passing different test gases and determined that these composites show high sensitivity towards LPG (Khasim and Al-Hartomy 2014).

In 2015, Pati et al synthesized undoped as well as indium doped nanocrystalline ZnO thin films via chemical solution deposition route. A doping level of 3 wt% of indium in ZnO is found to give optimum response and the lowest detection limit of hydrogen of 1 ppm or even lower. They observed further increase in the doping concentration resulted in reduced sensing performance. Through exploring this gas sensing mechanism, it is argued that the sensor performance can be dramatically improved by tailoring the indium concentration in ZnO for its practical application in various sectors as an effective gas sensor (Pati et al. 2015).

In 2016, Bian et al synthesized the ZnO nanostructures by electrospinning technique, and they reported of the gas-sensing property of the ZnO nanostructures. The porous network-like ZnO nanostructures were observed from the SEM micrographs. Gas sensing properties revealed that the porous network like ZnO nanostructures exhibited a higher response and fast response to acetone vapor and excellent selectivity, which was attributed to porous network structure and oxygen vacancies (Bian et al. 2016).

In 2016, Xie et al doped ZnO nanoparticles with yttrium by using solid state chemical reaction. The Y-doped ZnO nanoparticles have diameters around 20–50 nm. The gas-sensing test indicated that the Y-doped ZnO nanoparticles have higher sensitivity and fast response than the pure ZnO sensor, and the gas sensors based on the Y-doped ZnO nanoparticles exhibit excellent selectivity toward gasoline at 200⁰C, while to ethanol at 4000C. The results showed that the Y-doped ZnO nanoparticles can be used as the sensing materials for the temperature-regulated detectors (Xie et al. 2016).

In 2016, Hastir et al studied the influence of terbium doping on structural, morphological, optical and gas sensing properties of ZnO. A chemical route was adopted for synthesis of pure and terbium (Tb) doped zinc oxide. Gas sensors were fabricated out of synthesized samples and it was observed that doped samples have significantly high sensing response, temperature dependent selectivity toward ethanol and acetone, and sensors were able to detect even low concentration (~10 ppm) of these vapors. It was found that 4% Tb doped ZnO sensor exhibited maximum sensor response toward ethanol and acetone (Hastir et al. 2016).

In 2016, Gao et al published a research article discussing about fabrication of fully integrated wearable sensor arrays for perspiration analysis aiming towards realization of personal wearable sensors. Fully integrated and mechanically flexible wrist band, based on different electrochemical sensor has been developed to monitor sweat metabolites such as glucose, lactose and electrolytes such as sodium and potassium ions. This wearable sensor system can be used to measure detailed sweat profile of human being involved in prolonged indoor and outdoor physical activities (Gao et al. 2016).

“Portable cyber-physical system for indoor and outdoor gas sensing” was developed by Jarvinen et al using well established Arduino microcontroller and raspberry bi single board computer. Commercially available MQ-4, MQ-8 and custom fabricated Pt-WO₃ sensors were interfaced with microcontroller to monitor hydrogen concentration. Developed fully wireless sensor systems could be used to

acquire data from four different sensors and showed good performance and satisfactory operability (Järvinen et al. 2017).

Low cost gas sensors were developed by Bossche et al to monitor atmospheric methane using commercially available TGS2611 sensors and Seeeduno microcontroller. Designed sensor assembly was used to measure temperature and humidity, to supply power to gas sensor and its resistive heater and to control sensor read-outs and data storage. After calibrating with respect to methane concentration, humidity and temperature, the developed systems were capable of estimating methane in lab atmosphere with error of 1ppm (Bossche et al. 2017).

1.5 SCOPE OF WORK

Literature survey reveals that numerous research efforts were focused on ZnO based gas sensors during last few years. For sensor application, ZnO thin film have been prepared by various physical and chemical methods. In particular, chemical method like spray pyrolysis is potential technique to produce ZnO thin films for sensor application. It has capability to produce large area, high quality adherent films of uniform thickness at normal atmosphere. It is very simple and inexpensive and versatile technique; hence it is preferred for mass production in industries. Very few attempts have been done for the investigation of ZnO based thin film sensor using spray pyrolysis. Hence, spray pyrolysed ZnO thin film based sensor have been taken up to enhance the sensitivity of the thin film towards the analyte gas. One approach to enhance the properties is through surface modification by proper choice of additives or dopants to the base oxide material. So the present work focuses on the doping and surface modification of ZnO based sensor to improve sensitivity and selectivity towards analyte gas.

1.6 OBJECTIVES

- 1) To optimize the growth condition of zinc oxide based thin films using prepared by pyrolysis technique.
- 2) To study the structural, compositional, optical and electrical properties of zinc oxide based thin films.

- 3) To study the sensing behavior of zinc oxide based thin films for different volatile organic compounds and gases.
- 4) To study the effect of various gas sensing parameters on the sensitivity of prepared material.

1.7 THESIS OUTLINE

The research work contained in this thesis is concerned with doping of ZnO with group-II material (cadmium), group-III materials (Indium and Aluminum), mixing of ZnO with Group-I material and preparation of amorphous zinc-tin-oxide for gas sensor application using spray pyrolysis technique. Complete work carried out is formatted in six chapters as described below.

Chapter 1 gives general introduction about thin films, compound semiconductors, metal oxide and gas sensors. Brief history of gas sensors, ZnO based gas sensors and electronic instrumentation of gas sensors is also discussed in literature survey.

Chapter 2 discusses the experimental technique of preparation method and various characterization techniques used to analyses the prepared thin films.

Chapter 3 deals with preparation and characterization of cadmium, indium and aluminum doped ZnO thin films using spray pyrolysis technique. Particular attention was paid to get optimal doping condition to enhance electrical properties without disturbing optical properties.

Chapter 4 describes about effect of cadmium, indium and aluminum doping of ZnO and its concentration on volatile organic compound (VOC) sensing properties. This also focus on finding lower VOC detection limit, effect of doping concentration on sensitivity, gas concentration on sensitivity, response time and recovery time of sensing material.

Chapter 5 comprises of synthesis, characterization of mixed Cu-Zn-Oxide and Zn-Sn-Oxide thin films. This also pays special concentration on VOC sensing properties of two immiscible metal oxide (Copper-Zinc-Oxide system) and amorphous (Zinc-Tin-Oxide) systems.

Chapter 6 includes conclusion drawn from all the investigations carried out on ZnO based materials and summarizes all the result. This also discusses about scope of future work

CHAPTER 2

EXPERIMENTAL TECHNIQUES

2.1 THIN FILM PREPARATION

Thin film semiconductor processing is an important field because of the wide variety of applications. Most of the applications of semiconductors need to have particular thickness and that can be achieved by growing them on surface of substrate through deposition process. Essential properties of thin films can be achieved by selecting proper deposition technique and conditions. Various deposition techniques have been used to deposit thin films and they can be broadly classified into two main categories as physical method and chemical method. Physical method mainly involves molecular beam epitaxy (MBE), hot wall flash evaporation, close space sublimation, sputter deposition, vacuum evaporation etc. Most of these methods are modified variants of basic vapor deposition techniques, which are developed to balance advantage and disadvantage in terms of purity, rate of growth, deposition area, etc. Chemical methods consist of techniques such as spray pyrolysis, chemical bath deposition, chemical vapor deposition, electrochemical deposition, electro less deposition, metal organic chemical vapor deposition, etc. High quality thin film grown with sophisticated instrumentation which involve high temperature, high vacuum and precise control are highly expensive and limited to very smaller area. Applications such as solar cells, large area displays, sensors require deposition on large area substrates with advantages such as high reproducibility and batch process, which can bring down the cost of final fabricated device. Spray pyrolysis is an effective processing technique being considered in research to prepare thin and thick films, ceramic coating and powders. In this simple technique ionic solution (prepared by starting solution in appropriate stoichiometric proportions) containing the constituent elements of the compound is sprayed over a preheated substrate. Generally, the metals are in solution as their chlorides, nitrates or acetates. Droplets impact on the substrate surface, spread into different structures, and undergo thermal decomposition. The shape and size depends on the momentum and volume of the droplet, as well as the substrate temperature. Consequently, the film is usually

composed of overlapping of metal salt being converted into oxides on the heated substrates, the substrate provides thermal energy for thermal decomposition and subsequent recombination of the constituent species, followed by sintering and crystallization of clusters of crystallites and thereby resulting in coherent film. Figure 2.1 shows the schematic representation and photograph of spray pyrolysis system.

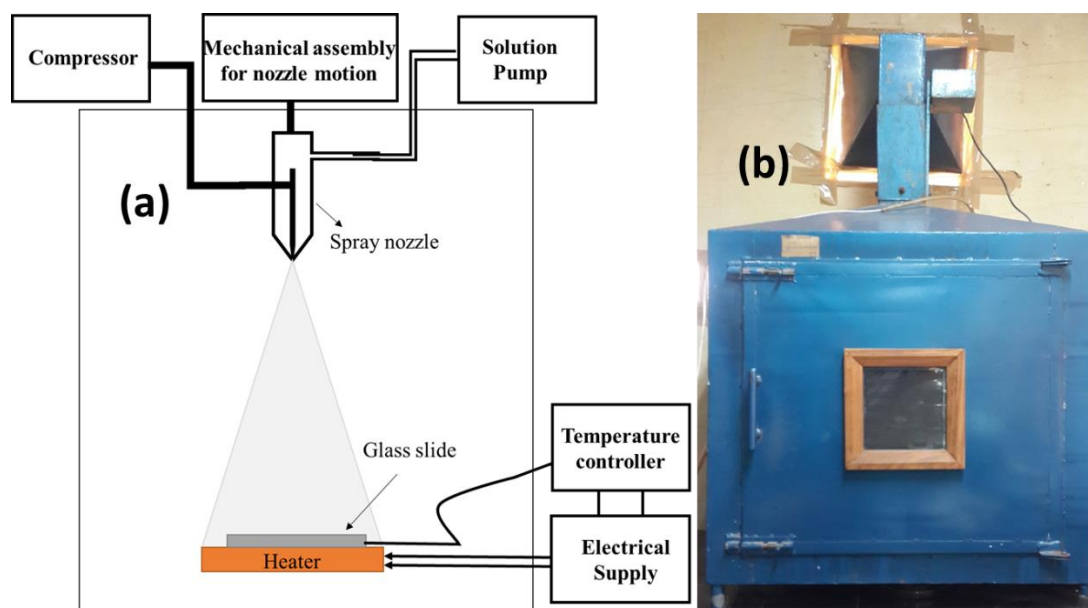


Figure 2.1: (a) Schematic representation and (b) photo graph of spray pyrolysis equipment

The spray pyrolysis mainly consists of a spray nozzle, hot plate, compressor and gas regulator valve as described below.

Spray nozzle: It is made up of glass and consists of the capillary tube surrounded by the glass bulb with outlet for compressed air. Required precursor solution will be pumped into capillary tube using external pump. With the help of compressed air, solution will disperse into aerosols and move towards below hot plate because of air pressure and gravity. Spray nozzle will be attached to a rotor which produces linear simple harmonic motion over the required length of the hot plate.

Hot plate: The stainless steel plate attached to nichrome coil will act as a hot plate. The chromel-alumel thermocouple is used to measure the temperature of the hot plate, which will be considered as substrate temperature. The temperature of the hot plate is monitored with the help of PID-temperature controller.

Compressor: It consists of assembly of electric motor connected to a piston cylinder and metal container, which compresses the normal atmospheric air. Compressed air will be channelized to spray nozzle using pipe, which helps in formation of aerosol of precursor solution material. Compressed gas flow can be regulated using a regulatory valve and pressure gauge assembly.

2.2 CHARACTERIZATION OF THIN FILMS

2.2.1 Thickness measurement

In present study, gravimetric method was used to estimate thickness of the deposited film. Thickness of material can be determined by knowing mass of deposited layer (m), deposited area (A) and bulk density of material. The mass of deposited material can be estimated by knowing difference in mass substrate before (m_1) and after (m_2) deposition by using high resolution weighing balance. The thickness (t) of the thin film can be calculated from formula.

$$t = \frac{m_2 - m_1}{\rho A} \quad (2.1)$$

2.2.2 X-ray Powder Diffraction (XRD)

X-ray diffraction (XRD) is a powerful non-destructive technique for characterising crystalline materials. It provides information on structures, phases, preferred crystal orientations, and other structural parameters such as average grain size, crystallinity, strain and crystal defects. X-ray diffraction peaks are produced by constructive interference of a monochromatic beam of x-rays scattered at specific angles from each set of lattice planes in a sample. The peak intensities are determined by distribution of atoms within the lattice. Consequently, the x-ray diffraction pattern is the fingerprint of periodic atomic arrangement in a given material. In present study, Rigaku miniflex-600 table top X-ray diffractometer working in Bragg-Brentano geometry (θ - 2θ) with vertical goniometer (radius of goniometer circle =150mm) and 600W characteristic X-ray source (Cu K_α , $\lambda=1.54\text{\AA}$) was used. This also consists of optics such as divergence slit, scattering slit, receiving slit, K_β foil filter, monochromator and soller slit with capability of scanning range from -3° to 145° (2θ) and scanning rate of 0.001 - 100° /min (2θ) at minimum step width of 0.005° (2θ). In

present study, a scan rate of $2^\circ/\text{min}$ was used as it provided good diffracted intensity. Interplanar distance (d) in crystallites of thin film produces characteristic peaks at particular 2θ angles, which is ruled by Bragg's law ($2d \sin \theta = n\lambda$). The standard 'd' values for materials are well documented in card format over the years by Joint Committee on Powder Diffraction Standards-International Center for Diffraction Data (JCPDS-ICDD). The calculated 'd' values, obtained from XRD pattern, were matched with the standard data to confirm crystal structure. Calculated 'd' values and lattice parameters were rounded off to two decimal places with an error about $\pm 0.02 \text{ \AA}$. Also, diffraction data was used to obtain dimension of unit cell and crystallinity.

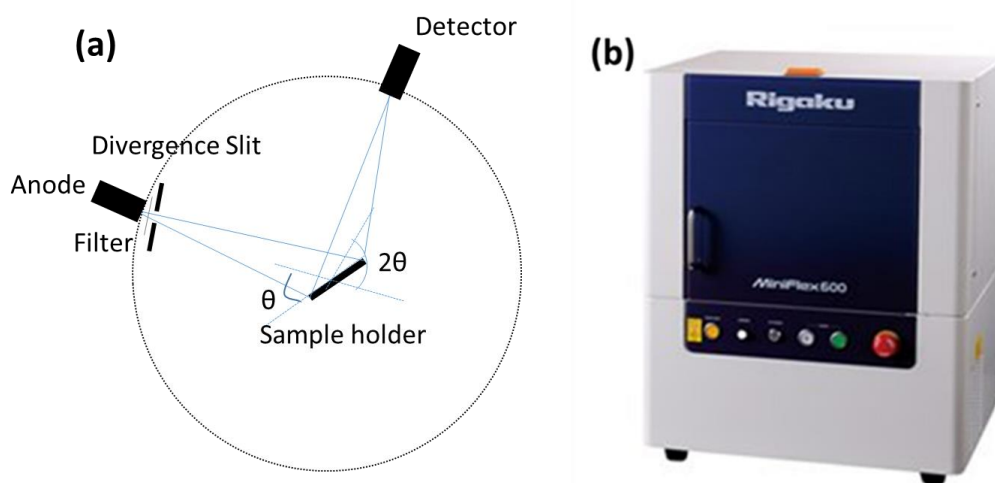


Figure 2.2: (a) Schematic representation of XRD, (b) Photograph of Rigaku-miniflex600

2.2.3 Scanning Electron Microscope (SEM):

Field emission scanning electron microscopy (FE-SEM) is one of the largely used techniques to analyse the surface microstructure. In this technique, an electron beam is focused in vacuum by electro-magnetic lens and scanned over the surface of the sample. The scattered secondary electrons from the surface of the sample are then fed to the detector, which gives the information of the sample. SEM comprises of a heated filament as a source of electron beam, condenser lenses, aperture, evacuated chamber for placing the sample, electron detector, amplifier, etc. Detectors also have the capability to collect x-rays, backscattered electrons and secondary electrons and convert them

into a signal that is sent to a screen to produces the final image. In present study, surface morphology was captured using Zeiss-Sigma FE-SEM model. The FE-SEM is capable of capturing image with resolution of 1nm at accelerating voltage of 20kV. Accelerating voltage of 5kV with working distance of 5-8mm was used during present study. Since, the samples were deposited on non-conducting soda-lime glass substrate, all the samples were sputtered with thin layer of gold and conductivity between surface of thin film to sample holder was established using carbon tape.



Figure 2.3: Photograph of FE-SEM model Zeiss-Sigma

Energy dispersive x-ray spectroscopy (EDS or EDX) is an analytical technique used predominantly for the elemental analysis or chemical characterization of a specimen. EDS technique detects x-rays emitted from the sample using drifted silicon detector during bombardment by an electron beam to characterize the elemental composition. The energy of x-ray generated is characteristic of that material, which can be used to quantitative and qualitative identification of chemical composition. However, accuracy of quantitative measurement depends on atomic number of sample, x-ray absorption coefficient and fluorescence factor of sample. EDX spectrum is a plot of how frequently an X-ray is released for each of scanned energy level in which highly intensive peak represents the more concentrated element of grown sample. In the present work, EDX data is corrected upto one decimal place with a possible error of 0.5 at. %.

2.2.4 Optical studies

The interaction of the semiconductor material with light is used to analyse the band structure. When light falls on the material part of the incident light may be reflected, some part may get absorbed and the remaining part may get transmitted. The amount of reflected, transmitted or absorbed light energy depends on the energy of the incident photons and the band structure of the material. The transmission or absorption measurements reveal valuable information about the band structure of the material. In a semiconductor, optical absorption may take place due to various mechanisms and each contributes to the total absorption. In present investigation, optical transmission spectra of all the prepared thin film was recorded using Princeton SpectraPro-2300i UV-Visible spectrometer in the wavelength range of 300-800nm. Newport made xenon lamp with 150W power was used as light source. The slit width of 1mm, scanning rate of 5nm/sec was fixed throughout the study.

2.2.5 Electrical studies

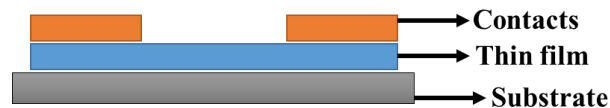


Figure 2.4: Schematic diagram of sample used for electrical measurement

The electrical properties of materials may depend on several factors such as deposition technique, optimization condition, thickness, crystallinity, defects, etc. Analysing electrical property of material gives insight into many property of material, which can be helpful for device fabrication. Thin films prepared using spray pyrolysis technique will be polycrystalline in nature, in which electrical property is dominated by grain boundaries and defect. In present study, electrical resistivity was measured using Keithley 2002 multimeter and 2400 sourcemeter. For this purpose, sample of known dimension was deposited with thin layer of aluminium using thermal evaporation technique. Two aluminium contact pads of 1cm x 1cm separated by distance of 1mm were deposited on surface of 1.5cm x 2.5cm thin film of known thickness.

The resistivity of the thin film is calculated by using the formula

$$\rho = RA/l \quad (2.2)$$

where 'R' is the resistance of the film, 'l' is the length of the contact and 'A' is the area between the contacts. Area between the contacts is given by

$$A = t \times d \quad (2.3)$$

where 't' is the thickness and 'd' is the gap between the contacts.

Type of electrical conductivity of deposited thin films were analysed using hot probe method. This method is based on Seebeck effect, in which sign of thermo emf generated between hot and cold is used to determine the type of conductivity. A soldering gun was used to heat one terminal and other terminal was maintained at room temperature. Then, hot end and cold end terminal of thin film were connected to positive and negative terminals of voltmeter respectively. Because of thermal gradient, thermally generated charge carriers diffuse from hot end to cold end leading to development of a potential, which can be measured using voltmeter. A positive and negative potential develops across the terminals for n type and p-type materials respectively.

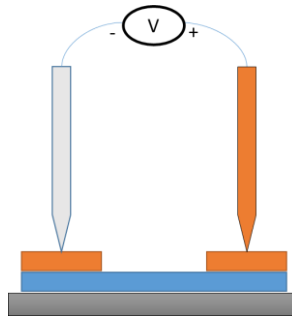


Figure 2.5: Schematic diagram of hot probe method

2.2.6 Gas sensor studies

Sensing behaviour is the most important and well known property of metal-oxide materials. Metal oxide demonstrate high sensitivity to surrounding chemical environment. The working mechanism of the metal oxide sensors is based on the variation of surface electrical conductance in the presence of a gaseous environment. This induces the change in electrical conductivity by the adsorption of gaseous species on the surface film by a chemical reaction. The metal oxide causes the gas to

dissociate in to charged ions or complexes on the surface, which result in the transfer of electrons from film to gas molecules or vice versa. This property has been exploited and used for detection of toxic gases. Gas sensing measurements were performed under laboratory condition (40 % relative humidity, 25⁰C) using custom made static gas-sensing system of volume 30L. The schematic representation of gas sensor is shown in figure 2.6. Prior to injection of test gas, air is admitted to the measuring chamber. To improve long term stability, the sensing element is heated for several hours at optimized temperature to reach a stable resistance in air (R_a). At this moment, a fixed volume of volatile organic compounds (VOCs) is injected into the chamber using a micro pipette, which readily evaporates to form vapours and the chamber is closed. Fan inside the chamber facilitate proper diffusion of air and vaporized VOC. The stable resistance of sensing element (R_g) at VOC environment is noted. Again air is admitted to measuring chamber, sensing element comes in contact with air and the resistance of sensing element returns to value which it had before VOC injection. The complete phenomenon of resistance variation of the sensing element was recorded using computer interfaced Keithley source meter-2400.

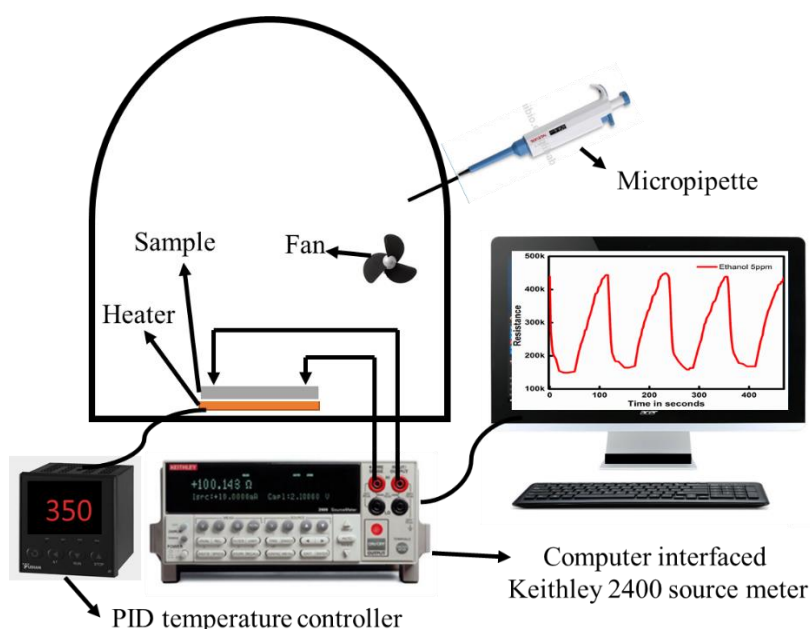


Figure 2.6: Schematic representation of gas sensing set up

CHAPTER 3

PREPARATION AND CHARACTERIZATION OF DOPED ZnO THIN FILMS

3.1 INTRODUCTION

ZnO is an extensively studied n-type metal oxide semiconductor material, which is non-toxic and abundant in nature. Wide band gap and good electrical property of ZnO based thin films can be exploited to make front panel electrode in solar cells (Bi et al. 2013), thin film transistors (Smith et al. 2009) and light emitting diodes (Tseng et al. 2016). Large exciton binding energy of 60meV makes it important candidate for highly efficient room temperature operable lasers (Bagnall et al. 1997). ZnO can be synthesized in the form of powders (Su et al. 2014), pellets (Ghosh et al. 2015), thick films (Borse et al. 2010), thin films (Pati et al. 2015) etc. Comparatively, thin films are most attractive because of low consumption of precursor material during synthesis and high surface to volume ratio. Many times the optical and electrical properties of ZnO thin film in pure form may not reach all the requirements of high performance semiconductor devices. It is possible to tune the optical band gap from the range of 1.8eV to 3.89eV in $Cd_xZn_{1-x}O$ and $Mg_xZn_{1-x}O$ alloys (Ma et al. 2011) (Wang et al. 2008). In order to enhance electrical properties, ZnO can be doped with different elements like Ga(Chin et al. 2016), In(Pati et al. 2015), Al(Tsubota et al. 1997) and Cd (Zhai et al. 2014). Cadmium(Cd) is an important doping material, could be an ideal doping candidate for ZnO to improve its opto-electronic properties. CdZnO films are useful in the construction of ZnO/CdZnO heterojunction and superlattice structures, which are important in fabrication of ZnO based light emitters and detectors (Vijayalakshmi et al. 2008). Another important dopant for ZnO is indium(In), which is used in the manufacturing of transparent electrodes, one of the most successful results achieved up to now is by incorporation of In as impurity into the ZnO lattice. No post- annealing treatment in a reducing or vacuum environment is required in order to obtain low resistivity values for In doped ZnO. In present days, group III elements, in particular aluminium is considered to be the most gifted alternative doping agent to costlier indium, because of its low cost, non-toxicity and

abundant availability. It is also reported that, Aluminium doped ZnO (AZO) thin films not only exhibit good electrical property and high optical transparency in the visible wavelength region (300-800 nm) but also offers good chemical, mechanical and thermal stability. So, the present work deals with the preparation of ZnO thin films doped with Cd [$\text{Cd}_x\text{Zn}_{1-x}\text{O}$ ($0 \leq x \leq 0.20$)], In [$\text{In}_x\text{Zn}_{1-x}\text{O}$ ($0 \leq x \leq 0.05$)] and Al [$\text{Al}_x\text{Zn}_{1-x}\text{O}$ ($0 \leq x \leq 0.05$)] thin film using spray pyrolysis technique and characterization to check phase consistency, surface morphology, optical, electrical properties.

3.2 EFFECT OF Cd DOPING ON THE PROPERTIES OF ZnO THIN FILMS

3.2.1 Experimental details

Cd doped ZnO [$\text{Cd}_x\text{Zn}_{1-x}\text{O}$ ($0 \leq x \leq 0.20$)] thin films were deposited on cleaned soda lime glass substrate using spray pyrolysis technique. Along with zinc diacetate dihydrate ($\text{Zn}(\text{CH}_3\text{COO})_2 \cdot 2\text{H}_2\text{O}$), cadmium chloride ($\text{CdCl}_2 \cdot 2\frac{1}{2}\text{H}_2\text{O}$) was used as dopant source to prepare $\text{Cd}_x\text{Zn}_{1-x}\text{O}$ thin films. The prepared solution was sprayed at rate of 2ml/min on preheated glass substrate held at optimized temperature of 400°C . The spray nozzle is fixed at a distance of 30 cm from the substrate. Air was used as carrier gas at the pressure of 2 bar. The sprayed droplets reach the hot glass substrate and decompose on glass substrate to form highly adherent thin films.

The thickness of the films was measured using gravimetric method and maintained $\sim 600\text{nm}$. The structural characterization was carried out by X-ray diffractometer (Rigaku Miniflex 600) using $\text{CuK}\alpha$ radiation. The surface morphology and chemical composition of the grown film were analysed using field emission scanning electron microscope (Carl-Zeiss FE-SEM) and energy dispersive X-ray (EDX) spectroscopy. The optical transmittance was measured using UV-Visible spectrophotometer (Princeton SpectraPro-2300i) in the wavelength range of 300–800nm at room temperature. The electrical measurements were carried out using Keithley source meter and multimeter.

3.2.2 X-ray Diffraction

The figure 3.1(a), shows the XRD pattern of the as-deposited pure ZnO thin film. The sharp diffraction peaks indicate the good crystallinity of polycrystalline pure ZnO thin film. The XRD pattern can be indexed as wurtzite-phase of ZnO with characteristic

peaks of (002), (101), (102) and (103) planes. As compared to the polycrystalline pattern of randomly oriented ZnO (JCPDS Card No. 01-079-0208), the (002) peak is greatly enhanced, indicating preferential orientation of grains along c-axis. The mechanism which dominates the preferential growth of films along this direction is not clearly understood. The hexagonal wurtzite structure has minimum surface energy and the highest atomic density of zinc atom along (002) plane, so growth along this plane is predominant (Pati et al. 2015), (Bao et al. 1998).

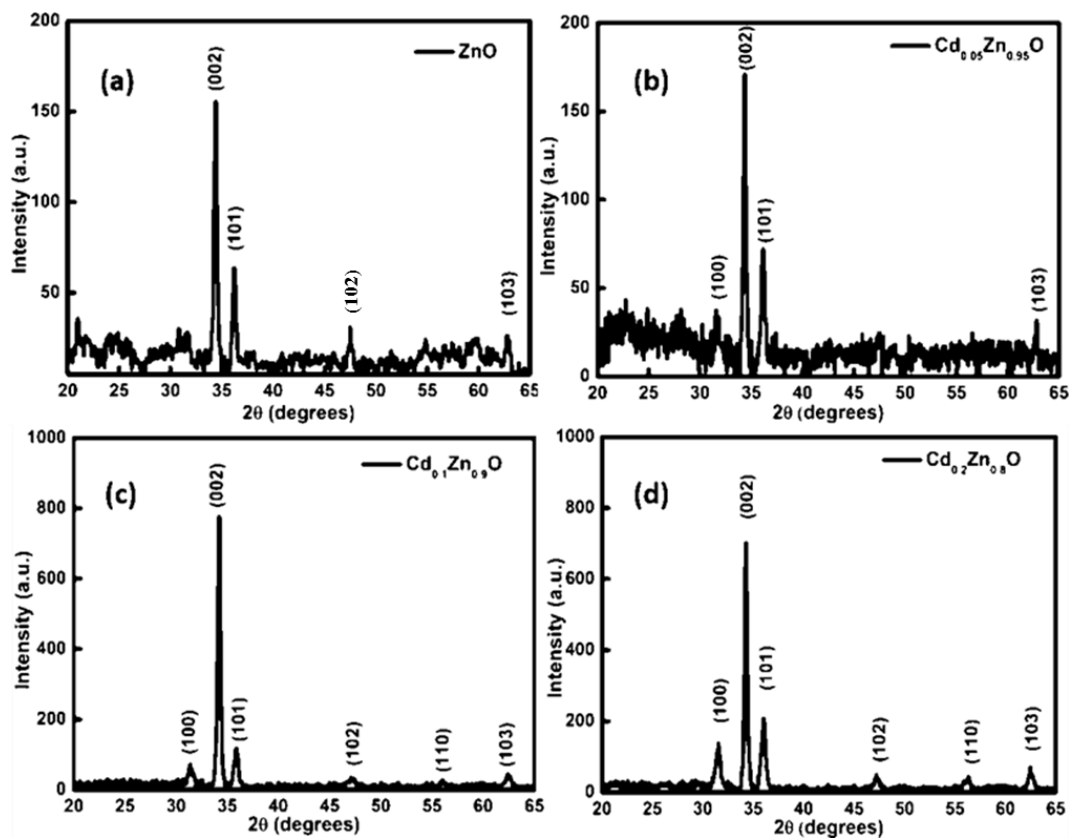


Figure 3.1: XRD patterns of Cd_xZn_{1-x}O thin films (a) 0%, (b) 5 at. %, (c) 10 at. %, (d) 20 at.%.

The figure 3.1(b - d) shows the XRD patterns of Cd_xZn_{1-x}O thin film with cadmium content 5, 10 and 20 at.%. The presence of only one predominant peak along (002) direction for all the composition indicate a strong preferred orientation. No other peak corresponding to possible impurities like CdO was detected. It is observed that the diffraction peak positions shift systematically towards lower angles with increase in Cd concentration. This indicates substitution of Zn²⁺ ions by Cd²⁺ ions resulting in changes in lattice parameters.

The inter planar distance ‘d’ is calculated using Bragg equation

$$2d_{hkl} \sin \theta = n\lambda \quad (1)$$

where ‘n’ is the order of diffraction, hkl the Miller indices of the plane of diffraction, ‘λ’ is the wavelength of X-ray radiation, ‘θ’ is the angle of incidence. The lattice parameters ‘a’ and ‘c’ for hexagonal structure can be calculated from relation

$$\frac{1}{d^2} = \frac{4}{3} \frac{(h^2+hk+k^2)}{(a^2)} + \frac{l^2}{c^2} \quad (2)$$

The calculated lattice parameters and inter planar distance is listed in the table 3.1. Since the ionic radius of Cd²⁺ ions (0.97 Å) is larger than that of Zn²⁺ ions (0.74 Å), increase in lattice parameters and inter planar distance can be observed.

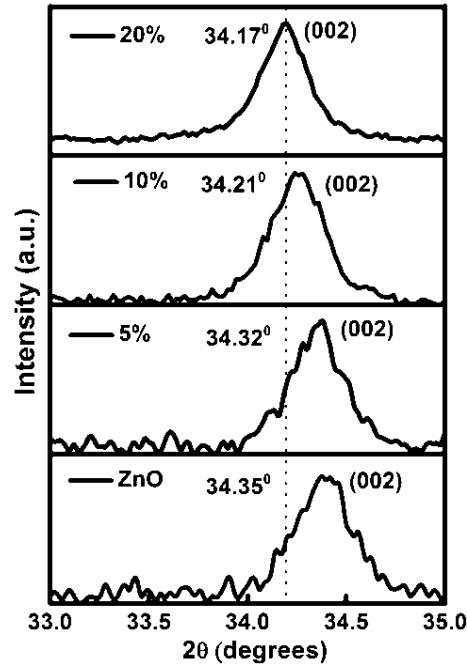


Figure 3.2: Shift in the (002) peak position of Cd_xZn_{1-x}O

Table 3.1: Structural parameters of Cd_xZn_{1-x}O estimated from XRD

Sample name	d (Å)	D (nm)	a (Å)	c (Å)
ZnO	2.607	23.00	3.252	5.214
Cd _{0.05} Zn _{0.95} O	2.609	25.30	3.260	5.218
Cd _{0.1} Zn _{0.9} O	2.617	26.60	3.282	5.234
Cd _{0.2} Zn _{0.8} O	2.620	26.20	3.297	5.241

The grain size ‘D’ is evaluated using the Scherrer’s equation

$$D = \frac{0.94\lambda}{\beta \cos \theta} \quad (3)$$

where β is the full width at half maxima in radian. Calculated grain sizes are tabulated in table 3.1. It is observed that, increase in Cd doping concentration brings marginal increase in the grain size.

3.2.3 Morphological and compositional analysis

Figure 3.3(a) shows the FE-SEM micrographs of ZnO thin films. The image shows the uniformity in the formation of the microstructure without any holes and cracks. It can be observed that thin films possess tightly packed and randomly arranged plate like structures.

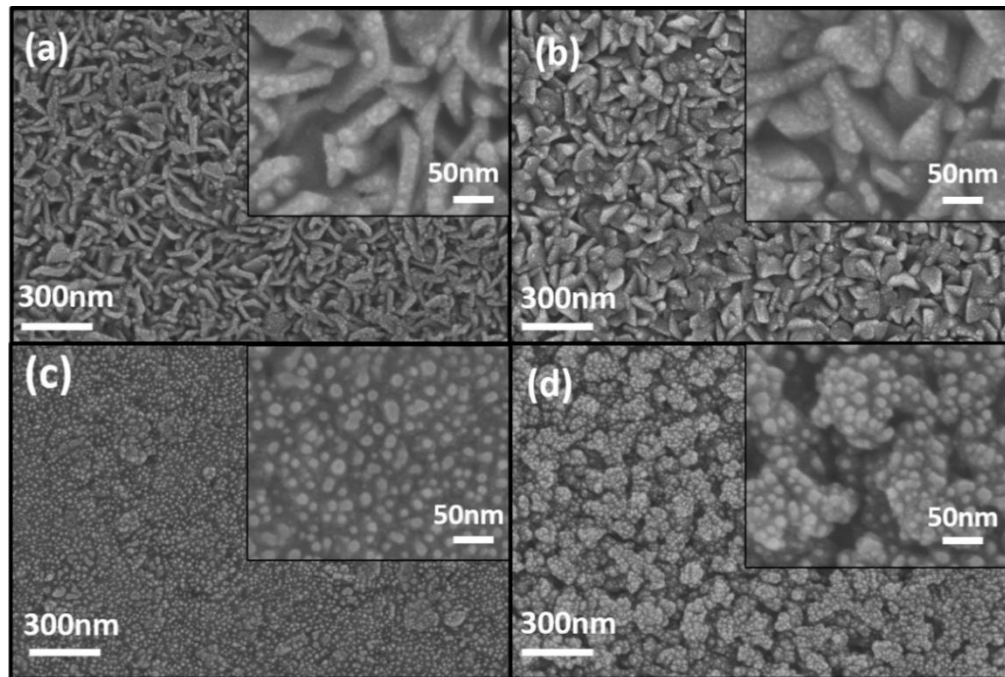


Figure 3.3: FE-SEM images of $\text{Cd}_x\text{Zn}_{1-x}\text{O}$ (a) 0%, (b) 5 at.%, (c) 10 at.% and (d) 20 at.%

With addition of 5 at.% Cd, the thin film surface contains randomly shaped grains as shown in the figure 3.3(b). Increasing the Cd concentration to value of 10 at.% and 20 at.%, leads to granular morphology. The mixture of smaller and larger tightly packed granular structure can be observed in figure 3.3(c) and (d). These results indicate that Cd incorporation modifies the surface morphology of the films by influencing the initial nucleation process. The structures obtained are very significant due to their high specific surface area and adsorption capacity.

The EDX analysis confirmed the presence of Zn and Cd elements in as-deposited thin films (shown in figure 3.4). It has also been observed that the amount of Cd in the thin film is slightly less than that in initial precursor solution. Similar behaviour was also observed by Vijayalakshmi et al (Vijayalakshmi et al. 2008). According to EDX-Elemental mapping results, Cd is uniformly distributed throughout the thin film (Figure 3.4(inset)).

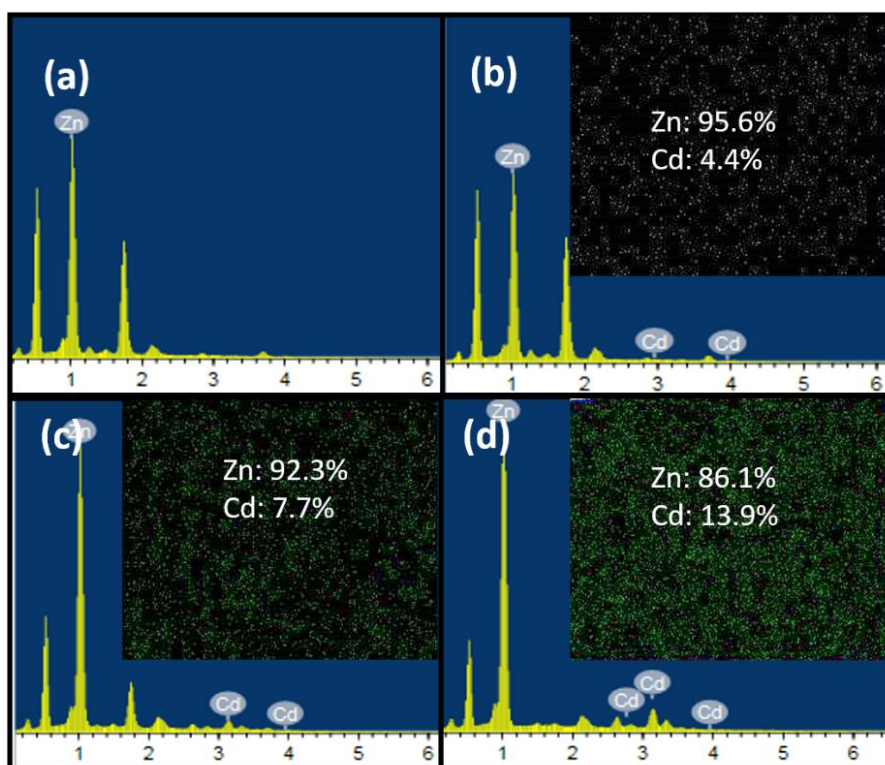


Figure 3.4: EDAX spectra (inset: mapping) of $Cd_xZn_{1-x}O$ thin films for different Cd concentration (a) 0%, (b) 5 at.%, (c) 10 at.% and (d) 20 at.%.

3.2.4 Optical properties

The optical transmittance spectra of $Cd_xZn_{1-x}O$ thin films are shown in the figure 3.5(a). The transmittance measurements show that pure ZnO thin films are highly transparent above wavelength of 350nm. As the Cd composition increases, the transmittance value decreased from 95% to 65%. The increase in the Cd composition up to 10 at. % does not cause much change in the transmittance value in visible region. Above this concentration level coloration is observed (transparent to pale yellowish colour) in thin films with a decrease in the transmittance values, i.e. the

average transmittance of these films decreased for higher Cd concentrations. Similar behaviour was observed by Vijayalakshmi et al (Vijayalakshmi et al. 2008). Along with increase in Cd concentration, successive shift in the transmission edge towards higher wavelength was observed, which clearly indicates decrease in bandgap values. The bandgap values of $\text{Cd}_x\text{Zn}_{1-x}\text{O}$ thin films determined from the plots of $(\alpha h\nu)^2$ vs. $(h\nu)$ are shown in figure 3.5(b). The extrapolation of linear portion of $(\alpha h\nu)^2$ to $(h\nu)$ axis provides bandgap values. The bandgap energy value decreases with increase in cadmium content in thin films (Table 3.2). The increase in the Cd concentration leads to band gap narrowing, which can be attributed to the large difference in the band gap values of ZnO and CdO. Shift in band gap is common phenomena when two materials with different band gap are properly mixed (Santhosh et al. 2017). The linearity in the plot indicates that $\text{Cd}_x\text{Zn}_{1-x}\text{O}$ films possess direct inter band transitions without any intermediate band gap belonging to CdO. This also confirm the successful substitution of Zn^{2+} ions by Cd^{2+} ions in ZnO lattice, which is in pact with the XRD and EDX mapping analysis.

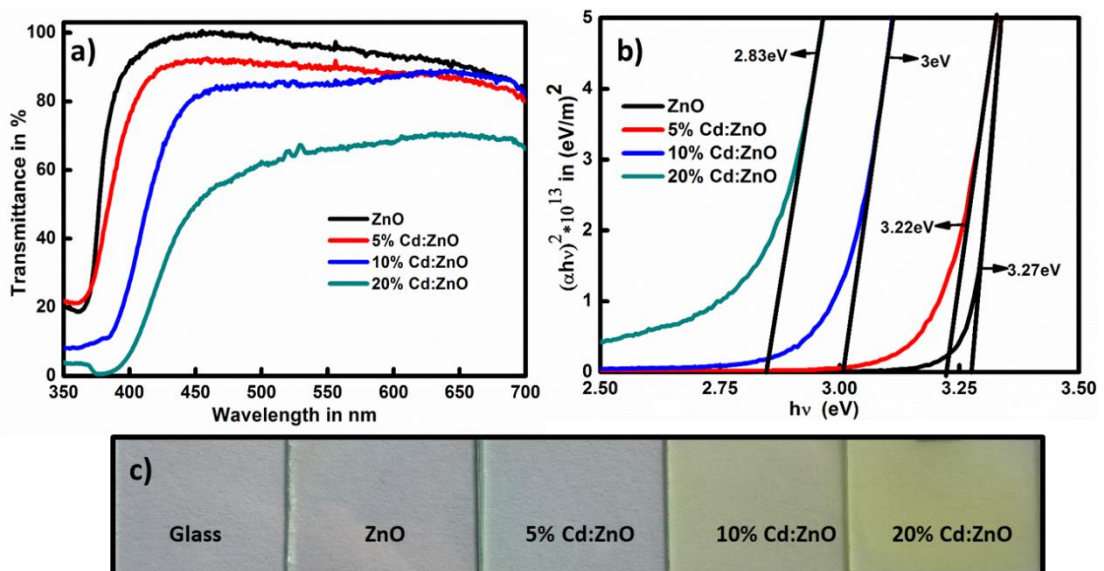


Figure 3.5: (a) Transmittance spectra, (b) Tauc's plots of $\text{Cd}_x\text{Zn}_{1-x}\text{O}$ thin film and (c) appearance of deposited $\text{Cd}_x\text{Zn}_{1-x}\text{O}$ thin films

3.2.5 Electrical properties

A hot probe experiment carried out confirm n-type conductivity for all as deposited thin films. The linear I-V characteristic curves in the figure 3.6 proves formation of ohmic contact between thin film and thermally evaporated aluminum

contact. The electrical resistivity values of $\text{Cd}_x\text{Zn}_{1-x}\text{O}$ are shown in table 3.2, it was observed that an increase in Cd concentration up to 10 at.% causes an decrease in its resistivity. The decrease in its resistivity may be because of interstitial occupation of some Cd^{2+} ions, which donates two electrons to conduction band. When the Cd concentration increases further up to 20 at.%, the resistivity increases. This may be because of increased lattice distortion and decreased grain size, as observed from XRD.

Table 3.2: Electrical resistivity and bandgap of $\text{Cd}_x\text{Zn}_{1-x}\text{O}$ thin films

Sample name	Resistivity (Ωm)	Bandgap (eV)
ZnO	13.30	3.27
$\text{Cd}_{0.05}\text{Zn}_{0.95}\text{O}$	0.30	3.22
$\text{Cd}_{0.1}\text{Zn}_{0.9}\text{O}$	0.02	3.00
$\text{Cd}_{0.2}\text{Zn}_{0.8}\text{O}$	0.39	2.83

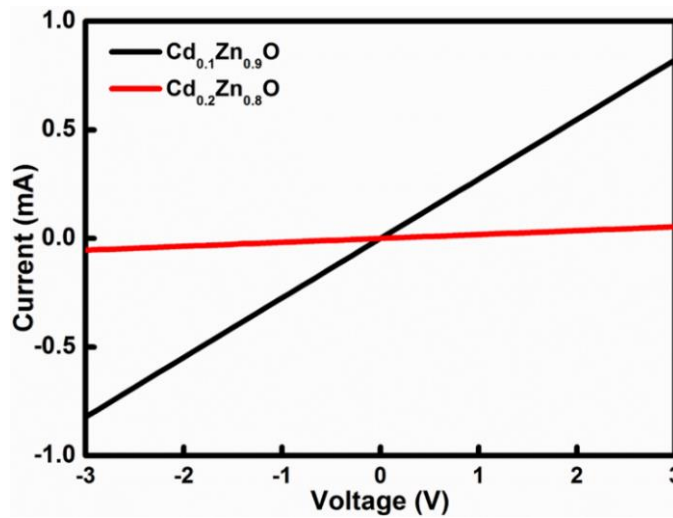


Figure 3.6: I-V characteristic curve of $\text{Cd}_x\text{Zn}_{1-x}\text{O}$ thin films with aluminum contact

3.3 EFFECT OF ANNEALING ON $\text{Cd}_x\text{Zn}_{1-x}\text{O}$ THIN FILMS

3.3.1 X-ray diffraction

To study thermal stability $\text{Cd}_x\text{Zn}_{1-x}\text{O}$ thin films, they were subjected to annealing in air at temperature of $400\text{ }^{\circ}\text{C}$ for 4hrs. The figure 3.7 displays the XRD spectrum of annealed $\text{Cd}_x\text{Zn}_{1-x}\text{O}$ thin films with different doping concentration. The XRD patterns revealed that the annealed $\text{Cd}_x\text{Zn}_{1-x}\text{O}$ thin films were also polycrystalline in nature, as compared with the as-deposited $\text{Cd}_x\text{Zn}_{1-x}\text{O}$ thin films. It also demonstrates

that preferred orientation of grains in $\text{Cd}_x\text{Zn}_{1-x}\text{O}$ thin films along (002) plane is unaffected by annealing process. In comparison with the as deposited sample, the shift in peak position of (002) plane is less for annealed $\text{Cd}_x\text{Zn}_{1-x}\text{O}$ thin films, peak positions are listed in the table 3.3. It was also observed that the a- and c-lattice parameters of annealed thin films were slightly reduced as compared to the as deposited $\text{Cd}_x\text{Zn}_{1-x}\text{O}$ thin films. This may be because of reduction in the Cd concentration, which may be evaporating because of high temperature annealing. Grain size increase for all the composition of $\text{Cd}_x\text{Zn}_{1-x}\text{O}$ thin films with annealing, this may be because of recrystallization process taking place during annealing.

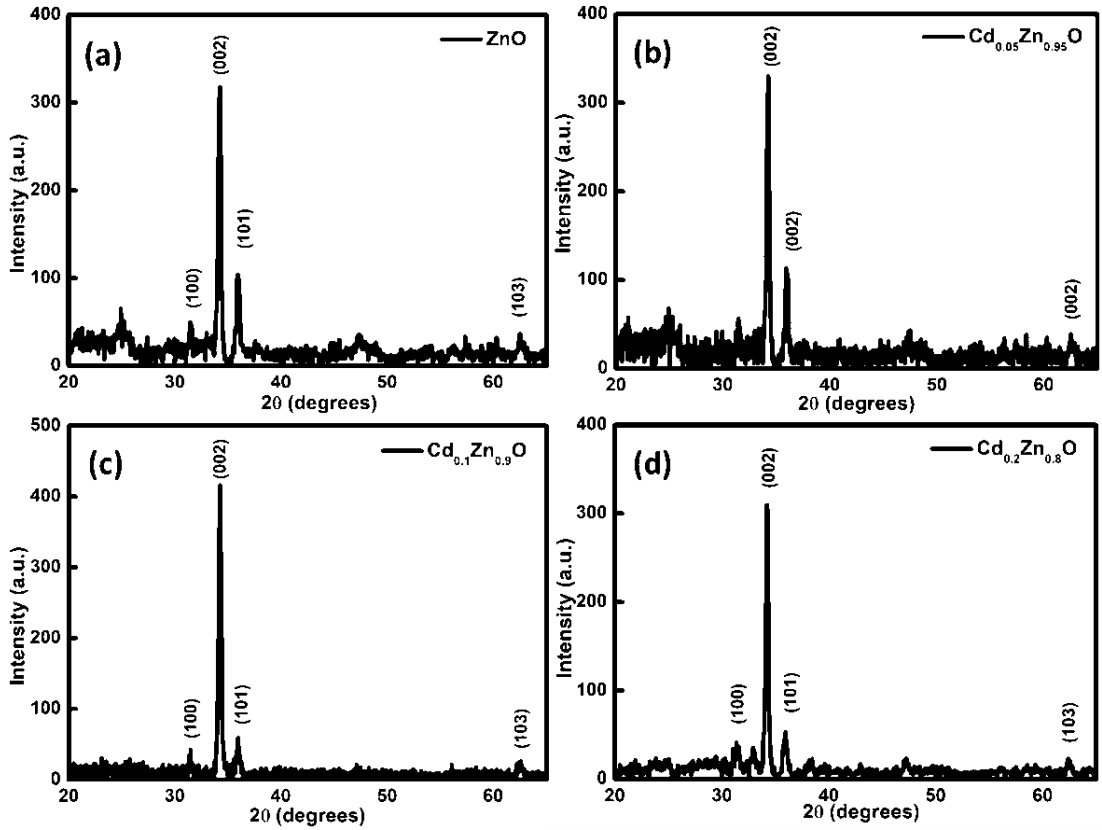


Figure 3.7: XRD patterns of annealed $\text{Cd}_x\text{Zn}_{1-x}\text{O}$ thin films (a) 0%, (b) 5 at.%, (c) 10 at.%, (d) 20 at.%

Table 3.3: Structural parameters of annealed $\text{Cd}_x\text{Zn}_{1-x}\text{O}$ estimated from XRD

Sample name	2θ (degree)	D (nm)	d (Å)	a (Å)	c (Å)
ZnO	34.33	26.00	2.608	3.253	5.217
$\text{Cd}_{0.05}\text{Zn}_{0.95}\text{O}$	34.32	28.00	2.609	3.256	5.218
$\text{Cd}_{0.1}\text{Zn}_{0.9}\text{O}$	34.28	34.00	2.616	3.276	5.224
$\text{Cd}_{0.2}\text{Zn}_{0.8}\text{O}$	34.21	27.00	2.617	3.278	5.235

3.3.2 Morphological and compositional analysis

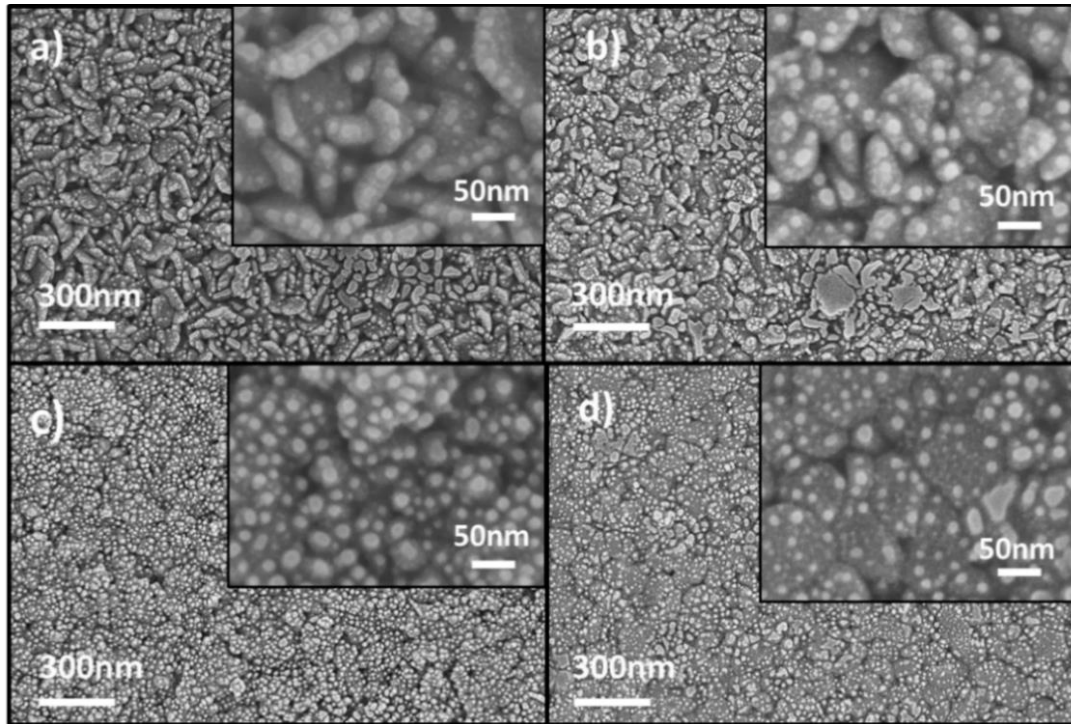


Figure 3.8: FE-SEM images of annealed $Cd_xZn_{1-x}O$ (a) 0%, (b) 5at.%, (c) 10at.%(d) 20at.%

Table 3.4: Compositional information $Cd_xZn_{1-x}O$ thin film

Cd at.%	Zn (at.%)	Cd(at.%)
ZnO	100%	0%
$Cd_{0.05}Zn_{0.95}O$	97.10%	2.89%
$Cd_{0.1}Zn_{0.9}O$	94.45%	5.55%
$Cd_{0.2}Zn_{0.8}O$	88.98%	11.02%

Annealing process modifies morphological structure of the material by changing nature of distribution of crystallites in the thin films. It also facilitates proper oxidation of the unreacted metal ions and helps in desorption of gaseous impurities. The figure 3.8 depicts morphology of annealed $Cd_xZn_{1-x}O$ thin films. For pure ZnO, plate like structure as seen in as-deposited thin film transforms to randomly shaped closely distributed granular structure. In all the remaining samples recrystallization can be observed clearly, in which smaller clusters are agglomerated to form bigger clusters as shown in figure 3.8(b)-(d). Compositional information of annealed thin films is presented in table 3.4. It is observed that the atomic concentration of Cd in

thin films reduced after annealing, considerable reduction may be because of evaporation of Cd atoms. This result is in corroboration with XRD analysis.

3.3.3 Optical properties

After annealing, the transmittance value remains almost constant, but as compared to the band gap of as deposited thin film, slight increase in the band gap was observed for annealed $\text{Cd}_x\text{Zn}_{1-x}\text{O}$ thin films. The tauc's plot for annealed $\text{Cd}_x\text{Zn}_{1-x}\text{O}$ is shown in the figure 3.9(b). The increase in band gap may be because of evaporation of Cd from ZnO lattice, as observed from XRD and EDX analysis.

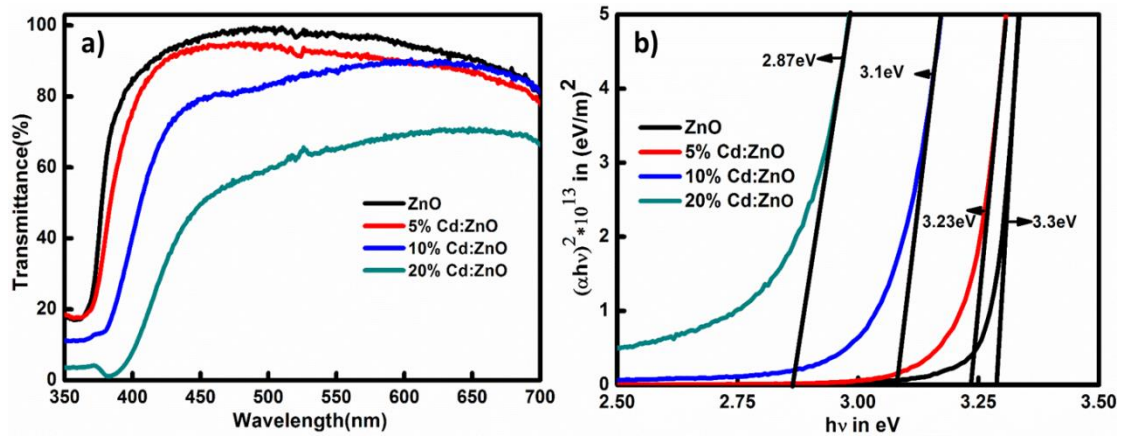


Figure 3.9: (a) Transmittance spectra, (b) Tauc's plots of annealed $\text{Cd}_x\text{Zn}_{1-x}\text{O}$ thin film

3.3.4 Electrical properties

Table 3.5: Electrical resistivity and bandgap of annealed $\text{Cd}_x\text{Zn}_{1-x}\text{O}$ thin films

Sample name	Resistivity (Ωm)	Bandgap (eV)
ZnO	64.8	3.3
$\text{Cd}_{0.05}\text{Zn}_{0.95}\text{O}$	15.0	3.23
$\text{Cd}_{0.1}\text{Zn}_{0.9}\text{O}$	1.08	3.1
$\text{Cd}_{0.2}\text{Zn}_{0.8}\text{O}$	1.38	2.87

As observed from hot-probe experiment, type of conductivity of $\text{Cd}_x\text{Zn}_{1-x}\text{O}$ thin films are unchanged by annealing. The measured resistance, calculated resistivity and conductivity of $\text{Cd}_x\text{Zn}_{1-x}\text{O}$ thin films are tabulated in the table 3.5. It was observed that the resistance of all $\text{Cd}_x\text{Zn}_{1-x}\text{O}$ thin films increased drastically after annealing. This increase in the resistance may be because of evaporation of Cd, as observed from

EDX analysis. This may be also because of diffusion of impurities from glass substrate and adsorption of oxygen from the atmosphere.

3.4 EFFECT OF In DOPING ON THE PROPERTIES OF ZnO THIN FILMS

3.4.1 Experimental details

$\text{In}_x\text{Zn}_{1-x}\text{O}$ thin films were deposited onto soda lime glass substrates using homemade assembly of spray pyrolysis unit. Zinc diacetate dihydrate ($\text{Zn}(\text{CH}_3\text{COO})_2 \cdot 2\text{H}_2\text{O}$) was used as precursor material and indium chloride (InCl_3) was used as dopant source, both the materials were dissolved in distilled water at different molar ratios to get resultant solution of 50mM concentration. In the deposition process, the solution was injected through nozzle and sprayed on top of pre heated glass substrate maintained at temperature of 350°C . A constant spray rate of 2ml/min and substrate to nozzle distance of 30cm was maintained during the deposition. Air was used as carrier gas, which was supplied by an air compressor at constant pressure of 2 bar.

3.4.2 XRD Analysis

The X-ray diffraction pattern of the as deposited pure ZnO thin film in figure 3.10(a) shows the polycrystalline nature of the thin films. The diffraction pattern of pure ZnO mainly consist of peak corresponding to (002) and (101) planes at an angle of 34.34° and 36.10° , which is in accordance with the standard XRD pattern of wurtzite-ZnO [JCPDS Card No. 01-079-020]. The high intensity of (002) peak indicates preferential orientation of grains along the same direction. Minimum surface energy of wurtzite structure and highest atomic density of zinc along (002) plane may be the reason for this preferential growth (Pati et al. 2015), (Bao et al. 1998).

Figure 3.10(b)-(d) shows the XRD spectra of In doped ZnO thin films corresponding to the doping concentration of 1 at. %, 3 at. % and 5 at. % respectively. Peaks corresponding to In or In compounds were not observed within detection limit of XRD, which proves the successful incorporation of In into the ZnO lattice. Slight shift in the (002) peak was also observed, indicating the substitution of In into ZnO lattice. Indium substitution has significant impact on film crystallinity and orientation. In doping concentration of 1 at. % do not cause any major changes in the

XRD peak intensities. Beyond 1 at.% In doping concentration, dominance of (002) peak decreases while the intensity of (100) and (101) increases. Similar behaviour is also observed by Shinde et al (Shinde et al. 2008).

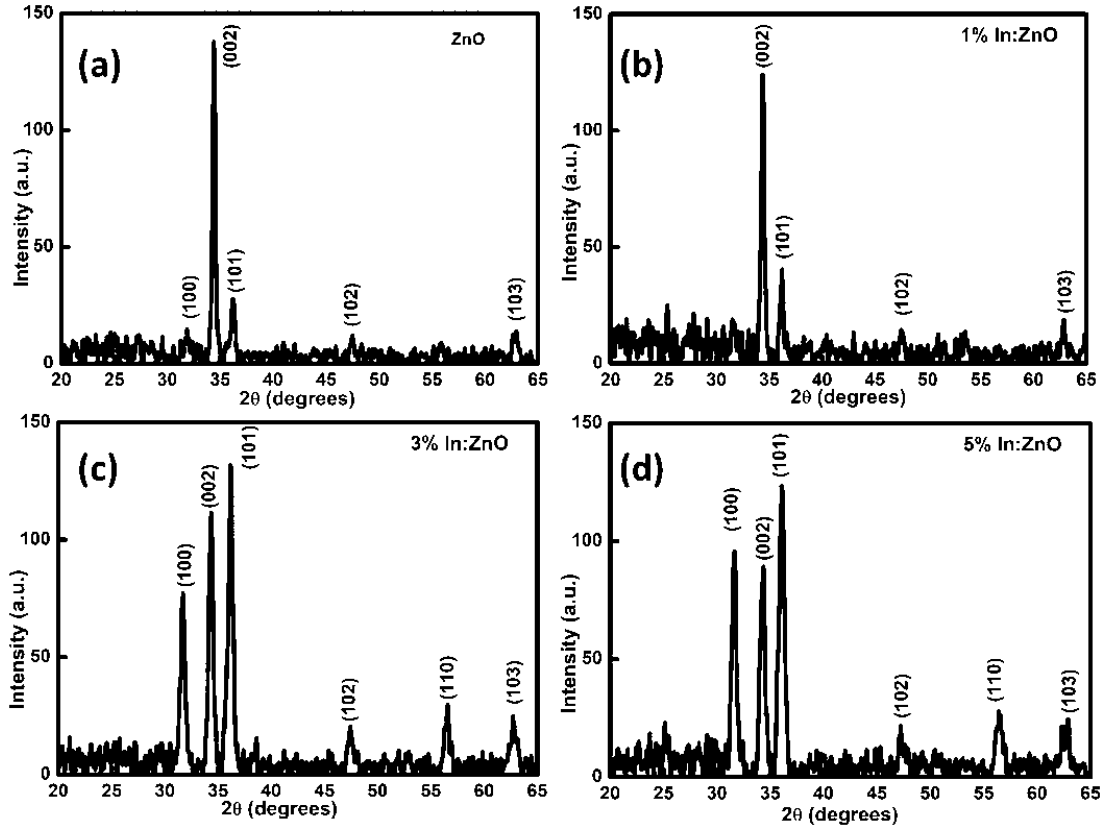


Figure 3.10: XRD patterns of $\text{In}_x\text{Zn}_{1-x}\text{O}$ thin films (a) 0 at. %, (b) 1 at. %, (c) 3 at. %, (d) 5 at. %

Table 3.6: Estimated structural parameters of $\text{In}_x\text{Zn}_{1-x}\text{O}$ thin films

Sample name	(hkl)	D in nm	d in Å	c in Å	a in Å
ZnO	(002)	23.20	2.605	5.210	
	(101)	18.17	2.475		3.248
$\text{In}_{0.01}\text{Zn}_{0.99}\text{O}$	(002)	21.64	2.605	5.211	
	(101)	24.92	2.479		3.255
$\text{In}_{0.03}\text{Zn}_{0.97}\text{O}$	(100)	14.41	2.827		
	(002)	14.56	2.609	5.219	
	(101)	13.78	2.481		3.257
$\text{In}_{0.05}\text{Zn}_{0.95}\text{O}$	(100)	12.47	2.825		
	(002)	12.88	2.611	5.222	
	(101)	11.96	2.485		3.263

Further to see the effect of In substitution at Zn site in ZnO lattice, grain size 'D' is evaluated using the equation (3). Calculated grain sizes are tabulated in Table

3.6. It can be observed that FWHM of $\text{In}_x\text{Zn}_{1-x}\text{O}$ thin films increases with increase in doping concentration indicating decrease in grain size. This may be because of distortion created in the ZnO lattice due to substitution of Zn^{2+} by In^{3+} ions. Adding indium ions disturbs periodicity of ZnO lattice because of mismatch in their size. This can lead to increase in defect site and grain boundaries, which decreases crystallite size.

The inter planar distance ‘d’ is calculated using the equation (1). Interplanar distance calculated for (100), (002) and (101) are tabulated in the table 3.6. The calculated interplanar distance, lattice parameters ‘a’ and ‘c’ are listed in the table 3.6, which increases with increase in doping concentration. This variation can be attributed to relative difference between ionic radii of In^{3+} (0.80 Å) and Zn^{2+} (0.74 Å).

3.4.3 Surface morphological and compositional analysis

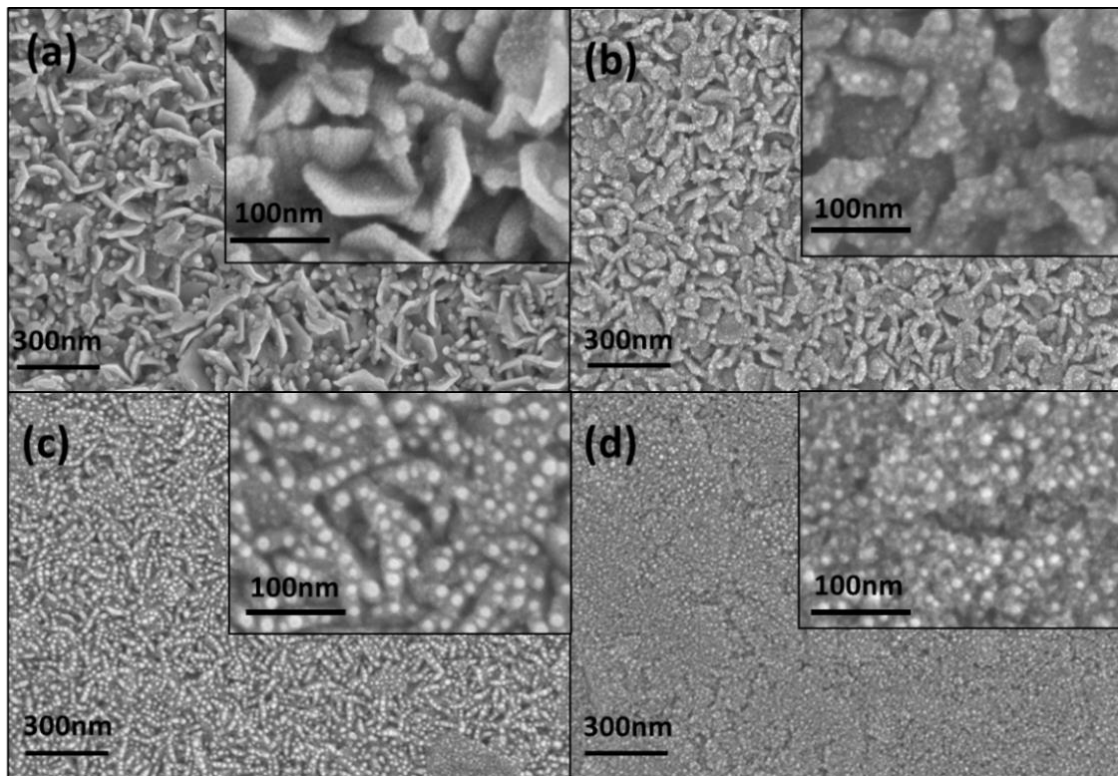


Figure 3.11: FE-SEM image of $\text{In}_x\text{Zn}_{1-x}\text{O}$ thin films (a) 0 at.%, (b) 1 at.%, (c) 3 at.% and (d) 5 at.%

SEM micrographs of In doped ZnO thin films are shown in the figure 3.11. All the deposited thin films exhibited a rough surface with uniform distribution of

particle-like structures. Holes and cracks free surface can be observed from low magnification images. These micrographs prove that, surface morphology of $\text{In}_x\text{Zn}_{1-x}\text{O}$ thin films robustly dependent on In doping concentration. Figure 3.11(a) shows surface morphology of undoped ZnO thin films with elongated plate like structure along with smaller grains. With increase in In concentration, visible grain density in given image increases and in figure 3.11(c) (In= 3 at. %) noticeable changes in the surface configuration can be observed as compared to figures 3.11(a). EDX analysis confirms the presence of the Zn and In in prepared thin films. Compositional data is tabulated in the table 3.7.

Table 3.7: Compositional information $\text{In}_x\text{Zn}_{1-x}\text{O}$ thin films

Sample name	Zn (at.%)	In (at.%)
ZnO	100	0
$\text{In}_{0.01}\text{Zn}_{0.99}\text{O}$	99.01	0.99
$\text{In}_{0.03}\text{Zn}_{0.97}\text{O}$	97.60	2.40
$\text{In}_{0.05}\text{Zn}_{0.95}\text{O}$	94.96	5.04

3.4.4 Optical analysis

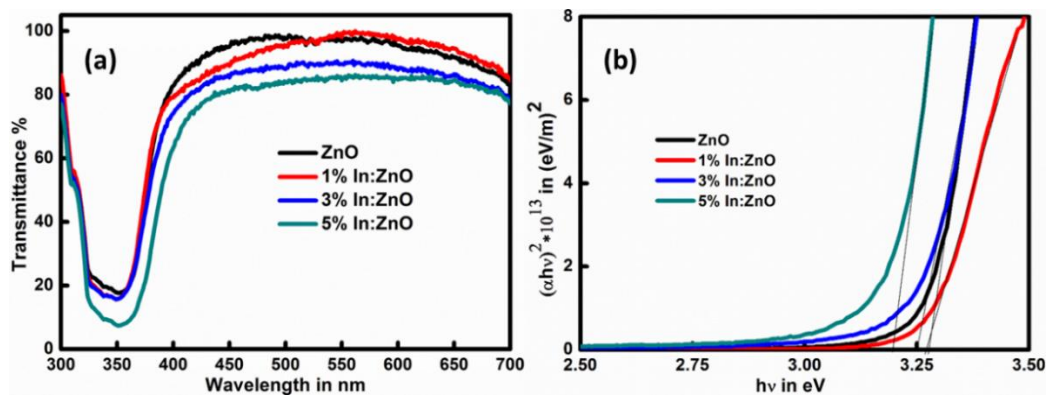


Figure 3.12: (a) Transmittance spectra, (b) Tauc's plots of In doped ZnO thin films

The optical transmission measurements carried out on In doped ZnO thin films in the wavelength range of 300 to 750nm are shown in figure 3.12(a). It can be observed that the transmission value decreases from >95% to >80% with increase in the doping concentration. This may be because of the decrease in the crystallinity of the film as observed in XRD, which induces scattering by surface of thin films. All the thin films have high absorption in UV region and high transmission in visible region. The high absorption in UV region is because of fundamental absorption

involving the transition of electron from valance band to conduction band, which can be used to calculate the optical bandgap of semiconductor material. The band gap of prepared thin films is shown in the Tauc's plot (Figure 3.12(b)). Also, the linearity observed in the tauc's plot proves the direct interband transitions. The estimated optical bandgaps ranges from 3.27eV (for pure ZnO) to 3.20eV (for 5 at. % In doped ZnO). Slight redshift in the bandgap is observed with increase in the In concentration. Similar behavior is also observed by Kim et al (Kim et al. 2012).

3.4.5 Electrical studies

Table 3.8: Electrical resistivity and bandgap of $\text{In}_x\text{Zn}_{1-x}\text{O}$ thin films

Sample name	Resistivity (Ωm)	Bandgap (eV)
ZnO	20.49	3.29
$\text{In}_{0.01}\text{Zn}_{0.99}\text{O}$	0.166	3.27
$\text{In}_{0.03}\text{Zn}_{0.97}\text{O}$	0.058	3.25
$\text{In}_{0.05}\text{Zn}_{0.95}\text{O}$	0.177	3.18

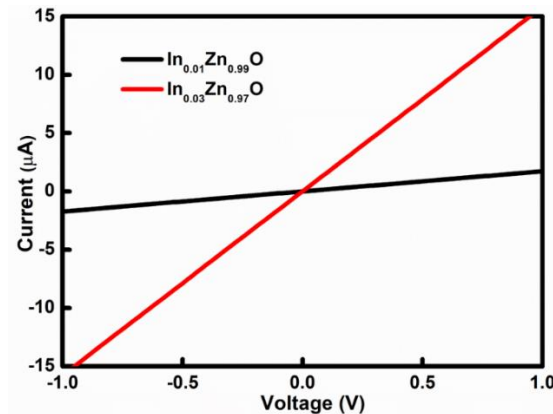


Figure 3.13: I-V characteristics of $\text{In}_x\text{Zn}_{1-x}\text{O}$ thin films

The n-type of electrical conductivity of as deposited thin films were identified by using hot probe setup. The linearity in the current-voltage measurements (Figure 3.13) proves the formation of ohmic contact between thin films and aluminium contact. The variation in electrical resistivity with respect to indium doping concentration are listed in the table 3.8. At lower doping concentration (1 at. % and 3 at. %) an decrease in resistivity was observed. This may be because of substitution of In^{3+} in place of Zn^{2+} , which donates an electron to conduction band. Further increase in doping concentration leads to increase in resistivity may be

because of decrease in crystallinity, as observed from XRD. Increase in resistivity is attributed to decrease in crystallinity of thin films, which leads to increase in distortion of lattice and hence a decrease in mobility of electrons. $\text{In}_{0.03}\text{Zn}_{0.97}\text{O}$ thin films were showing good conductivity with good transmission in UV-VIS range. So, these samples can be used for transparent conductor application. Current results are comparable with dip coated and Sol-Gel process synthesized $\text{In}_x\text{Zn}_{1-x}\text{O}$ thin films (Alamdari et al. 2017)(Kim et al. 2015).

3.5 EFFECT OF Al DOPING ON THE PROPERTIES OF ZnO THIN FILMS

3.5.1 Experimental details:

Aluminum doped ZnO thin films were deposited onto sodalime glass substrate by using spray pyrolysis technique. Zinc diacetate dihydrate ($\text{Zn}(\text{CH}_3\text{COO})_2 \cdot 2\text{H}_2\text{O}$) was used as precursor material and aluminum chloride (AlCl_3) was used as dopant source, both the materials were dissolved in distilled water at different molar ratios to get resultant solution of 50mM concentration. In the deposition process, the solution was injected through nozzle and sprayed on top of pre heated glass substrate maintained at temperature of 350°C . During complete deposition process optimized spray rate and substrate to nozzle distance were maintained. Air was used as carrier gas, which was supplied by an air compressor at constant pressure of 2 bar.

3.5.2 XRD Analysis

The X-ray diffraction pattern pure ZnO deposited in this batch was comparable with 3.10 (a). Figure 3.14(b-f) displays the XRD spectra of $\text{Al}_x\text{Zn}_{1-x}\text{O}$ thin films corresponding to the doping concentration of 0.5 at. %, 1 at. %, 1.5 at. %, 3 at. % and 5 at. % respectively. All the $\text{Al}_x\text{Zn}_{1-x}\text{O}$ thin films exhibited multiple peaks indicating polycrystalline nature. It was observed that dominant peak in XRD spectra for all $\text{Al}_x\text{Zn}_{1-x}\text{O}$ thin films was along (002) direction, this type of c-axis orientation of $\text{Al}_x\text{Zn}_{1-x}\text{O}$ thin film is essential when used as a buffer layer in CdS/CdTe based solar cells. No impurity peaks were observed even upto 5 at. % Al doping to ZnO host matrix, indicates successful Al substitution into ZnO host matrix without creating any impurity phase.

Table 3.9: Estimated structural parameters of $\text{Al}_x\text{Zn}_{1-x}\text{O}$ thin films

Sample name	D (nm)	d (Å)	c (Å)	a (Å)
$\text{Al}_{0.005}\text{Zn}_{0.995}\text{O}$	23.24	2.599	5.199	3.260
$\text{Al}_{0.01}\text{Zn}_{0.99}\text{O}$	22.58	2.607	5.214	3.259
$\text{Al}_{0.015}\text{Zn}_{0.985}\text{O}$	20.40	2.603	5.207	3.255
$\text{Al}_{0.03}\text{Zn}_{0.97}\text{O}$	18.25	2.603	5.207	3.267
$\text{Al}_{0.05}\text{Zn}_{0.95}\text{O}$	12.25	2.605	5.211	3.283

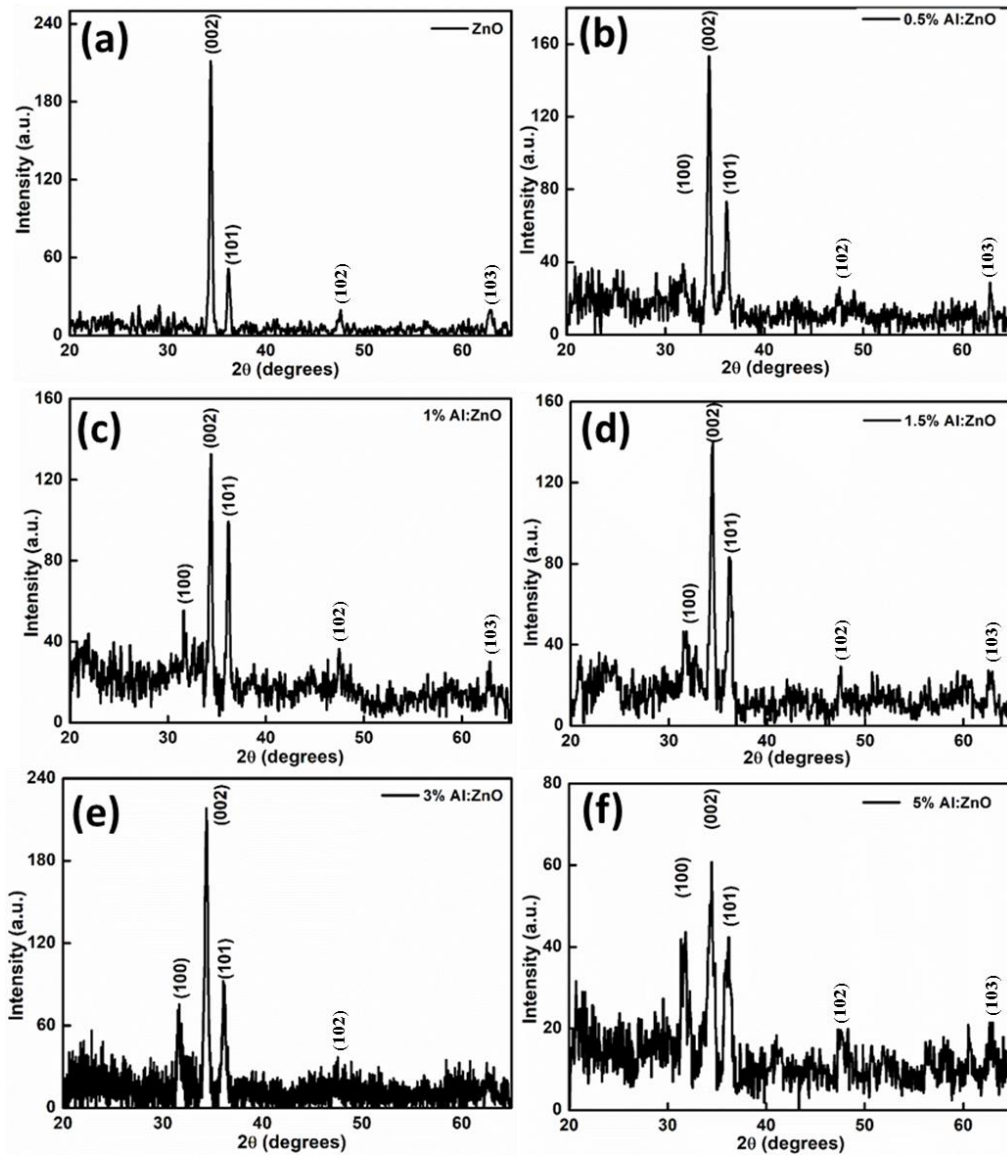


Figure 3.14: XRD patterns $\text{Al}_x\text{Zn}_{1-x}\text{O}$ thin films (a) ZnO, (b) $\text{Al}_{0.005}\text{Zn}_{0.995}\text{O}$, (c) $\text{Al}_{0.01}\text{Zn}_{0.99}\text{O}$, (d) $\text{Al}_{0.015}\text{Zn}_{0.985}\text{O}$, (e) $\text{Al}_{0.03}\text{Zn}_{0.97}\text{O}$, (f) $\text{Al}_{0.05}\text{Zn}_{0.95}\text{O}$

Furthermore, to see the effect of Al substitution in ZnO, grain size, interplanar distance and lattice parameters were calculated for highest intensity peak using the equation and tabulated in table 3.9. It is inferred from table that an increase in aluminium doping concentration causes the decrease in the grain size. During initial crystallization doped atom may act as nucleation centres and increase in doping concentration leads to increase in nucleation centres, which subsequently leads to increase number of smaller crystals. This decrease in crystal size may also be attributed to distortion created by substitution of Al³⁺ ions, which acts as impurity in ZnO lattice. The estimated lattice parameter and interplanar distance are well matched with JCPDS data with minor random variation, similar nonlinear trend in the structural parameters are also reported in literature (Raghu et al. 2017). In conclusion, Al substitution has less impact on the lattice parameters and interplanar distance.

3.5.3 Surface morphological and compositional analysis

SEM micrographs of Al_xZn_{1-x}O thin films shown in the figure 3.15 exhibits homogeneous and uniform distribution of particle-like nanostructures with holes and cracks free surface, which can be observed from low magnification images. Variation of surface morphology with an increase in aluminum doping concentration can be clearly noticed from high magnification images (inset of figure 3.15). Aluminum doping changes plate like morphology of ZnO into granular morphology (figure 3.15(b-f)). EDX analysis confirms the presence of the Zn and Al in prepared thin films. Compositional data is tabulated in the table 3.10.

Table 3.10: Compositional information Al_xZn_{1-x}O thin films

Sample name	Zn (at. %)	Al (at. %)
Al _{0.005} Zn _{0.995} O	99.48	0.51
Al _{0.01} Zn _{0.99} O	99.07	0.93
Al _{0.015} Zn _{0.985}	98.46	1.54
Al _{0.03} Zn _{0.97} O	96.8	3.2
Al _{0.05} Zn _{0.95} O	95.12	4.88

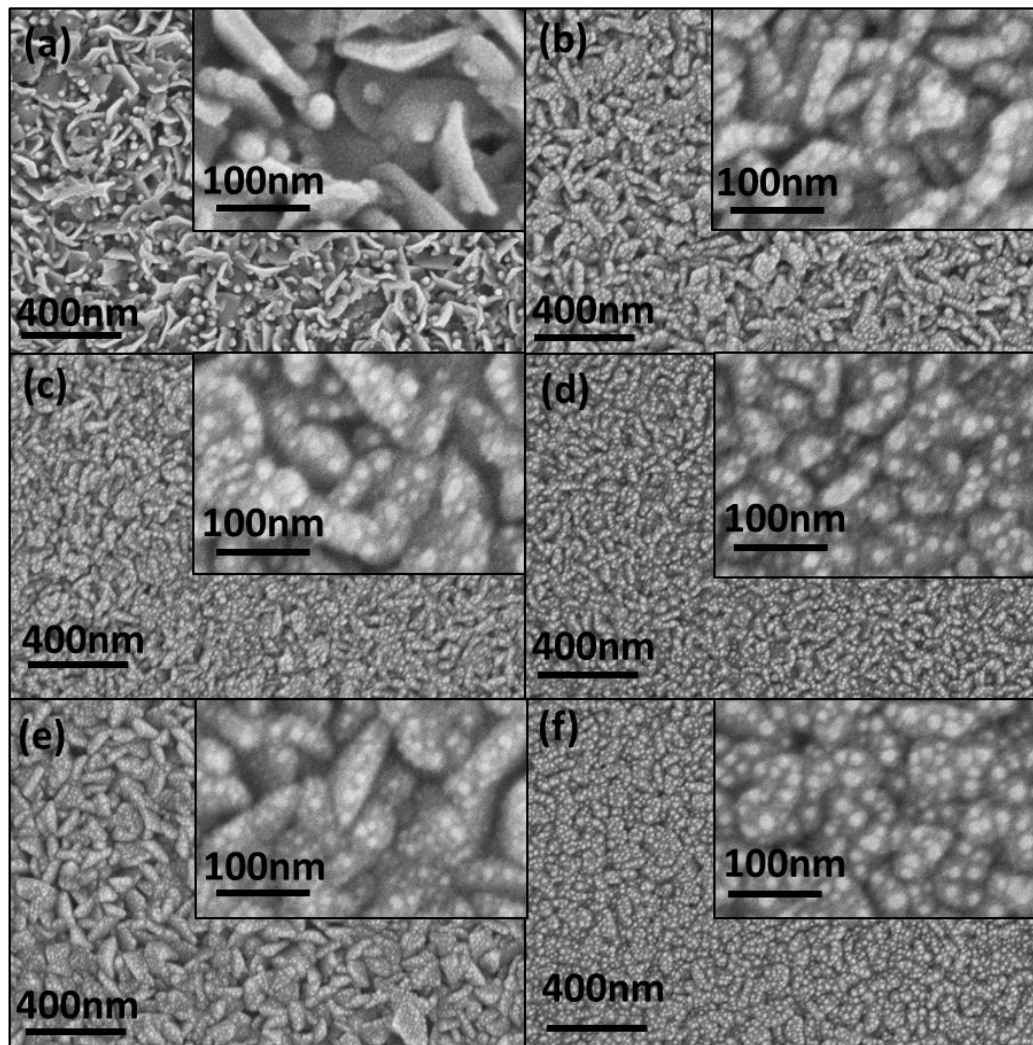


Figure 3.15: FE-SEM images of $\text{Al}_x\text{Zn}_{1-x}\text{O}$ thin films (a) ZnO, (b) $\text{Al}_{0.005}\text{Zn}_{0.995}\text{O}$, (c) $\text{Al}_{0.01}\text{Zn}_{0.99}\text{O}$, (d) $\text{Al}_{0.015}\text{Zn}_{0.985}\text{O}$, (e) $\text{Al}_{0.03}\text{Zn}_{0.97}\text{O}$, (f) $\text{Al}_{0.05}\text{Zn}_{0.95}\text{O}$

3.5.4 Optical properties

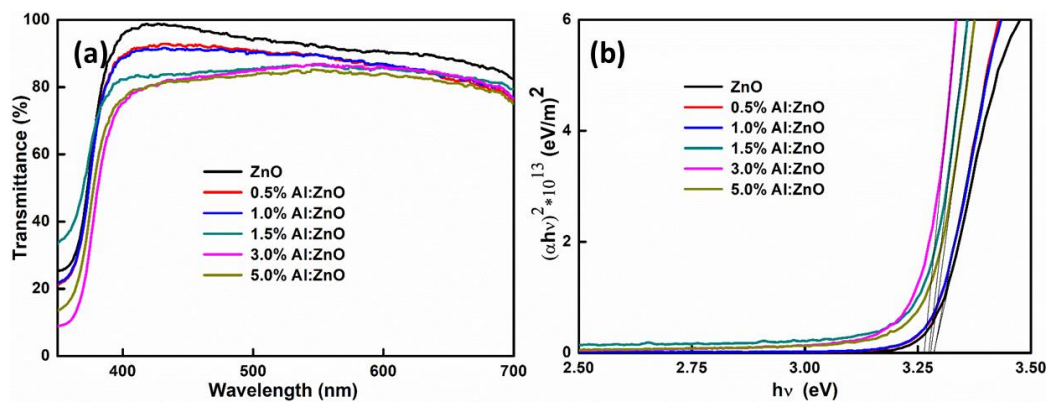


Figure 3.16: (a) Transmittance spectra, (b) Tauc's plots of $\text{Al}_x\text{Zn}_{1-x}\text{O}$ thin films

To investigate the effect of Al doping into ZnO thin films on optical transmission and bandgap, UV-Visible measurements carried out in the wavelength range of 300 to 700nm (shown in figure 3.16 (a)). >80% transmittance was achieved for $\text{Al}_{0.015}\text{Zn}_{0.985}\text{O}$ and $\text{Al}_{0.03}\text{Zn}_{0.97}\text{O}$ thin films and also it can be seen that transmission value decreased from >95% to >80% with an increase in the Al doping concentration. This may be because of decrease in the crystallinity thin film, as observed in XRD. The band gap of $\text{Al}_x\text{Zn}_{1-x}\text{O}$ thin films is displayed in the Tauc's plot (figure 3.16 (b)). The band gap is determined by the extrapolation of linear portion of $(\alpha h\nu)^2$ versus $h\nu$ plots at $\alpha=0$ using the equation. Also, the linearity observed in the tauc's plot proves the direct interband transitions. Aluminum doping produces very minimal effect on bandgap, the estimated optical bandgaps are in the range of 3.29eV for all the thin films.

3.5.5 Electrical Properties

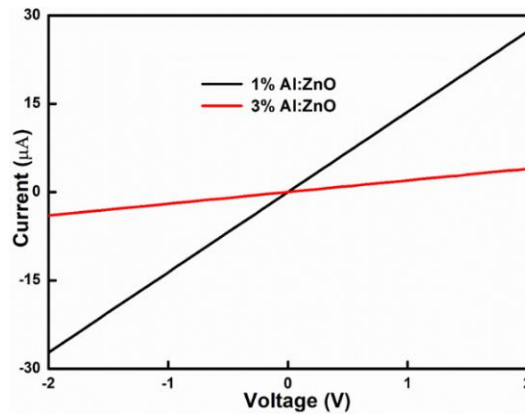


Figure 3.17: I-V characteristics of $\text{Al}_x\text{Zn}_{1-x}\text{O}$ thin films

Table 3.11: Electrical resistivity and band gap of $\text{Al}_x\text{Zn}_{1-x}\text{O}$ thin films

Sample name	Resistivity (Ωm)	Band gap (eV)
$\text{Al}_{0.005}\text{Zn}_{0.995}\text{O}$	12.24	3.28
$\text{Al}_{0.01}\text{Zn}_{0.99}\text{O}$	6.18	3.28
$\text{Al}_{0.015}\text{Zn}_{0.985}$	4.212	3.27
$\text{Al}_{0.03}\text{Zn}_{0.97}\text{O}$	0.5178	3.27
$\text{Al}_{0.05}\text{Zn}_{0.95}\text{O}$	1.572	3.26

The n-type of electrical conductivity of as deposited thin films were identified by using hot probe measurement. The linearity in the current-voltage measurements (figure 3.17) proves the ohmic contact between deposited aluminum contact and thin

films. The variation in electrical resistivity with respect to Al doping are listed in the table 3.11. At lower doping concentration decrease in resistivity was observed. This may be because of substitution of Al^{3+} ions in place of Zn^{2+} ions, which donates an electron to conduction band. Increase in resistivity at higher doping concentration may be because of decrease in crystallinity, as observed from XRD. ZnO thin films with 3 at. % Al doping were showing good conductivity with good transmission in UV-VIS range. So, these samples can be used for transparent conductor application.

CHAPTER 4

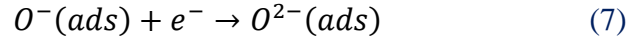
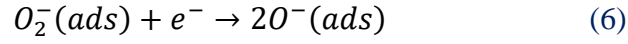
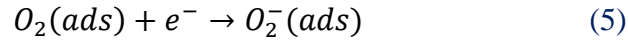
GAS SENSING PROPERTIES OF DOPED ZnO THIN FILMS

4.1 INTRODUCTION

Every activity in daily life results in the release of organic species to the atmosphere. Some examples of specific sources and processes that commonly emit high levels of volatile organic compounds (VOCs) include vent gas, water separation techniques, industrial waste water, petroleum refining, natural gas processing, petrochemical processes, and paints. Consequently, the increased emissions of volatile organic compounds (VOCs) and their resulting impact on the air quality are now considered as a major environmental concern. VOCs like Acetone and Ethanol are colourless highly inflammable liquids which can evaporate easily. Methanol is another example for VOC which is highly toxic. Literature survey reveals that the ZnO based thin film is a promising candidate for detection of VOCs (Zhang et al. 2009),(Öztürk et al. 2016). Among different ways, doping with metal ions is the easiest way to improve the sensitivity of ZnO based sensors. Till the date, very limited attempts have been carried out to improve sensitivity of ZnO thin film sensor with Cd, In and Al as dopant using spray pyrolysis technique. The present work deals with the preparation of ZnO doped with Cd [$\text{Cd}_x\text{Zn}_{1-x}\text{O}$ ($0 \leq x \leq 0.20$)], In [$\text{In}_x\text{Zn}_{1-x}\text{O}$ ($0 \leq x \leq 0.05$)] and Al [$\text{Al}_x\text{Zn}_{1-x}\text{O}$ ($0 \leq x \leq 0.05$)] thin film using spray pyrolysis technique and characterization to check gas sensing properties.

4.2 GAS SENSING STUDIES OF CADMIUM DOPED ZnO THIN FILMS

Mechanism for n-type semiconductor sensor is explained in the literature (Pati et al. 2015), (Shinde et al. 2012), (Xing et al. 2015). When sensor element is heated at an optimal temperature, various forms of oxygen from the atmosphere are adsorbed on the surface. The adsorbed oxygen traps the electron from the conduction band of metal oxide and causes the increase in resistance. Oxygen adsorption attains saturation and sensor element attains stable resistance in air. The mechanism can be given by following equation (Wang et al. 2008):



When the metal oxide sensor surface is exposed to different gas vapours, it react with the adsorbed oxygen species and then releases back the trapped electron to metal oxide thereby decreasing the sensor resistance (Pati et al. 2015).

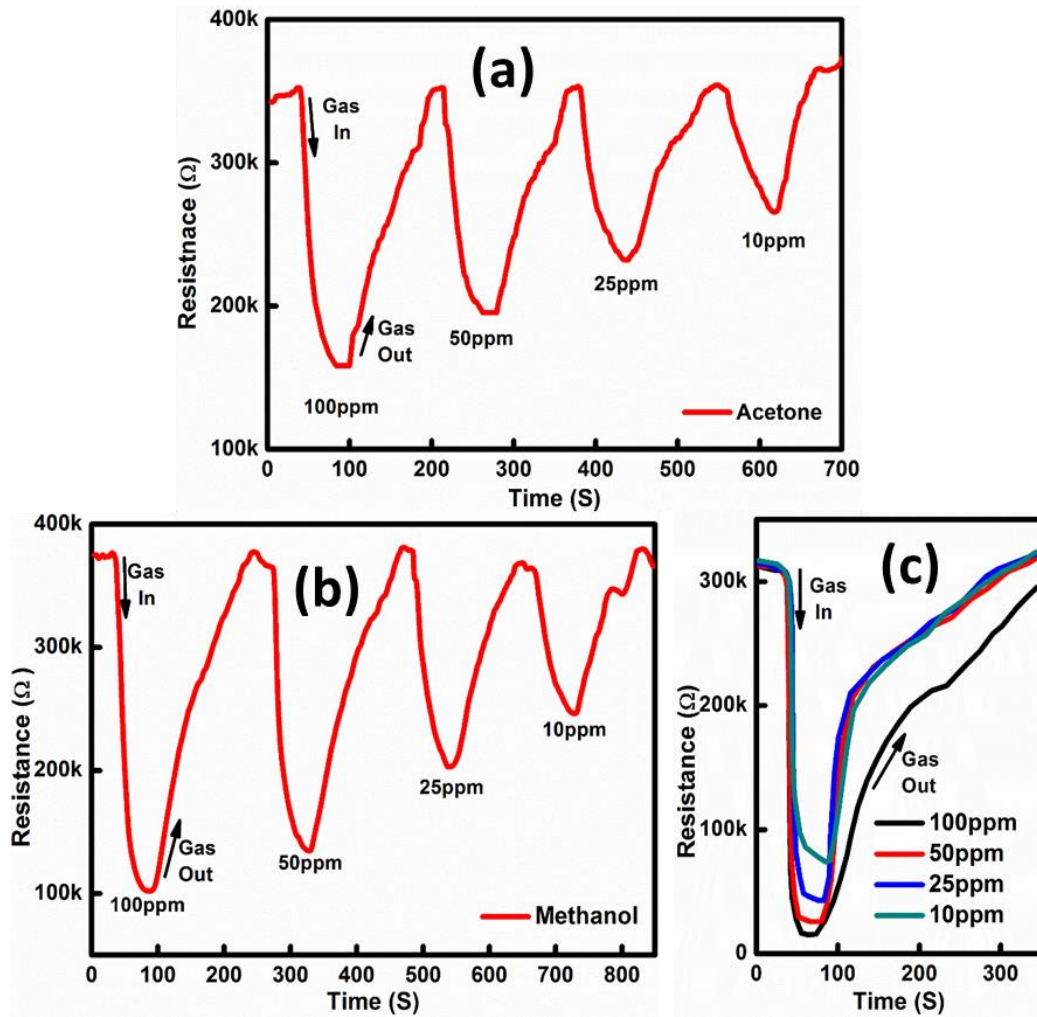


Figure 4.1: Resistance transient response of Cd_{0.1}Zn_{0.9}O thin film (a) Acetone, (b) Methanol and (c) Ethanol

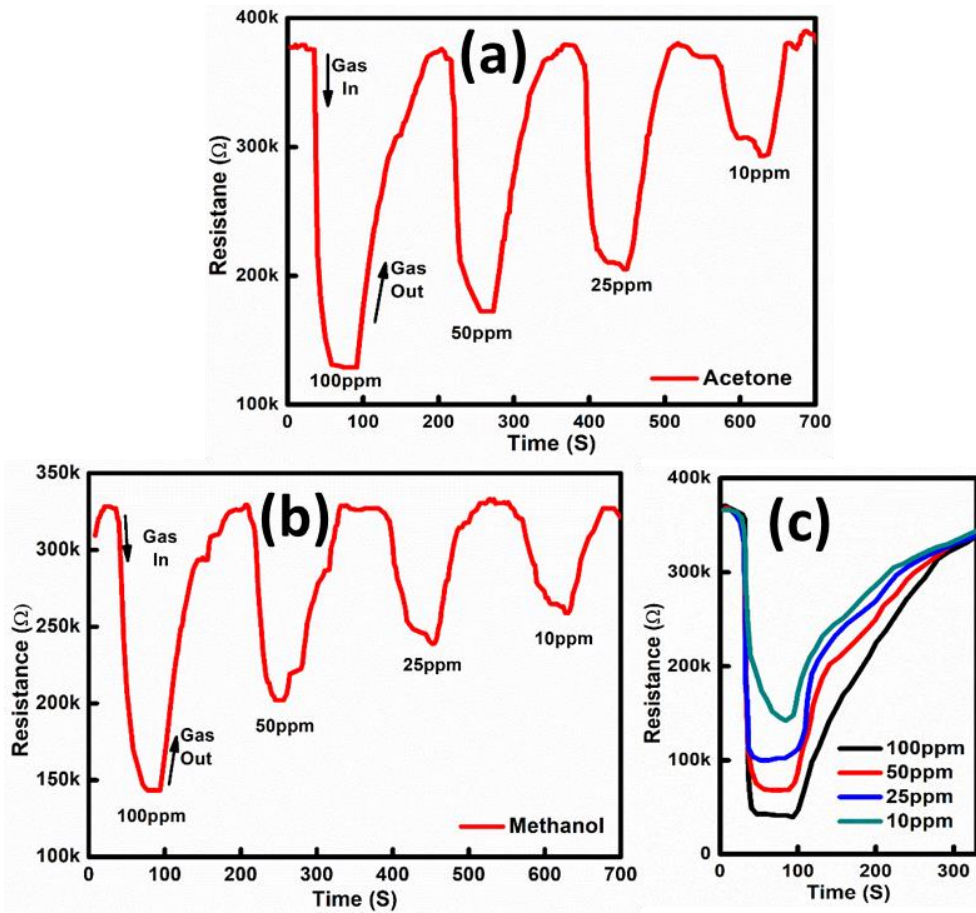


Figure 4.2: Resistance transient response of $\text{Cd}_{0.2}\text{Zn}_{0.8}\text{O}$ thin film (a) Acetone, (b) Methanol and (c) Ethanol

The gas sensing characteristics of as deposited $\text{Cd}_x\text{Zn}_{1-x}\text{O}$ films were investigated in presence of various gas vapours, such as acetone, ethanol and methanol at an optimised temperature of 350°C . Before starting the sensing experiment, the sensing element are kept at 350°C for 4 to 6 hours to establish stable base line resistance. The real-time resistance transient curves of $\text{Cd}_{0.10}\text{Zn}_{0.90}\text{O}$ and $\text{Cd}_{0.20}\text{Zn}_{0.80}\text{O}$ thin films upon exposure to different gas vapours at different concentrations are demonstrated in figure 4.1 and figure 4.2 respectively.

Decrease in the resistance of sensor element confirms that the $\text{Cd}_x\text{Zn}_{1-x}\text{O}$ based sensors are n-type semiconductor gas sensor. It can be observed from the above result that the $\text{Cd}_x\text{Zn}_{1-x}\text{O}$ thin film sensors show maximum resistance variation for ethanol vapours. So the experiment is carried out for the lower concentration of ethanol. The resistance transients of $\text{Cd}_{0.1}\text{Zn}_{0.9}\text{O}$ and $\text{Cd}_{0.2}\text{Zn}_{0.8}\text{O}$ thin films for lower

concentration of ethanol are shown in the figure 4.3 (a) and (b) respectively. Further, to check the reproducibility, the Cd_{0.1}Zn_{0.90}O sensors are exposed to four successive pulses of 5ppm of ethanol, which is shown in figure 4.3 (c). This shows that results are reproducible with a very minimal base line drift.

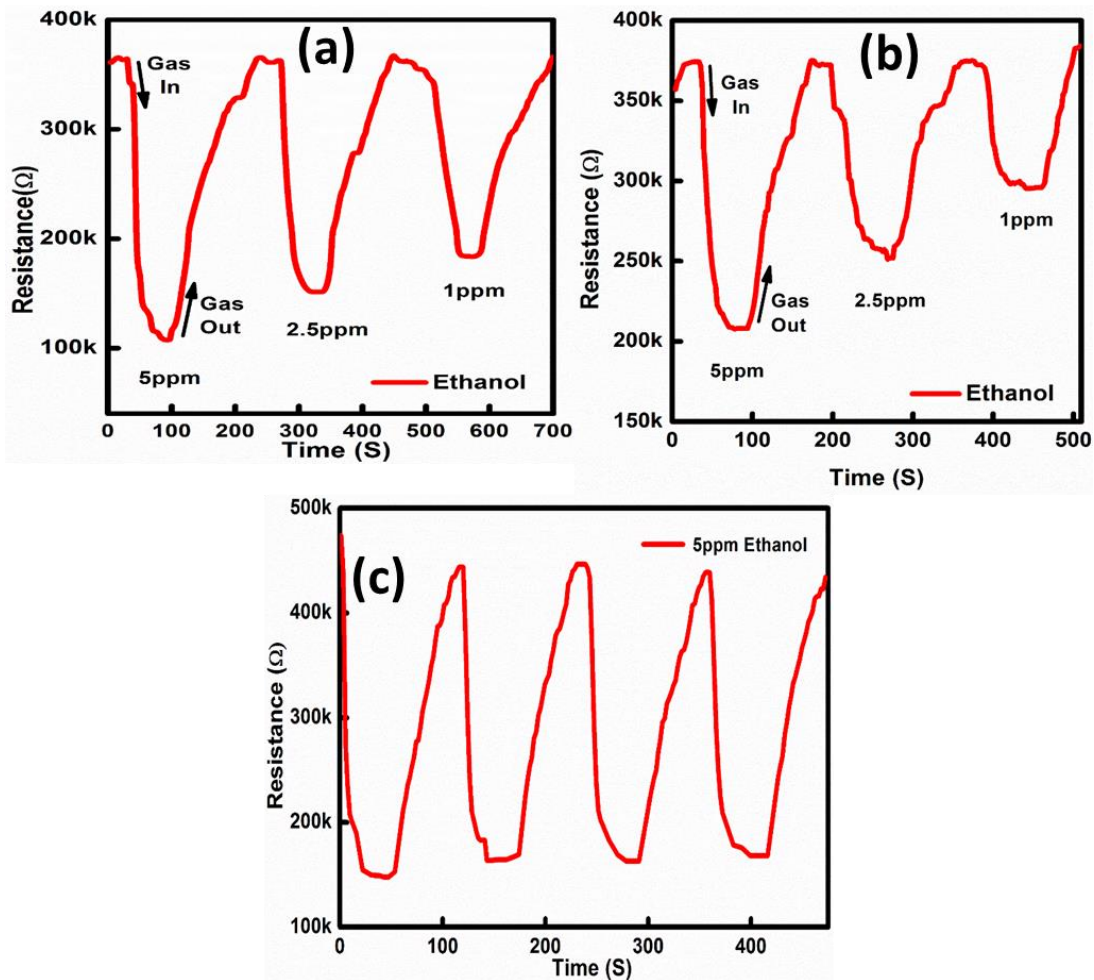


Figure 4.3: Resistance transient response for 5ppm, 2.5ppm and 1ppm of ethanol for (a) Cd_{0.10}Zn_{0.90}O and (b) Cd_{0.20}Zn_{0.80}O thin film and (c) reproducibility for 5ppm of ethanol for Cd_{0.10}Zn_{0.90}O thin film

Sensitivity of sensor can be defined as the ratio of the resistance change in presence of gas vapour to the resistance in air. This can be calculated from the formula

$$S = \left(\frac{R_a - R_g}{R_a} \right) \times 100 \quad (8)$$

where R_a = Resistance in air, R_g = resistance in gas atmosphere. The response curves drawn for Cd_{0.1}Zn_{0.9}O and Cd_{0.2}Zn_{0.8}O film for different gas vapour by varying concentration are shown in figure 4.4 and figure 4.5 respectively. The response

percentage of $Cd_xZn_{1-x}O$ thin film gas sensors for different concentration of acetone, methanol and ethanol is shown in the figure 4.6. It can be concluded from the above result that the $Cd_{0.1}Zn_{0.9}O$ thin film sensors are highly sensitive for ethanol vapours. This exhibits the sensitivity of 71%, 58% and 50% for 5, 2.5 and 1 ppm respectively.

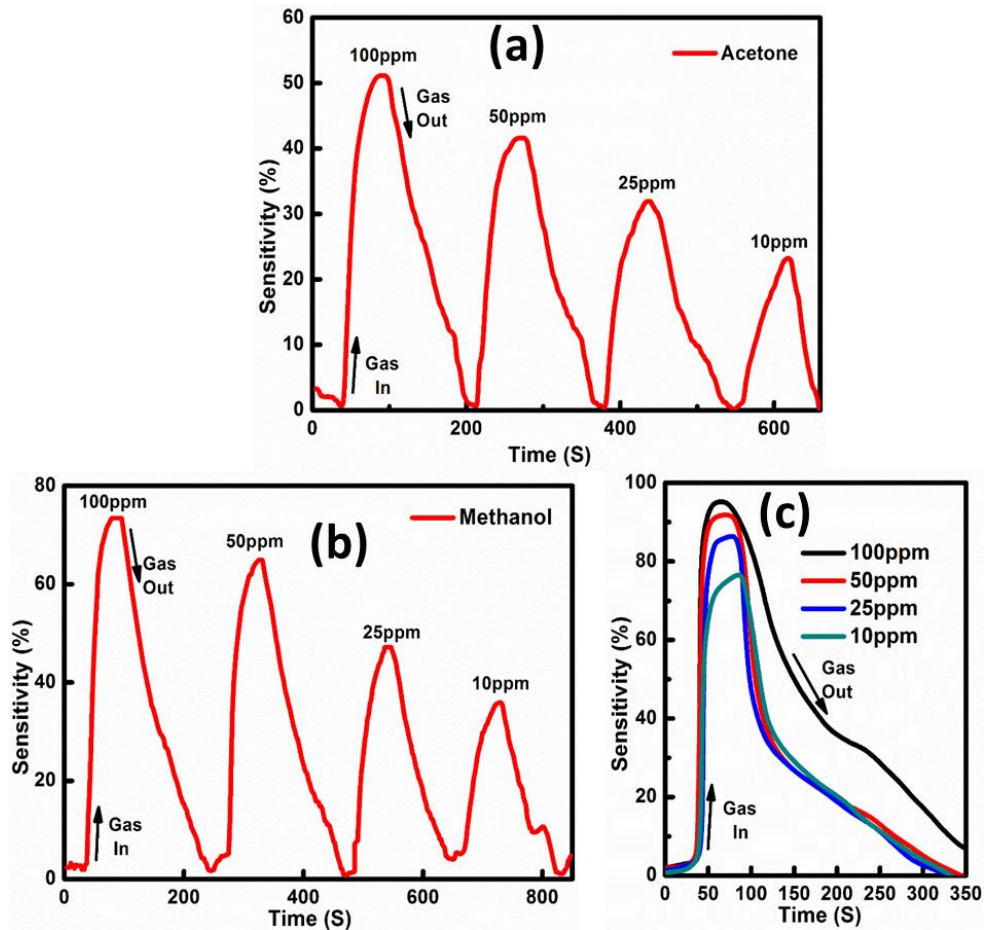
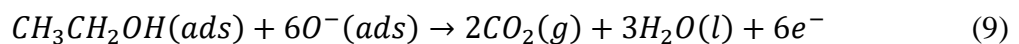


Figure 4.4: Response of $Cd_{0.1}Zn_{0.9}O$ thin film (a) Acetone, (b) Methanol and (c) Ethanol

Many reports suggest that ZnO based sensors are highly sensitive to ethanol (Wang et al. n.d.), (Hemmati et al. 2011), (Qin et al. 2014a) . Ethanol may be highly reactive on $Cd_xZn_{1-x}O$ thin film surface. The possible reaction mechanism involved in ethanol sensing is as shown below (Wang et al. n.d.):



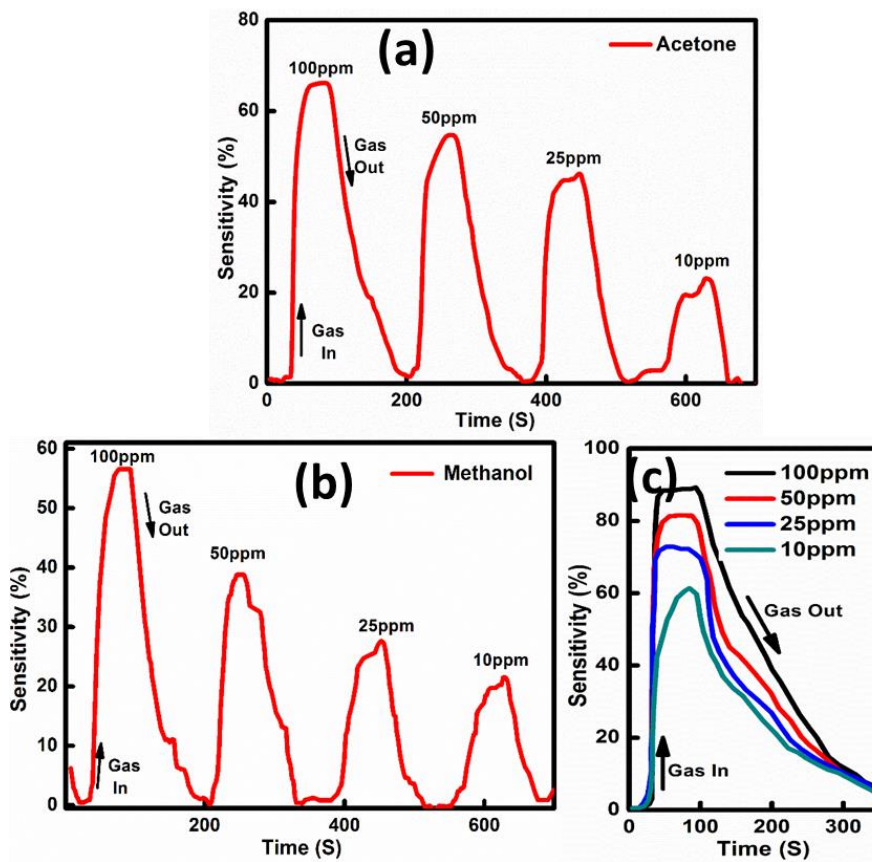


Figure 4.5: Response of $Cd_{0.2}Zn_{0.8}O$ thin film (a) Acetone, (b) Methanol and (c) Ethanol

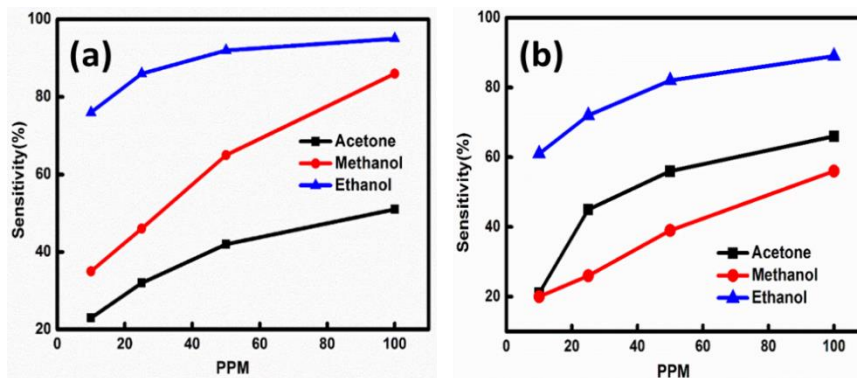


Figure 4.6: Comparison of sensitivity for different ppm of vapours (a) $Cd_{0.1}Zn_{0.9}O$, (b) $Cd_{0.2}Zn_{0.8}O$

The time taken for the sensor to attain 90% of the maximum change in resistance upon exposure to the gas is called response time. The time taken by the sensor to get back to 90% of the original resistance is the recovery time (Shinde et al. 2012). The response and recovery time of $Cd_{0.1}Zn_{0.9}O$ for lower concentration like

5ppm, 2.5ppm and 1ppm of ethanol are shown in the figure 4.7. The response time and recovery time of $Cd_{0.1}Zn_{0.9}O$ films for different gases are displayed in table 4.1. The response time for all the gases increase with decrease in concentration. At higher concentrations more gas molecules may interact with sensor surface to bring down the response time. Recovery time are found to increase with an increase in gas vapour concentration. This is because of larger concentration of adsorbed gas species on the sensor surface.

Table 4.1: Comparison of sensitivity of $Cd_{0.2}Zn_{0.8}O$ and $Cd_{0.1}Zn_{0.9}O$ thin films

Concentration (ppm)	$Cd_{0.2}Zn_{0.8}O$			$Cd_{0.1}Zn_{0.9}O$		
	Acetone	Methanol	Ethanol	Acetone	Methanol	Ethanol
100ppm	65	57	89	55	72	95
50ppm	55	39	86	42	61	91
25ppm	44	30	81	34	43	85
10ppm	20	20	71	16	30	75

Table 4.2: Response and recovery time of $Cd_{0.1}Zn_{0.9}O$ thin film for ethanol

Concentration (ppm)	Response time (Sec)			Recovery time (Sec)		
	Acetone	Methanol	Ethanol	Acetone	Methanol	Ethanol
100	31	30	14	97	129	318
50	32	35	16	92	120	226
25	38	43	17	89	94	216
10	49	49	20	33	76	210

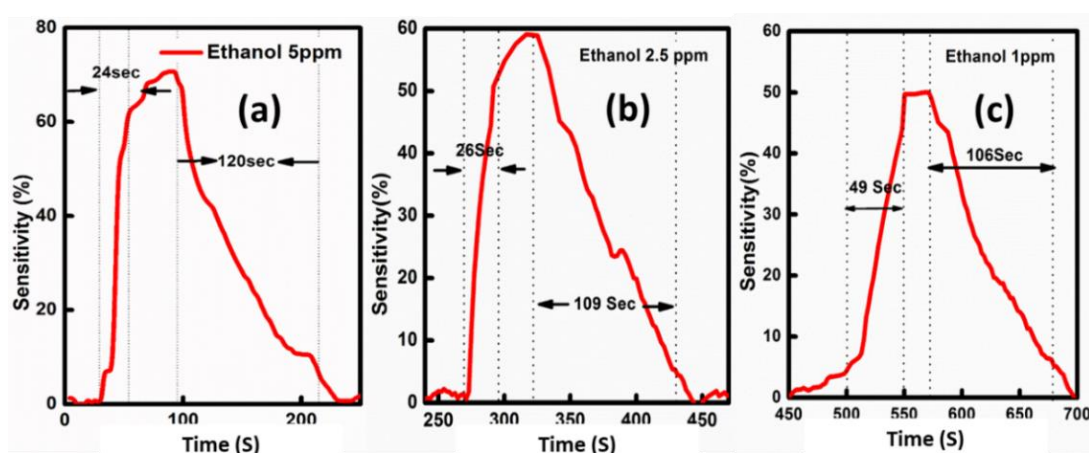


Figure 4.7: Response and recovery time of $Cd_{0.1}Zn_{0.9}O$ thin film for (a)5ppm, (b)2.5ppm and (c) 1ppm of ethanol

4.3 GAS SENSING STUDIES OF INDIUM DOPED ZnO THIN FILMS

The sensing characteristics of $\text{In}_x\text{Zn}_{1-x}\text{O}$ thin films were investigated for volatile organic compound vapours like acetone, ethanol and methanol at an optimised sensing temperature of 350°C . All the $\text{In}_x\text{Zn}_{1-x}\text{O}$ thin films exhibited n-type metal oxide sensor behaviour, in which base line resistance of sensing element decreases with exposure to different reducing vapours, so it follows same mechanism as explained in the previous section 2.3. It is well known that the gas sensing mechanism in the oxide based materials is surface controlled, here the grain size and oxygen adsorption also play an important role. It can be observed from the XRD and FE-SEM images that with an increase in indium concentration grain size decreases and effective surface area increases. The more number of grain boundaries and larger surface area offers more adsorption–desorption sites and thus enhances sensitivity. In indium doped ZnO thin films, the In^{3+} facilitates adsorption of more number of oxygen species.

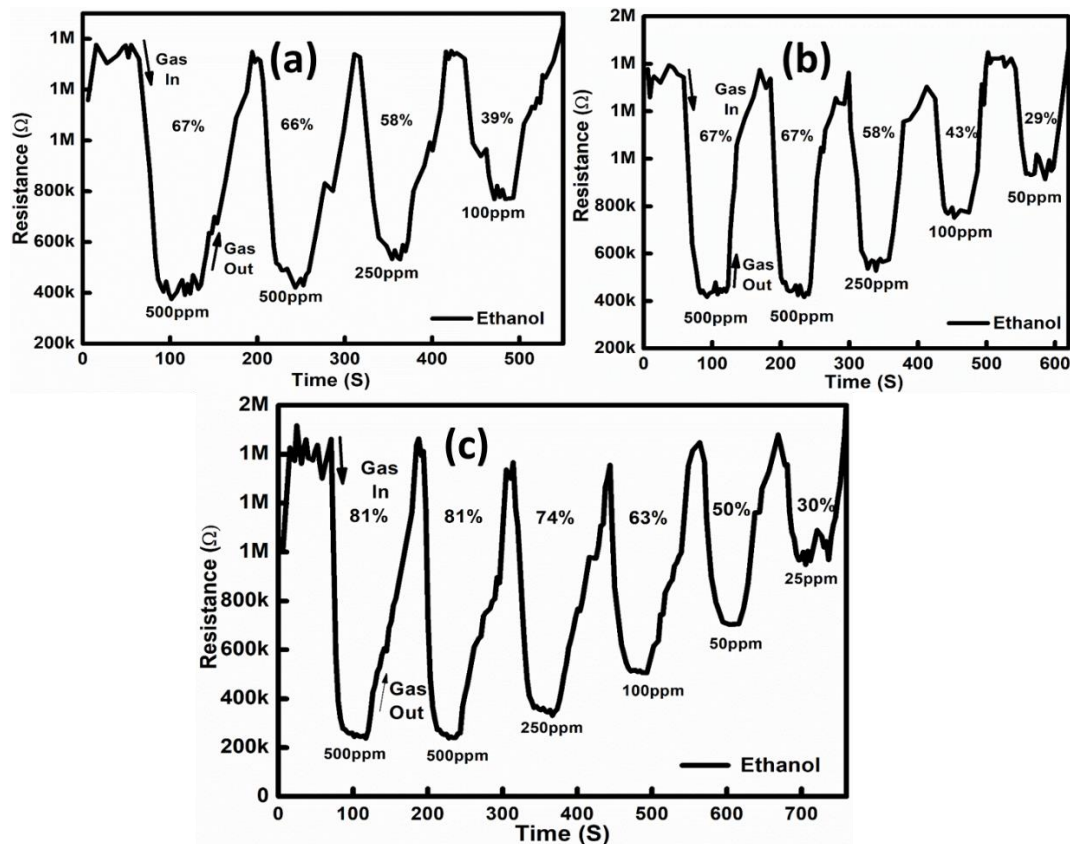


Figure 4.8: Resistance variation curves of (a) $\text{In}_{0.01}\text{Zn}_{0.99}\text{O}$, (b) $\text{In}_{0.05}\text{Zn}_{0.95}\text{O}$, (c) $\text{In}_{0.03}\text{Zn}_{0.97}\text{O}$

The figure 4.8 (a), (b) and (c) shows the resistance transient response plot recorded for 1 at.%, 3 at.% and 5 at.% In doped ZnO thin films towards different concentration of ethanol vapours respectively. It can be observed from the graph that the 3 at.% In doping is the optimal doping concentration with maximum resistance variation for ethanol vapours as compared to 1 at. % and 5 at. % In doped ZnO thin films. 3 at.% In doped ZnO sensor can detect up to 25ppm of ethanol, it can be used as effective ethanol sensor. 3 at.% In doped ZnO thin films are also subjected to detect acetone and methanol. Resistance transient curves for acetone and methanol is shown in figure 4.9 (a) and (b), these thin films were capable of detecting 250ppm of acetone and methanol respectively. So it can be concluded that $\text{In}_x\text{Zn}_{1-x}\text{O}$ thin films were selective toward ethanol. Further, to check the consistency of In doped ZnO sensor, the 3 at. % In doped ZnO thin film is exposed to four successive pulses of 250ppm ethanol, figure 4.9 (c) shows the resistance variation for 250ppm ethanol. As observed from figure 4.9 (c) the sensor element exhibit good reproducibility with very less baseline shift.

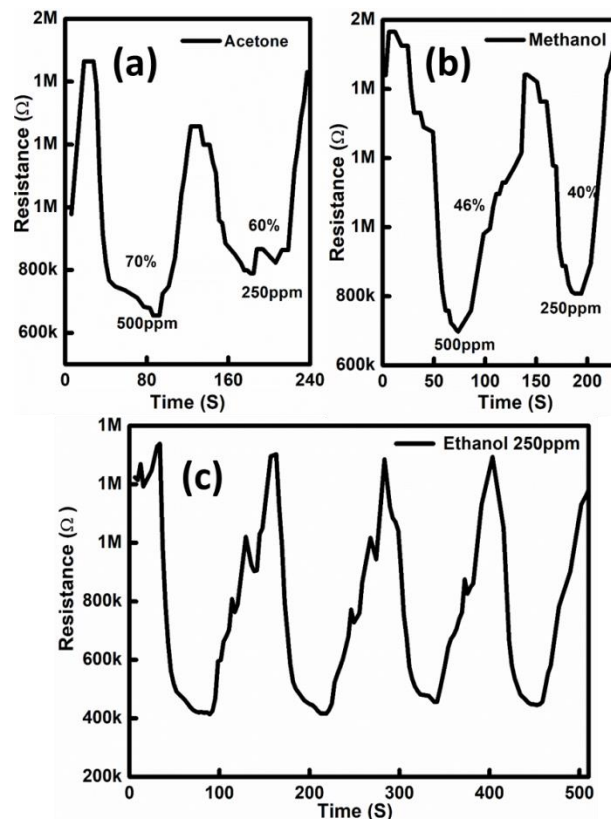


Figure 4.9: Resistance variation curves of $\text{In}_{0.03}\text{Zn}_{0.97}\text{O}$ thin films for (a) Acetone, (b) Methanol and (c) reproducibility of 250ppm of ethanol

The response curves drawn for $\text{In}_{0.03}\text{Zn}_{0.97}\text{O}$ thin film for ethanol vapour by varying concentration of ethanol are shown in figure 4.10 (a), response percentage decrease with decrease in ethanol concentration. The response percentage of In doped ZnO thin film gas sensors for 250ppm of acetone, methanol and ethanol is compared in the figure 4.10 (b). It can be concluded from the above result that the $\text{In}_{0.03}\text{Zn}_{0.97}\text{O}$ thin film sensors are highly sensitive for ethanol vapours.

The response and recovery time of $\text{In}_{0.03}\text{Zn}_{0.97}\text{O}$ for 250ppm ethanol is shown in the figure 4.11. The response time and recovery time of $\text{In}_{0.03}\text{Zn}_{0.97}\text{O}$ thin films for different gases are displayed in table 4.2.

Table 4.3: Comparison of sensitivity of $\text{In}_x\text{Zn}_{1-x}\text{O}$ thin films

Concentration (ppm)	Sensitivity towards ethanol (%)		
	$\text{In}_{0.01}\text{Zn}_{0.99}\text{O}$	$\text{In}_{0.03}\text{Zn}_{0.97}\text{O}$	$\text{In}_{0.05}\text{Zn}_{0.95}\text{O}$
500	67	81	67
250	58	74	58
100	39	63	43
50	-	50	29

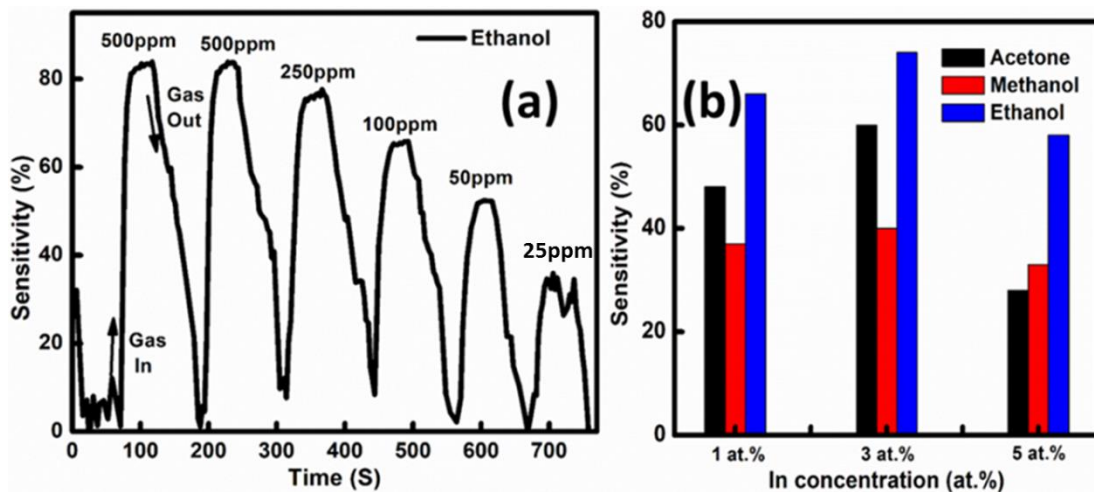


Figure 4.10: (a) Sensitivity curve for $\text{In}_{0.03}\text{Zn}_{0.97}\text{O}$ thin films, (b) Comparison of sensitivity of 250 ppm of Acetone, Ethanol and Methanol

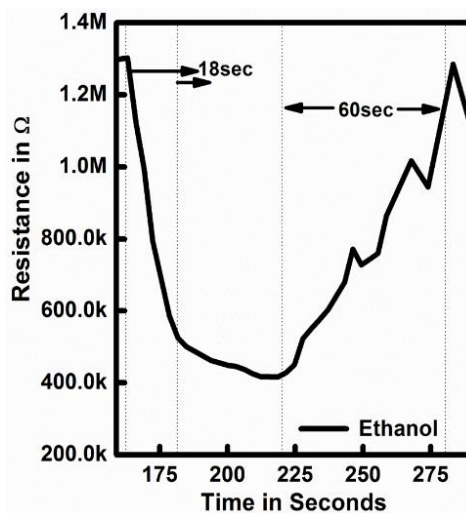


Figure 4.11: Response and recovery time of $\text{In}_{0.03}\text{Zn}_{0.97}\text{O}$ thin film for 250ppm of ethanol

Table 4.4: Response and recovery time of $\text{In}_x\text{Zn}_{1-x}\text{O}$ thin film for ethanol

Ethanol concentration (ppm)	Response time (Sec)	Recovery time (Sec)
500	22	69
250	18	60
100	17	55
50	16	40
25	12	17

4.4 GAS SENSING STUDIES OF ALUMINIUM DOPED ZnO THIN FILMS

The sensing characteristics of $\text{Al}_x\text{Zn}_{1-x}\text{O}$ thin films were investigated for volatile organic compound vapours like acetone, ethanol and methanol at an optimised sensing temperature of 350°C . Prior to sensing experiment, all samples were kept at optimised temperature for 4 hours to attain stable baseline resistance. Measurements were not acquired for pure ZnO thin films because of its highly resistive nature. $\text{Al}_x\text{Zn}_{1-x}\text{O}$ thin films exhibited n-type metal oxide sensor behaviour, in which base line resistance of sensing element decreases with exposure to different reducing vapours.

The figure 4.13 shows variation of resistance for $\text{Al}_{0.03}\text{Zn}_{0.97}\text{O}$ thin films for different concentration of ethanol, acetone and methanol. $\text{Al}_x\text{Zn}_{1-x}\text{O}$ samples were

proved to be ethanol sensitive because it showed less resistance variation towards acetone and methanol as compared to ethanol. Figure 4.12 (a) and (b) shows resistance transient variation for multiple trials of different concentration of acetone and ethanol, it can be observed from same figure that results were reproducible with very minimal variation in baseline shift and sensitivity. The sensitivity curve for different concentration of ethanol and acetone are given in the figure 4.13. Sensitivity of ethanol, acetone and methanol are also compared in the table 4.3. $Al_xZn_{1-x}O$ samples were highly sensitive and selective towards ethanol, so it can be used for affective ethanol sensor application.

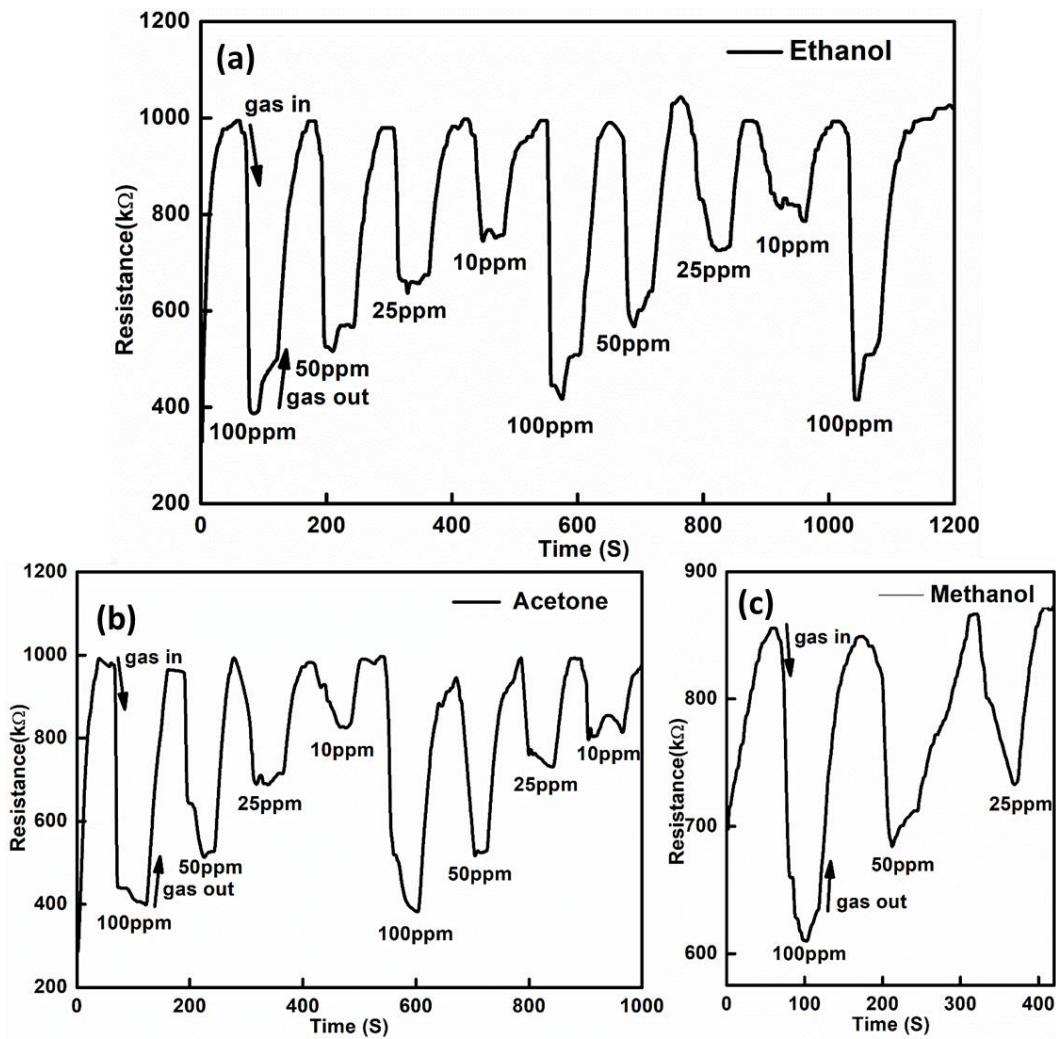


Figure 4.12: Resistance transient of $Al_{0.03}Zn_{0.97}O$ thin films for (a) ethanol, (b) Acetone and (c) Methanol

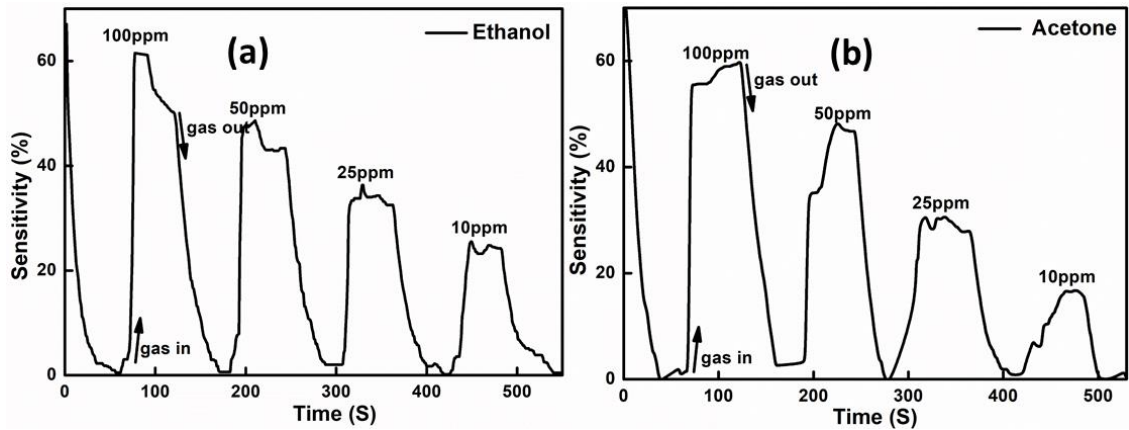


Figure 4.13: Sensitivity curve for $\text{Al}_{0.03}\text{Zn}_{0.97}\text{O}$ thin films (a) Ethanol, (b) Acetone

Table 4.5: Comparison of sensitivity of $\text{Al}_x\text{Zn}_{1-x}\text{O}$ thin films

Concentration (ppm)	Sensitivity (%)		
	Ethanol	Acetone	Methanol
100	61	58	28
50	48	47	18
25	34	29	14
10	24	16	--

The response and recovery time of $\text{Al}_x\text{Zn}_{1-x}\text{O}$ thin film for different gases is shown in table 4.4. It can be observed that response time decreases with increase in gas concentration and recovery time decreases with decrease in ethanol concentration.

Table 4.6: Response and recovery time of $\text{Al}_x\text{Zn}_{1-x}\text{O}$ thin film for ethanol and acetone

Concentration (ppm)	Response time (Sec)		Recovery time (Sec)	
	Ethanol	Acetone	Ethanol	Acetone
100	3	4	28	36
50	7	21	24	22
25	9	30	20	20
10	17	43	15	13

CHAPTER 5

SYNTHESIS, CHARACTERIZATION AND GAS SENSING PROPERTIES OF MIXED METAL OXIDE THIN FILMS

5.1 INTRODUCTION

Volatile Organic Compounds (VOCs) are easily evaporable and highly flammable organic compounds, which are major source of air pollution in outdoor and indoor atmosphere nowadays. Outdoor VOCs may originate from human activities such as petroleum refining, natural gas processing, paint industries, coal and biomass combustion (Bharath et al. 2017) . The most common indoor VOC sources include combustion processes like smoking, cooking and usage of air fresheners, mothballs, cleaners, personal care products (Bari et al. 2015). VOCs are most common solvent and reagents in research and clinical laboratories. Most of the VOCs are toxic in nature and exposure to these may result in potential chronic and acute health outcomes (Bari et al. 2015). Enormous research work is going on to identify and regulate release of VOCs into atmosphere to maintain indoor and outdoor air quality. To serve this purpose, metal oxide semiconductor gas sensors are best suitable candidates with many advantages such as low cost, portability, ease of operation and production and it can work at normal atmosphere. In various literature, different metal oxides like SnO₂(Zhang et al. 2018), ZnO(Bharath et al. 2017), TiO₂(Li et al. 2017), WO₃(Zhang and Xie 2015), NiO(Wang et al. 2015), CuO(Yu et al. 2012) based materials were extensively explored for gas sensor application. Sensing properties of metal oxide can be improved by doping (Bharath et al. 2017), decoration with other catalytic material (Zhang et al. 2018) and by using composite material (Yu et al. 2012). ZnO, CuO and Sn-O based multicomponent gas sensors are gaining significant attention nowadays because of their improved sensitivity and selectivity. Recently, CuO-sensitised ZnO and SnO₂ nanostructures were developed and studied for efficient H₂S and isopropanol sensing properties respectively (Vuong et al. 2016) (Zhang et al. 2018), in both the reports, increase in sensitivity was attributed to catalytic behaviour of CuO. Reduced graphene oxide decorated with CuO was developed and studied for ammonia and formaldehyde sensing application (Zhang et al. 2017), report suggests that increase in sensitivity is

because of heterojunction created at interface of reduced graphene oxide and CuO. Ghosh et al and Yu et al prepared CuO-ZnO composite thin film for carbon monoxide and ethanol sensing application respectively (Ghosh et al. 2017)(Yu et al. 2012). Most of the literature concentrates on H₂S sensing properties of CuO based composite system (Katoch et al. 2015)(Park et al. 2016), and it also reveals that very few studies were carried out using ZnO-CuO composite material for VOC sensor application. Recently, amorphous multicomponent ZnO based oxides such as Zn-Sn-O systems also have attracted much attention as transparent conducting oxide (TCO) materials. Since amorphous TCO films have smoother surface morphology and cleaner etched profiles compared with crystalline TCO films, can be advantageous in the field of organic light emitting diodes and thin film transistor-liquid crystal display. Also, ZnO and SnO based metal oxides are well known gas sensor materials. So, present study concentrates on preparation of CuO-ZnO and Sn-Zn-Oxide thin film using industrially applicable spray pyrolysis technique and on the structural, morphological, electrical analysis of deposited thin film for most commonly used VOC such as acetone, methanol and ethanol sensing application.

5.2 SYNTHESIS AND CHARACTERIZATION OF Cu_{1-x}Zn_xO COMPOSITE THIN FILMS FOR SENSOR APPLICATION

5.2.1 Experimental details

Pure CuO and Cu_{1-x}Zn_xO composite thin films were deposited on soda lime glass substrate using spray pyrolysis technique. Aqueous solution of 50mM concentration was prepared by dissolving copper (II) acetate monohydrate (Cu(OOCCH₃)₂·H₂O) and zinc acetate dihydrate (Zn(OOCCH₃)₂·2(H₂O)) in desired molar ratio. Prepared solution was atomized and sprayed using nozzle on top of preheated glass substrate. A spray rate of 2ml/min, substrate temperature of 350⁰C, substrate to nozzle distance of 30cm was maintained throughout the process and air was used as carrier gas at pressure of 2bar.

5.2.2 XRD analysis

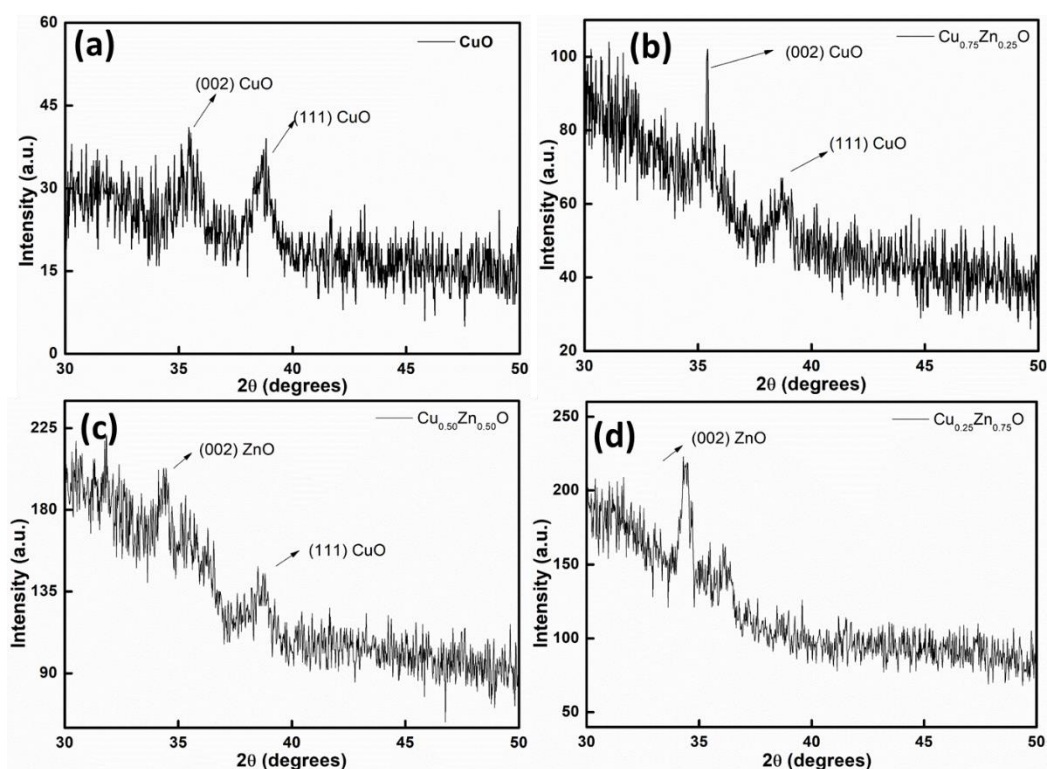


Figure 5.1: XRD patterns of $\text{Cu}_{1-x}\text{Zn}_x\text{O}$ thin films (a) CuO , (b) $\text{Cu}_{0.75}\text{Zn}_{0.25}\text{O}$ and (c) $\text{Cu}_{0.50}\text{Zn}_{0.50}\text{O}$, (d) $\text{Cu}_{0.25}\text{Zn}_{0.75}\text{O}$

Figure 5.1 shows XRD pattern of polycrystalline $\text{Cu}_{1-x}\text{Zn}_x\text{O}$ thin films. The lower intensity diffraction peaks in XRD pattern prove the poor crystallinity of as deposited $\text{Cu}_{1-x}\text{Zn}_x\text{O}$ thin films. Figure 5.1 (a) displays XRD pattern of pure copper oxide thin film with two peaks, which belongs to (111) and (002) orientation of monoclinic structured CuO (JCPDS card no. 01-080-1917), absence of peaks corresponding to Cu_2O , confirms the formation of single phased CuO . Figure 5.1 (b) shows XRD spectra of $\text{Cu}_{0.75}\text{Zn}_{0.25}\text{O}$ thin films, which also consists of two peaks corresponding to (002) and (111) peak of CuO . Figure 5.1 (c) shows the XRD spectra of $\text{Cu}_{0.50}\text{Zn}_{0.50}\text{O}$ thin film, it consists of 2 peaks which corresponds to (002) oriented hexagonal ZnO (JCPDS card no. 01-080-0075) and (111) peak of monoclinic CuO . Figure 5.1 (d) shows XRD pattern of $\text{Cu}_{0.25}\text{Zn}_{0.75}\text{O}$ thin film, it consists of (002) and (101) peaks of ZnO along with residual peak of CuO . Presence of peak corresponds to both ZnO and CuO confirms the formation of composite thin films, which consists of

separate ZnO and CuO crystallites. Ionic radius of Zn^{2+} (0.074nm) and Cu^{2+} (0.073nm) are almost same, but, in ZnO lattice Zn^{2+} ions prefers tetrahedral coordination and Cu^{2+} ions in CuO lattice prefers Jahn-Teller distorted octahedral coordination. This difference in coordination condition results in low degree solid state solubility between CuO and ZnO and leads to the formation of phase separated CuO-ZnO composite thin film.

5.2.3 Morphological and compositional analysis

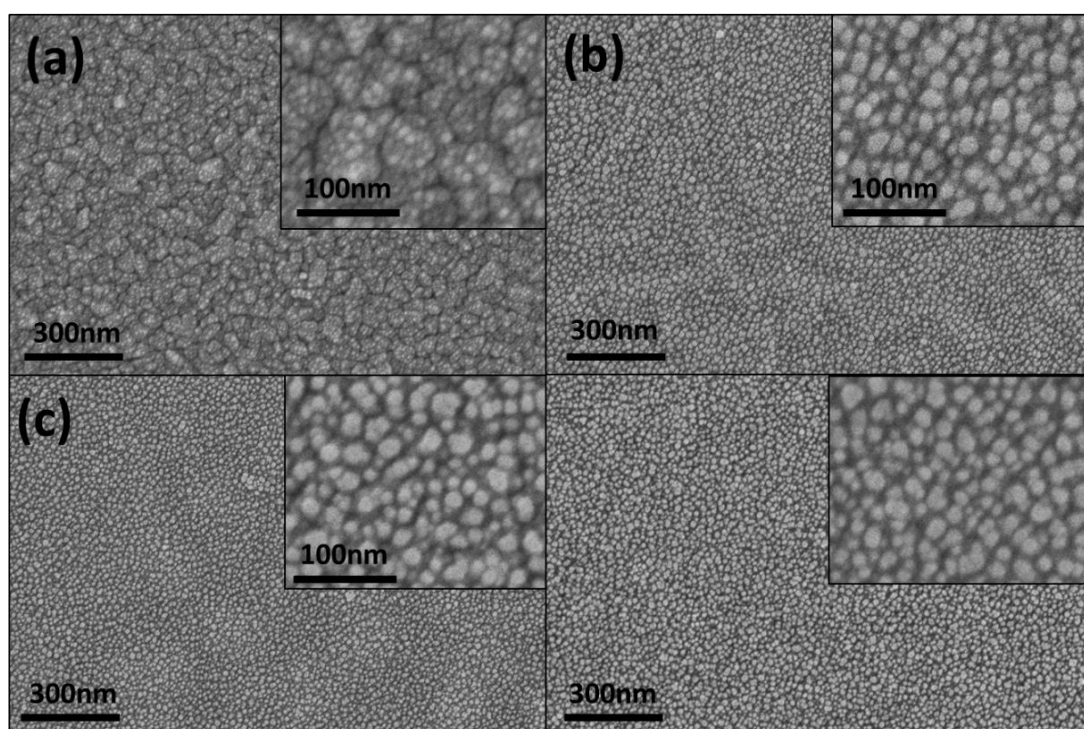


Figure 5.2: Surface morphology of $Cu_{1-x}Zn_xO$ thin films (a) CuO, (b) $Cu_{0.75}Zn_{0.25}O$ and (c) $Cu_{0.50}Zn_{0.50}O$, (d) $Cu_{0.25}Zn_{0.75}O$

Figure 5.2 (a)-(d) displays the surface morphology of $Cu_{1-x}Zn_xO$ thin films. It can be observed from low magnification images that all the thin films are continuous, without any cracks and pin holes. Densely packed nanostructured granular morphology of deposited thin film can be clearly depicted from high magnification images (inset of figure 5.2). Individual grains of CuO and ZnO cannot be differentiated in deposited composite thin films because of their very small size. During crystallization, ZnO undergo faster nucleation and growth followed by heterogeneous nucleation of CuO on

agglomerated ZnO (Ghosh et al. 2017). Compositional analysis was carried out using EDX to estimate atomic concentration of Zn and Cu in prepared thin films. EDX confirms the presence of Cu and Zn in thin films and also confirms the uniform distribution of ZnO and CuO grains throughout complete thin film. EDX spectra and composition of Zn and Cu in thin films are displayed in figure 5.3. The amount of Cu and Zn in final composite thin film was comparable with initial precursor concentration.

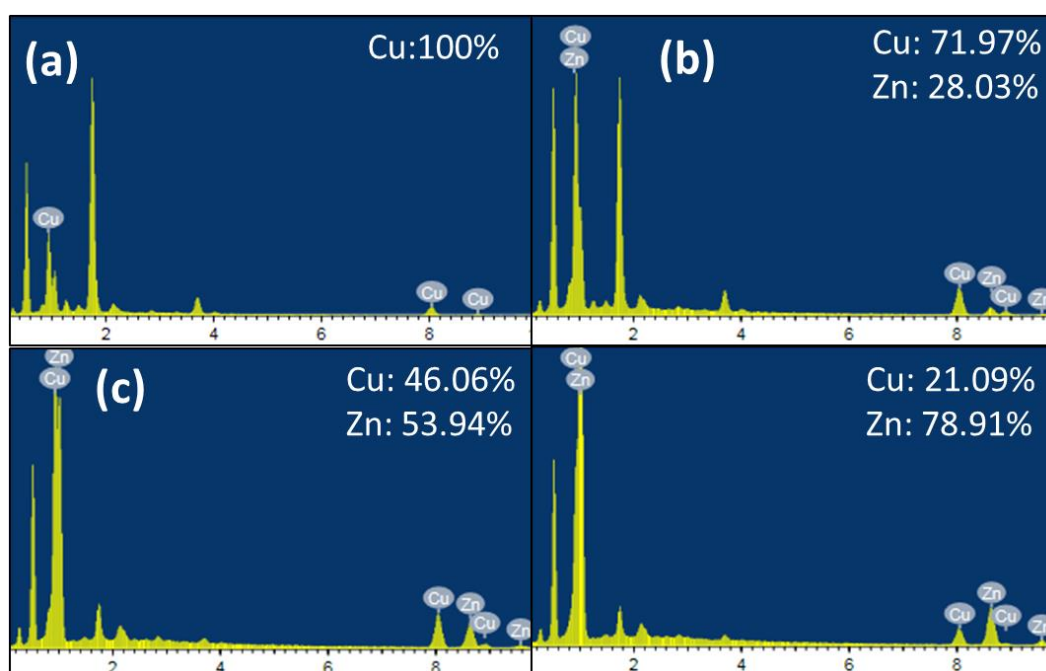


Figure 5.3: EDX spectra of $\text{Cu}_{1-x}\text{Zn}_x\text{O}$ thin films (a) CuO, (b) $\text{Cu}_{0.75}\text{Zn}_{0.25}\text{O}$ and (c) $\text{Cu}_{0.50}\text{Zn}_{0.50}\text{O}$, (d) $\text{Cu}_{0.25}\text{Zn}_{0.75}\text{O}$

5.2.4 Optical properties

The optical transmission measurements carried out on $\text{Cu}_{1-x}\text{Zn}_x\text{O}$ thin films in the wavelength range of 300 to 700nm are shown in figure 5.4 (a). It can be observed that transmission value decreased from >90% to ~50% with an increase in the copper concentration, which may be because of poor crystallinity of deposited thin films. The band gap of $\text{Cu}_{1-x}\text{Zn}_x\text{O}$ thin films is displayed in the Tauc's plot (figure 5.4 (b)). The band gap is determined by the extrapolation of linear portion of $(\alpha h\nu)^2$ versus $h\nu$ plots at $\alpha=0$ using the equation. The linearity observed in the tauc's plot proves the direct

interband transitions. The bandgap decreases from 3.29eV to ~2eV with increase in copper concentration.

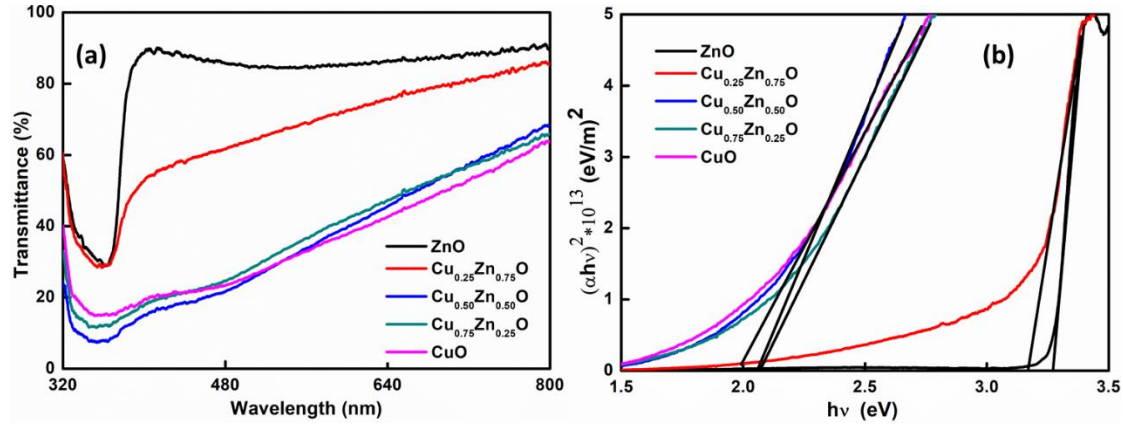


Figure 5.4: (a) Transmission spectra of Cu_{1-x}Zn_xO thin films, (b) Tauc's plot of Cu_{1-x}Zn_xO thin films

5.2.5 Electrical properties

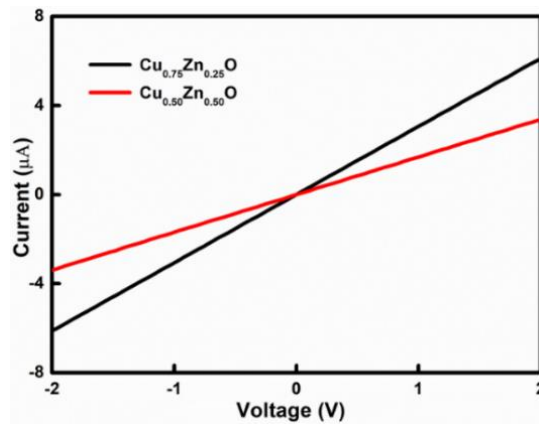


Figure 5.5: I-V characteristics of Cu_{1-x}Zn_xO thin films

The current-voltage (I-V) characteristics of as deposited Cu_{1-x}Zn_xO thin films with thermally evaporated aluminium as contacts were measured using two probe method. The curve of I-V characteristics was linear (as shown in figure 5.5), indicating the formation of ohmic contact between Cu_{1-x}Zn_xO composite thin film and aluminium contact. Estimated electrical resistivity of Cu_{1-x}Zn_xO thin film is tabulated in table 5.1. Minimum electrical resistivity was achieved for Cu_{0.75}Zn_{0.25}O composite thin film.

Table 5.1: Electrical data of $\text{Cu}_{1-x}\text{Zn}_x\text{O}$ thin films

Sample name	Resistivity (Ωm)
CuO	2.73
$\text{Cu}_{0.75}\text{Zn}_{0.25}\text{O}$	1.38
$\text{Cu}_{0.50}\text{Zn}_{0.50}\text{O}$	24.39

5.2.6 Gas sensing properties

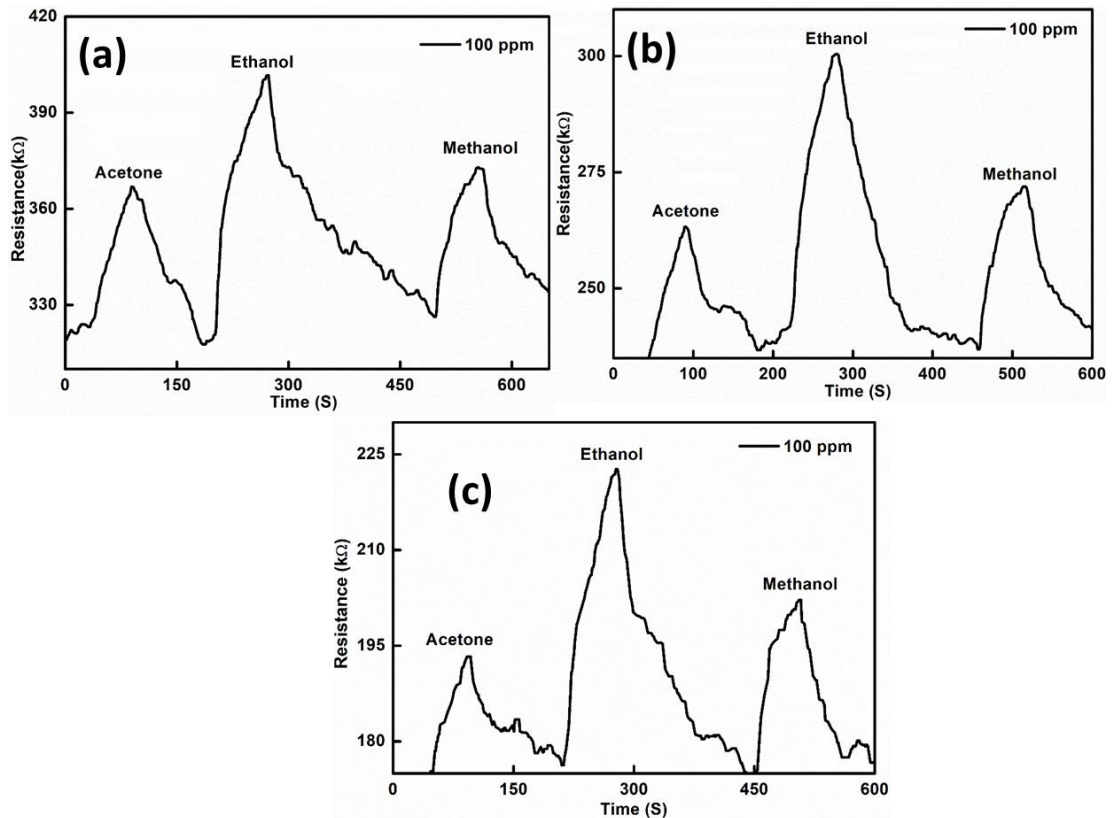


Figure 5.6: Resistance transient response of CuO for acetone, Ethanol and Methanol at different operating temperature (a) 270°C (b) 290°C (c) 310°C

The gas sensing characteristics of as deposited $\text{Cu}_x\text{Zn}_{1-x}\text{O}$ thin films were explored in presence of various gas vapours, such as acetone, ethanol and methanol. Before starting sensing experiment all the thin films were maintained at operating temperature for few hours. When p-type metal oxide sensor heated at high temperature, oxygen molecules adsorb on surface of metal oxide and ionize into O_2^- , O^- , and O^{2-} species. Ionization of oxygen traps the electron from grains and acts as hole donor. This adsorption leads to decrease in sensor resistance and attains saturation to establish stable baseline resistance. On exposure to gas atmosphere at appropriate temperature, gas molecule

will react with adsorbed ionic oxygen species and release back electron to recombine with holes, which leads to increase in sensor resistance. Resistance transient curves recorded for pure CuO thin films at different operating temperature such as 270⁰C, 290⁰C and 310⁰C are shown in figure 5.6. It can be observed that resistance increases after exposure to different test gases, which confirms the p-type conductivity of CuO samples and also explained sensing mechanism can be observed in same figure (figure 5.6). CuO thin films were capable of detecting 100 ppm of all test gases.

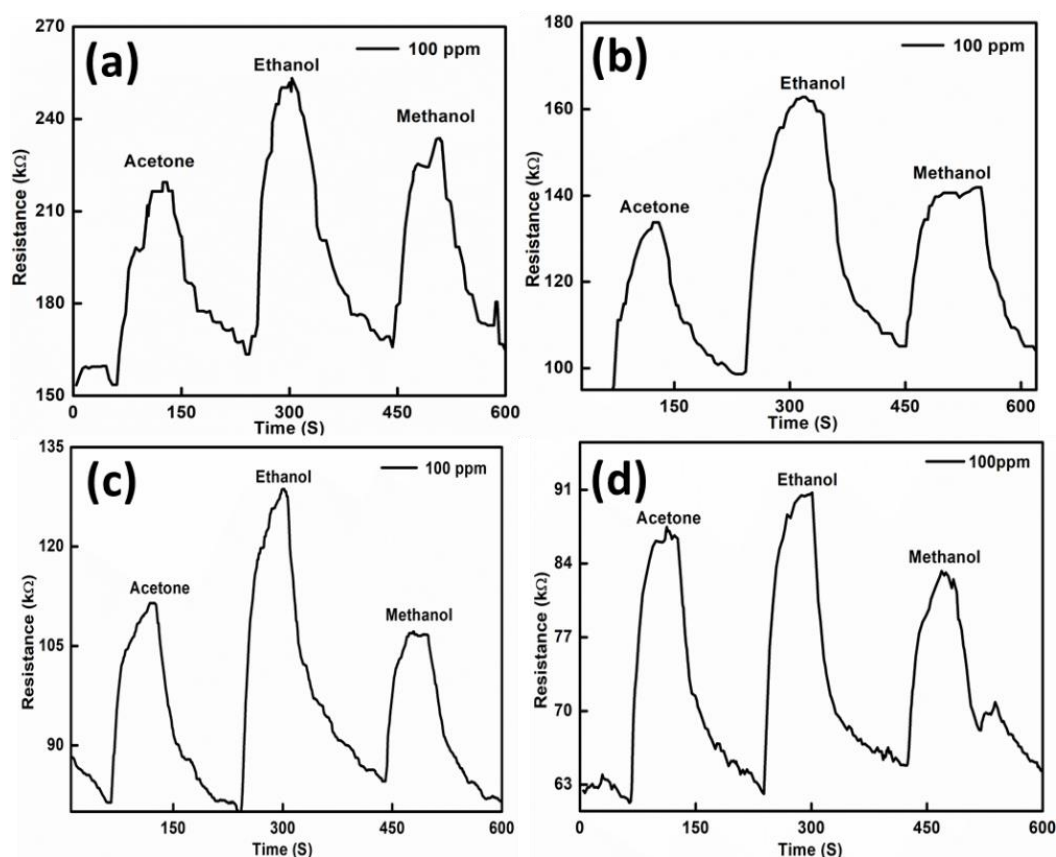


Figure 5.7: Resistance transient response of Cu_{0.50}Zn_{0.50}O composite thin films for 100ppm of acetone, ethanol and methanol at different operating temperature (a) 270⁰ C (b) 290⁰ C (c) 310⁰ C (d) 330⁰ C

Figure 5.7 (a), (b), (c) and (d) shows the temperature dependent sensing characteristics of Cu_{0.50}Zn_{0.50}O thin films at 270⁰C, 290⁰C, 310⁰C and 33⁰0C respectively, each graph consists of three peaks corresponding 100ppm of acetone, ethanol and methanol respectively. Sensing characteristics acquired at 250⁰C were noisy with very less resistance variation (not shown in figure). As the temperature increases sensing

characteristics improves and shows maximum variation at 310⁰C and again decreases. It can be observed in figure 5.7 (c) that the samples were showing large resistance variation at 310⁰C as compared to all other operating temperature with good resolution between peak corresponding to different gases. So, it can be concluded that optimal operating temperature for Cu_{0.50}Zn_{0.50}O thin film sensors is 310⁰C. Gas molecules to be sensed do not have sufficient thermal energy at lower operating temperature to react with surface adsorbed oxygen species, hence lower response at lower temperature can be expected. At optimal temperature gas molecules acquires enough thermal energy to react with adsorbed oxygen species and results in release of trapped electron (Shinde et al. 2007).

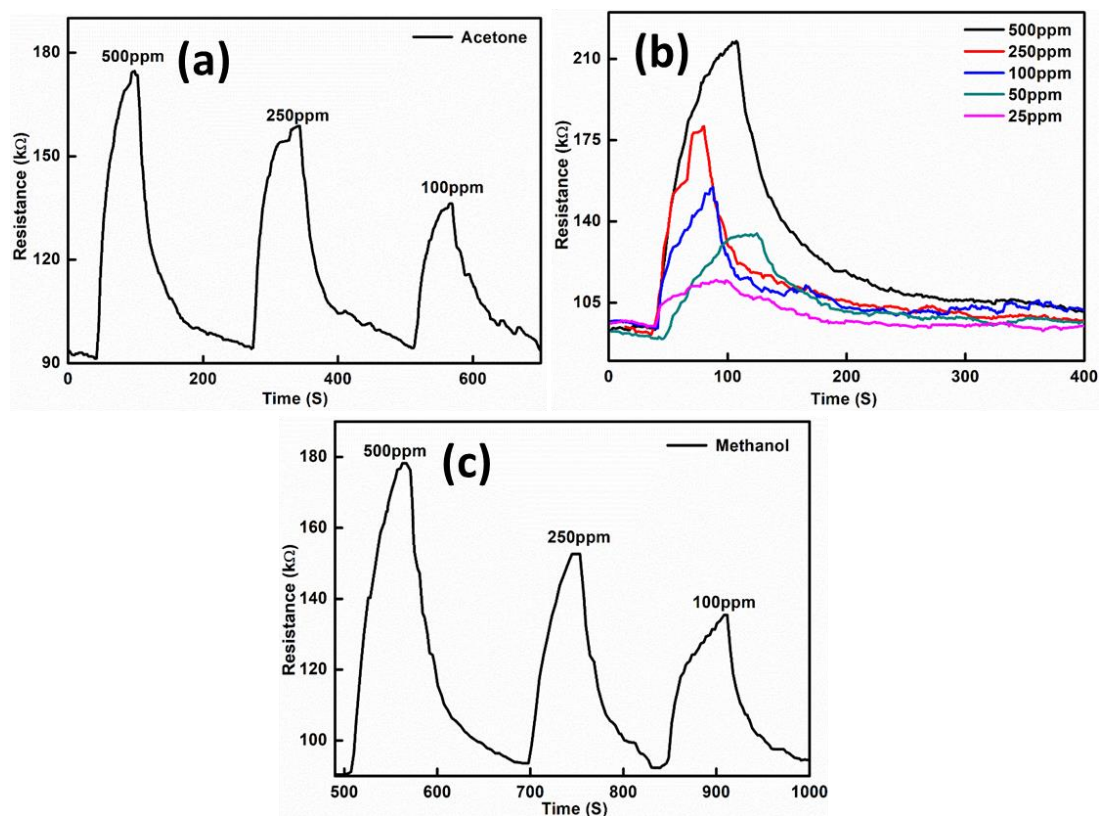


Figure 5.8: Resistance transient response of Cu_{0.50}Zn_{0.50}O composite thin films at operating temperature of 310⁰ C (a) acetone, (b) ethanol, (c) Methanol

Therefore, at optimised operating temperature of 310⁰ C sensing behaviour of Cu_{0.50}Zn_{0.50}O thin film was recorded for different quantity of different gases like ethanol, methanol and acetone. Figure 5.8 (a), (b) and (c) shows resistance transient curve for different concentration of acetone, ethanol and methanol respectively. It was

also observed that the samples were showing good sensitivity for ethanol than other VOC and were capable of detecting 1ppm of ethanol. Figure 5.9 shows resistance transient for 10, 5 and 1ppm of ethanol.

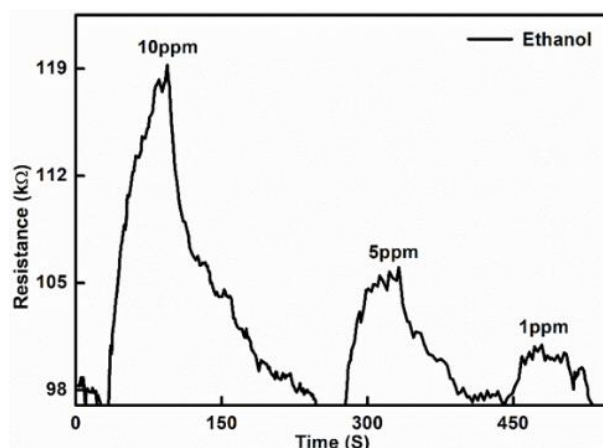


Figure 5.9: Resistance transient response of $\text{Cu}_{0.50}\text{Zn}_{0.50}\text{O}$ thin films for 1-10 ppm of ethanol

Further, $\text{Cu}_{0.75}\text{Zn}_{0.25}\text{O}$ thin films were subjected to sensing studies at different operating temperature like 270°C , 290°C and 310°C . The resistance transients correspond to different operating temperature for $\text{Cu}_{0.75}\text{Zn}_{0.25}\text{O}$ thin films for acetone, ethanol and methanol are given in figure 5.10, 5.11 and 5.12. By observing resistance transients of $\text{Cu}_{0.75}\text{Zn}_{0.25}\text{O}$ thin films at different temperature, it can be deduced that optimal operating temperature for $\text{Cu}_{0.75}\text{Zn}_{0.25}\text{O}$ thin film was 290°C , which is 20°C lesser as compared to $\text{Cu}_{0.50}\text{Zn}_{0.50}\text{O}$ thin films. It was also observed that $\text{Cu}_{0.75}\text{Zn}_{0.25}\text{O}$ thin films showed good sensitivity for all test gases than $\text{Cu}_{0.50}\text{Zn}_{0.50}\text{O}$ thin films. The resistance transients of $\text{Cu}_{0.75}\text{Zn}_{0.25}\text{O}$ thin films for lower concentration of ethanol are shown in the figure 5.13(a). Generally metal oxide gas sensors show higher response towards oxygen functionalized VOCs because these molecules can induce chemisorption at higher temperature, which involves exchange of electron hole pair between gas molecule and sensor surface (Cho et al. 2016). Further, to check the reproducibility, the $\text{Cu}_{0.75}\text{Zn}_{0.25}\text{O}$ sensors are exposed to successive pulses of 10ppm of ethanol, which is shown in figure 5.13(b). This proves that results are reproducible with a very minimal base line shift.

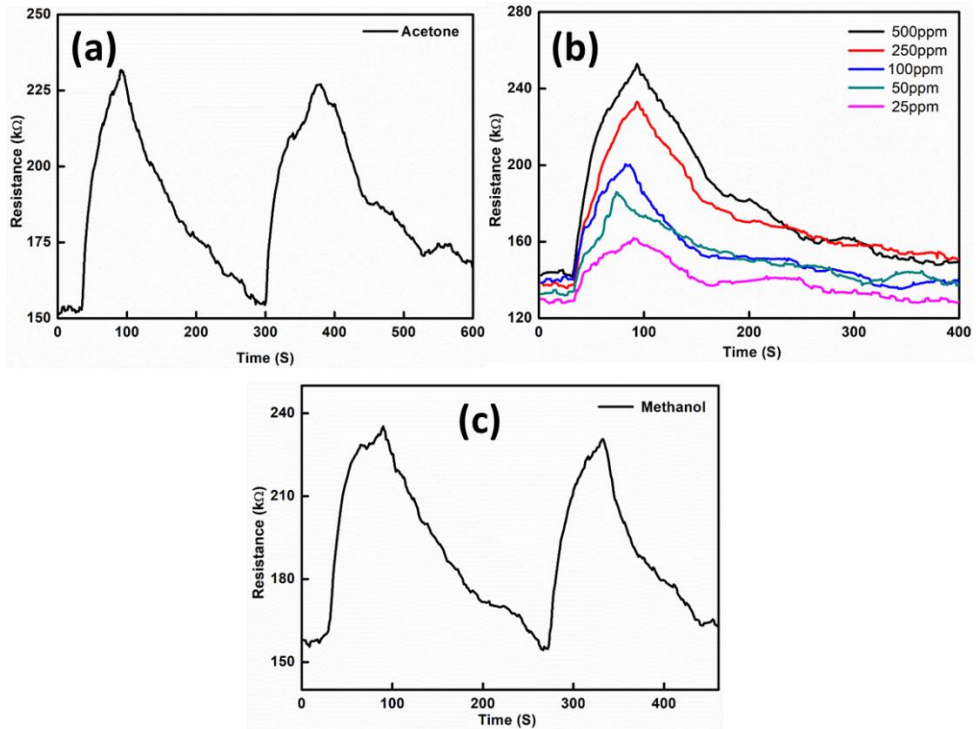


Figure 5.10: Resistance transient response of $\text{Cu}_{0.75}\text{Zn}_{0.25}\text{O}$ thin films at operating temperature 270°C (a) acetone, (b) ethanol, (c) Methanol

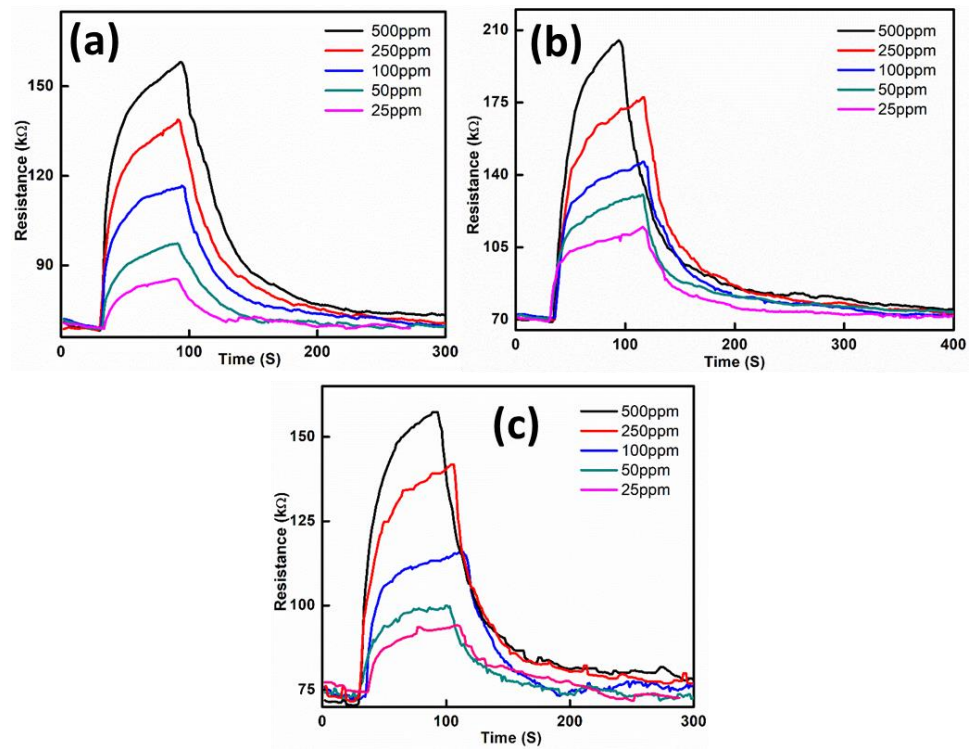


Figure 5.11: Resistance transient response of $\text{Cu}_{0.75}\text{Zn}_{0.25}\text{O}$ thin films at operating temperature 290°C (a) acetone, (b) ethanol, (c) Methanol

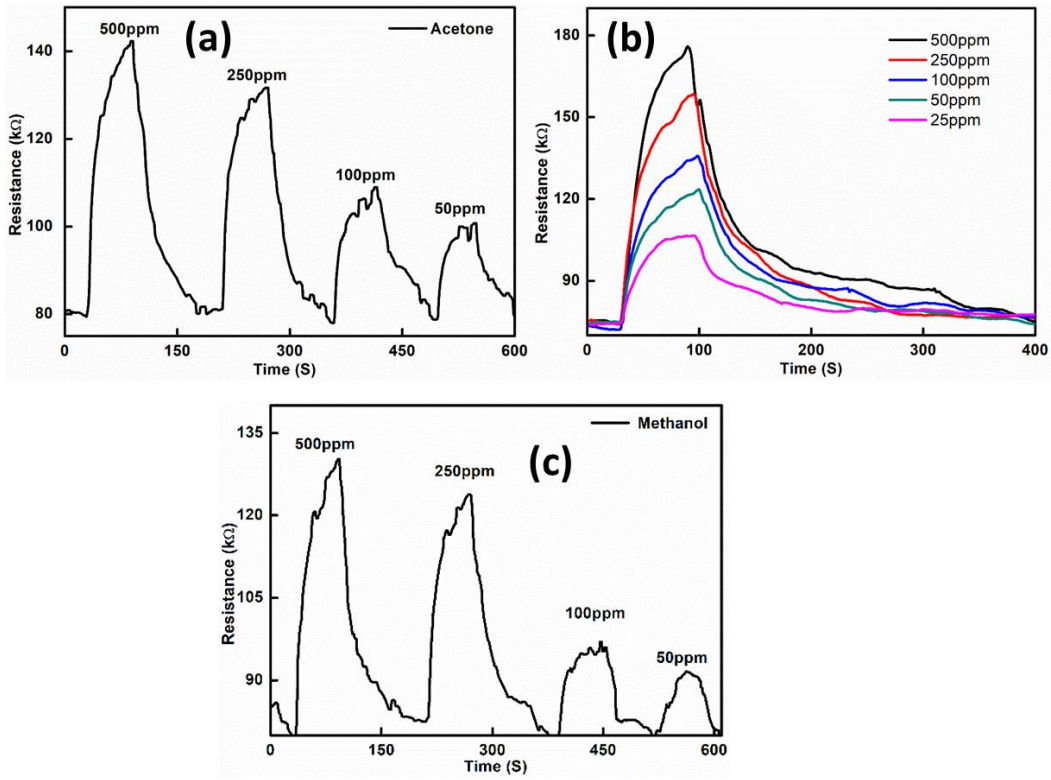


Figure 5.12: Resistance transient response of $\text{Cu}_{0.75}\text{Zn}_{0.25}\text{O}$ thin films at operating temperature 310°C (a) acetone, (b) ethanol, (c) Methanol

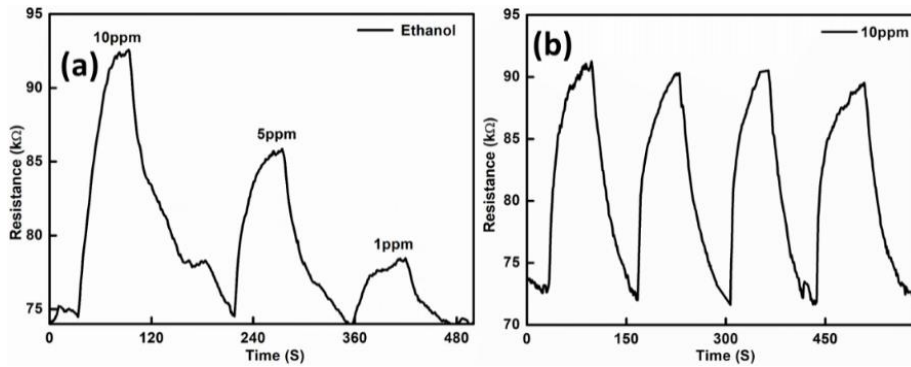


Figure 5.13: (a) Resistance transient response of $\text{Cu}_{0.75}\text{Zn}_{0.25}\text{O}$ thin films for 10-1 ppm of ethanol (b) Reproducibility curve of $\text{Cu}_{0.75}\text{Zn}_{0.25}\text{O}$ thin films for 10ppm of ethanol

Responsivity (%) of p type semiconductor gas sensor can be defined as the ratio of the resistance change in presence of gas vapour to the resistance in gas atmosphere. This can be calculated from the formula

$$S = \left(\frac{|R_a - R_g|}{R_g} \right) \times 100 \quad (8)$$

where R_a =Resistance in air, R_g = resistance in gas atmosphere. The response percentage of $\text{Cu}_{0.75}\text{Zn}_{0.25}\text{O}$ thin film gas sensors for different concentration of acetone, ethanol and methanol is shown in the table 5.2. $\text{Cu}_{0.75}\text{Zn}_{0.25}\text{O}$ thin films exhibited sensitivity of 18%, 11% and 4% for 10, 5 and 1 ppm of ethanol respectively. Comparison of calculated responsivity of different composition of $\text{Cu}_{1-x}\text{Zn}_x\text{O}$ thin films for 100ppm of ethanol at their optimal sensing temperature is shown in figure 5.14(a). By observing figure 4.14(b), it can be concluded that the $\text{Cu}_{0.75}\text{Zn}_{0.25}\text{O}$ thin film sensors are best suited for ethanol vapours at optimal operating temperature of 290°C .

Table 5.2: Responsivity of $\text{Cu}_{0.75}\text{Zn}_{0.25}\text{O}$ thin films

Concentration (ppm)	Sensitivity (%)				
	Ethanol (at 270°C)	Ethanol (at 310°C)	Ethanol (at 290°C)	Acetone (at 290°C)	Methanol (at 290°C)
500	43	56	65	56	54
250	40	52	63	49	48
100	30	47	52	39	37
50	27	38	46	29	28
25	19	30	39	18	23

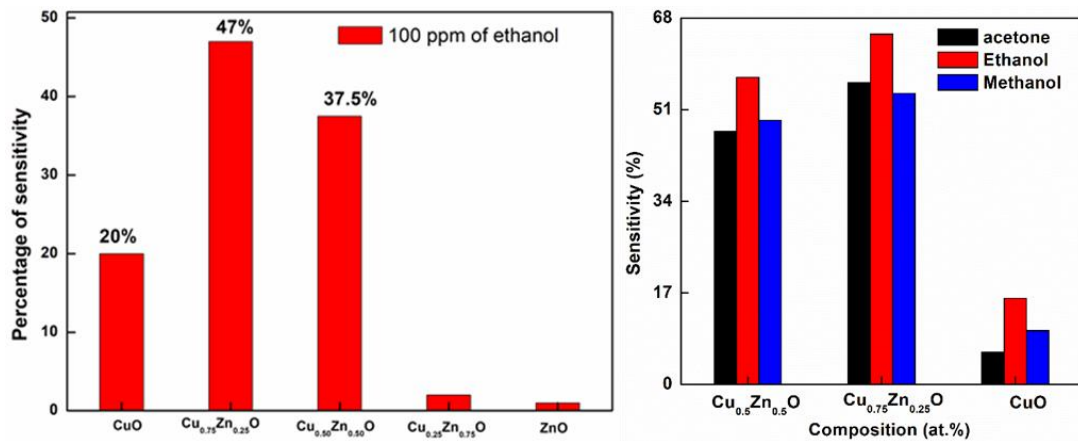


Figure 5.14: Comparison of sensitivity of $\text{Cu}_{1-x}\text{Zn}_x\text{O}$ thin films for 500 ppm of ethanol

It can be observed from figure 5.10, 5.11 and 5.12 that response time and recovery time is temperature dependent. At 270°C , time taken to reach its baseline resistance was very large as compared to higher temperature. Chemisorption and desorption of gas molecule is thermally activated process. At lower temperature reaction rate is very low which increases the response time and recovery time. The response time and recovery

time of $\text{Cu}_{0.75}\text{Zn}_{0.25}\text{O}$ thin films at optimized temperature of 290°C for different concentration of acetone, ethanol and methanol is displayed in table 5.3. The response time decreases with an increase in VOC concentration. More gas molecules come into interaction with sensor surface at higher concentration to bring down response time. Recovery time decreases with decrease in gas vapour concentration, because very small number of gas molecule interact with sensor surface which brings down recovery time.

Table 5.3: Response and recovery time of $\text{Cu}_{0.75}\text{Zn}_{0.25}\text{O}$ thin film for acetone, ethanol and methanol

Concentration (ppm)	Response time (S)			Recovery time (S)		
	Acetone	Ethanol	Methanol	Acetone	Ethanol	Methanol
500	20	24	22	154	300	160
400	22	28	26	132	238	126
300	26	30	28	83	209	100
200	37	34	31	49	170	89
100	40	40	34	33	117	74

5.3 SYNTHESIS AND CHARACTERIZATION OF $\text{Zn}_{1-x}\text{Sn}_x\text{O}$ COMPOSITE THIN FILMS FOR SENSOR APPLICATION

5.3.1 Experimental details

Zinc-Tin-Oxide ($\text{Zn}_{1-x}\text{Sn}_x\text{O}$) thin films were deposited onto sodalime glass substrate by using spray pyrolysis unit. Zinc diacetate dihydrate (ZnCl_2) and Tin chloride dihydrate ($\text{SnCl}_2 \cdot 2\text{H}_2\text{O}$) was used as precursor source, both the materials were dissolved in isopropyl alcohol at different molar ratios to get resultant solution of 25mM concentration. In the deposition process, the solution was injected through nozzle and sprayed on top of pre heated glass substrate maintained at temperature of 350°C . During complete deposition process optimised spray rate and substrate to nozzle distance were maintained. Air was used as carrier gas, which was supplied by an air compressor at constant pressure of 2 bar.

5.3.2 XRD analysis

The figure 5.15(a-d) displays X-ray diffraction profiles of $\text{Zn}_{1-x}\text{Sn}_x\text{O}$ thin films after the annealing treatment at 350°C for 2h. XRD profiles of as-deposited $\text{Zn}_{1-x}\text{Sn}_x\text{O}$ thin films are matching with annealed thin films, hence they are not provided. Figure 5.15

(a) displays the X-ray profile of ZnO thin film, where all the peaks (100), (002) and (101) are in consistent with standard XRD pattern of hexagonal structure ZnO (JCPDS Card No.-01-080-0075). Figure 5.15(e) shows the X-ray profiles of the SnO₂ thin films, where all the peaks (110), (200) and (211) are matching with the standard tetragonal structured SnO₂(JCPDS card no. 00-041-1445). The sharper (002) peak of ZnO and (110) peak of SnO₂ X-ray profiles proves the good crystallinity of thin films. X-ray profiles for intermediate compositions of Zn_{1-x}Sn_xO (25% to 75%) thin films are shown in figure 5.15 (b) to (d). It is observed that all the mixed oxide thin films showed characteristic profile of stable amorphous nature. For all the samples of intermediate composition, peaks of ZnO, SnO₂, ZnSnO₃ and Zn₂SnO₄ are absent, which confirms the formation of pure amorphous ZTO thin films.

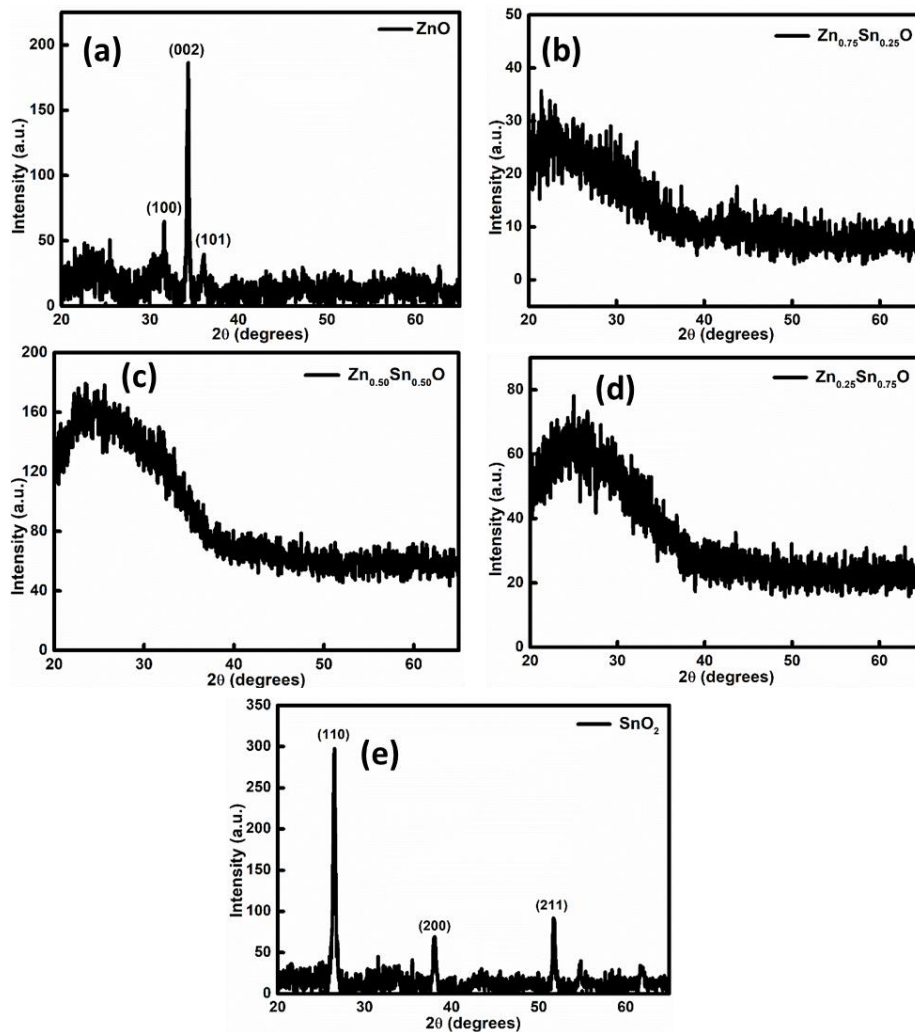


Figure 5.15: XRD patterns of Zn_{1-x}Sn_xO thin films (a) ZnO, (b) Zn_{0.75}Sn_{0.25}O, (c) Zn_{0.50}Sn_{0.50}O, (d) Zn_{0.25}Sn_{0.75}O, (e) SnO₂

5.3.3 Surface morphology and compositional analysis

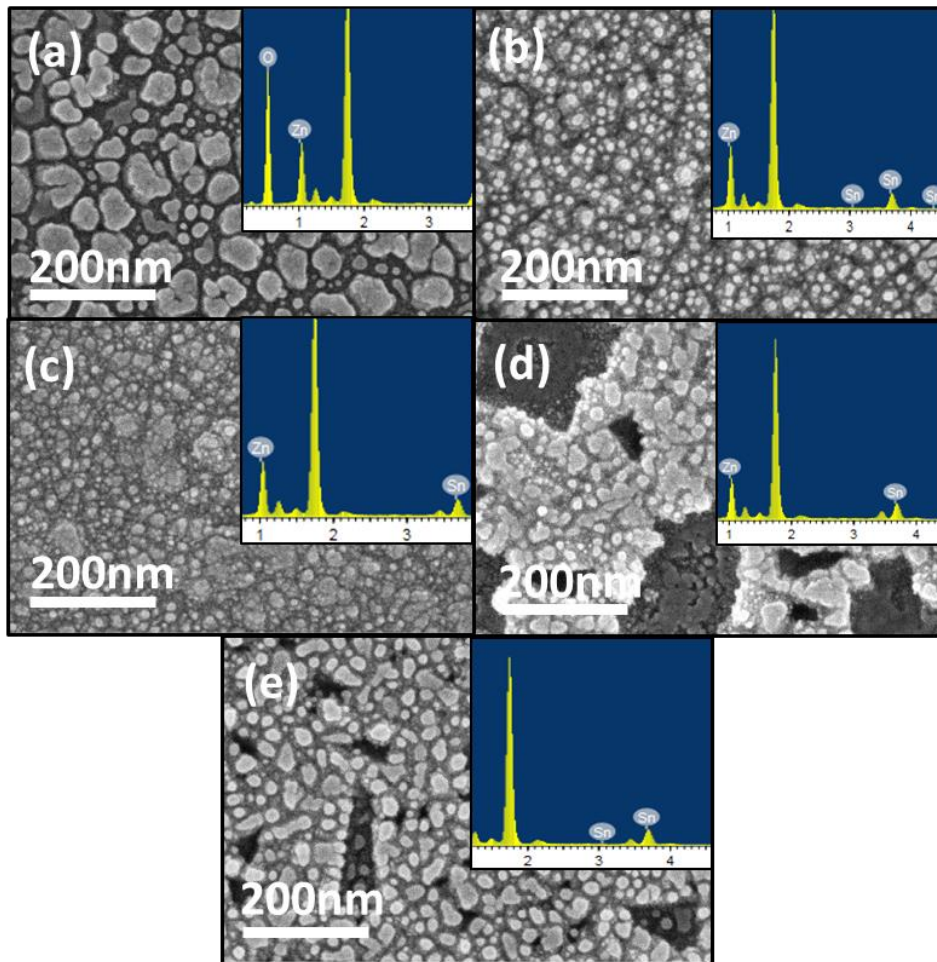


Figure 5.16: FE-SEM images of $Zn_{1-x}Sn_xO$ thin films (a) ZnO, (b) $Zn_{0.75}Sn_{0.25}O$, (c) $Zn_{0.50}Sn_{0.50}O$, (d) $Zn_{0.25}Sn_{0.75}O$, (e) SnO_2

Figure 5.16 presents the high resolution SEM image of annealed $Zn_{1-x}Sn_xO$ samples. It is observed that all the thin films are free from cracks and pin holes with uniformly distributed microstructures. Figure 5.16 (a) and (e) shows the surface morphology of pure ZnO and SnO_2 respectively, in these films sharp distinction between neighboring grains can be observed which may be because of its crystalline structure. As the Sn concentration increases the sharp distinction between agglomerated structure diminishes, which may be because of its amorphous nature (as observed from X-ray profiles). The atomic composition of annealed $Zn_{1-x}Sn_xO$ thin films, analysed by EDX, are shown in the figure 5.16. EDX spectra consists peak of Zn, Sn and O from constituent material and also it shows peak for sodium and silicon from soda-lime glass

substrate material. Atomic percentage of Zn and Sn are tabulated in table 5.4. It is observed that atomic percentage of Sn is less in prepared thin films as compared to starting precursor solution.

Table 5.4: Compositional information of $Zn_{1-x}Sn_xO$ thin film

Sample name	Zn (at. %)	Sn (at. %)
ZnO	100	0
$Zn_{0.75}Sn_{0.25}O$	86.64	13.36
$Zn_{0.50}Sn_{0.50}O$	74.49	25.5
$Zn_{0.25}Sn_{0.75}O$	49.17	50.83
SnO ₂	0	100

5.3.4 Optical properties

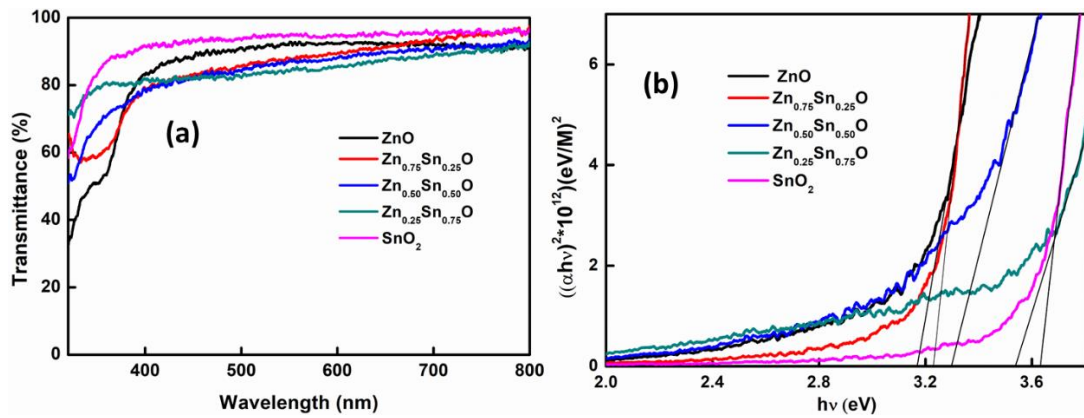


Figure 5.17: (a) Optical transmittance spectra and (b) Tauc's plot of $Zn_{1-x}Sn_xO$ thin films

The optical transmission measurements carried out on 350⁰C annealed $Zn_{1-x}Sn_xO$ thin films in wavelength range of 200-800nm is shown in figure 5.17. It was observed that pure ZnO and SnO₂ were showing highest transmittance of ~90%. At all the intermediate compositions, decrease in transmittance was observed and it was ~80%. It also can be observed that all the thin films have high absorption in UV region and high transmission in visible region. Estimated band gap from tauc's plot (as shown in fig) shows increase in band gap with increase in Sn content, and reaches maximum 3.6eV for pure SnO₂ thin films.

5.3.5 Electrical properties

The type of electrical conductivity of $Zn_{1-x}Sn_xO$ thin films was identified using hot probe set up, shows n-type conductivity. The current-voltage (I-V) characteristics of $Zn_{1-x}Sn_xO$ thin films with co-planar aluminium contacts were recorded and is shown in figure 5.18. The linearity in current voltage measurements proves the formation of ohmic contact between thin film and contact material. The variation of electrical resistivity of 350⁰C annealed $Zn_{1-x}Sn_xO$ thin films are summarised in table 5.5. As the Sn concentration increases the resistivity decreases up to 50% and with further increase in Sn concentration causes increase in resistivity.

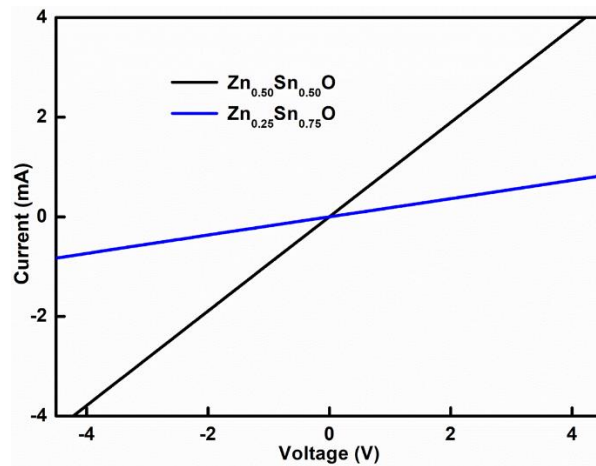


Figure 5.18: I-V characteristics of $Zn_{1-x}Sn_xO$ thin films

Table 5.5: Electrical resistivity and bandgap of $Zn_{1-x}Sn_xO$ thin films

Sample name	Resistivity(Ωm)	Band gap (eV)
ZnO	13.2	3.18
$Zn_{0.75}Sn_{0.25}O$	0.468	3.23
$Zn_{0.50}Sn_{0.50}O$	0.0144	3.30
$Zn_{0.25}Sn_{0.75}O$	0.0984	3.54
SnO_2	0.336	3.64

5.3.6 Gas sensing characteristics

$Zn_{1-x}Sn_xO$ thin films are n-type in conductivity, so it follows same mechanism as explained in the previous section 2.3. It is well known that the gas sensing mechanism in the oxide based materials is surface controlled, here surface morphology and oxygen adsorption also play an important role. Generally, thin films with lesser

grain size shows high sensitivity towards gases. It can be observed from the XRD all the intermediate composition $Zn_{1-x}Sn_xO$ thin films are amorphous in nature, so the present study concentrates on gas sensing behaviour of amorphous $Zn_{1-x}Sn_xO$ thin films. The gas sensing characteristics of $Zn_{1-x}Sn_xO$ thin films are investigated for gas vapours like acetone, ethanol and methanol at an optimised temperature of $350^{\circ}C$. The figure 5.19 (a) shows the resistance transient response plot recorded for $Zn_{0.50}Sn_{0.50}O$ thin films towards different concentration of ethanol, acetone and methanol vapours. Figure 5.19 (b) shows reproducibility curve for $Zn_{0.50}Sn_{0.50}O$ thin films for three successive pulse of 1000 ppm of ethanol, shows that results are reproducible with very minimal base line drift. Further $Zn_{0.50}Sn_{0.50}O$ thin films were subjected to detect acetone and methanol, resistance transient curves are shown in figure 5.20 (a) and (b) respectively.

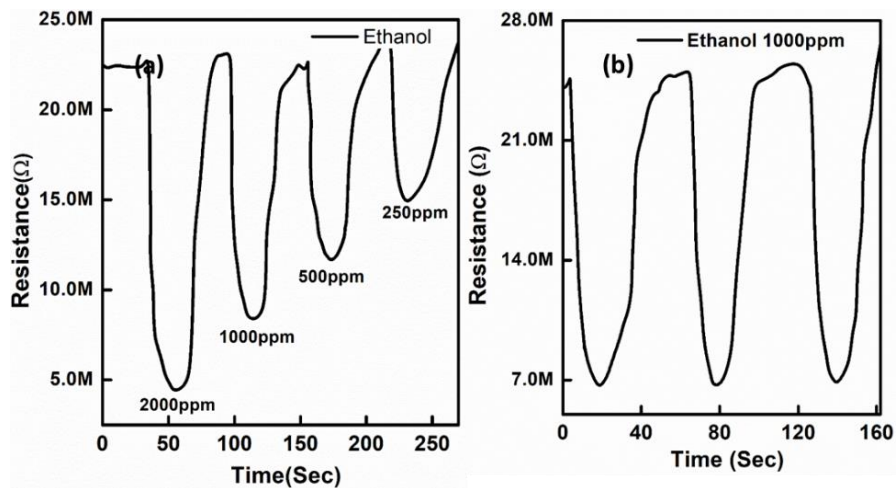


Figure 5.19: (a) Resistance transient response of $Zn_{0.50}Sn_{0.50}O$ thin films for ethanol, (b) reproducibility curve for 1000ppm of ethanol for $Zn_{0.50}Sn_{0.50}O$ thin films

Responsivity of sensor can be defined as the ratio of the resistance change in presence of gas vapour to the resistance in air. This can be calculated from the equation (8). $Zn_{0.50}Sn_{0.50}O$ thin films were capable of detecting 250 ppm of ethanol with 33% sensitivity. Responsivity curve of $Zn_{0.50}Sn_{0.50}O$ thin films for ethanol is shown in 5.21 (a). Comparison of sensitivity for different concentration of acetone, ethanol and methanol can be seen in 5.21 (b).

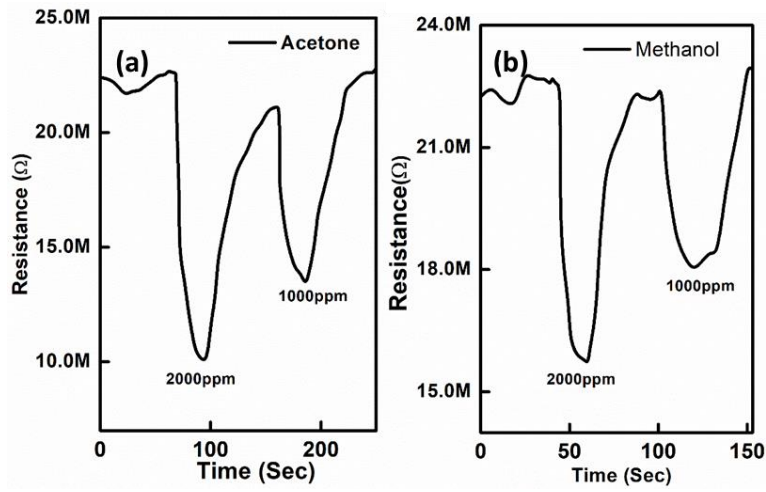


Figure 5.20: Resistance transient response of Zn_{0.50}Sn_{0.50}O thin films for (a) Acetone, (b) Methanol

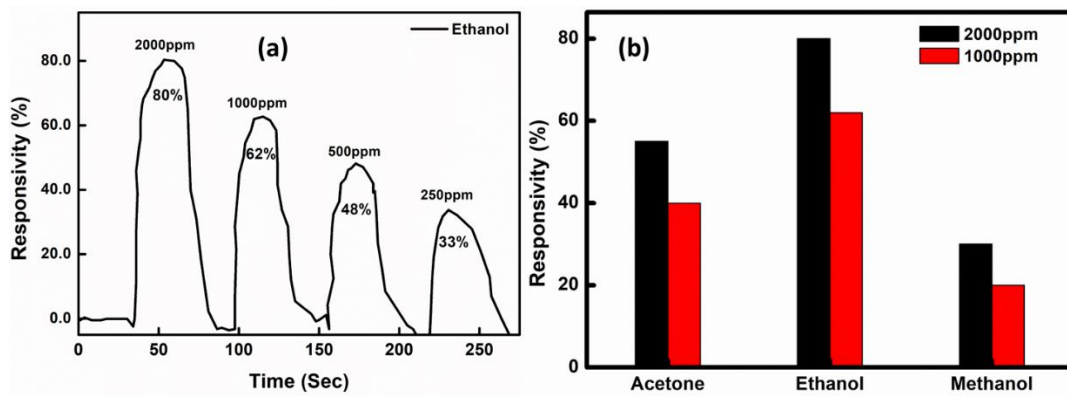


Figure 5.21: (a) Responsivity curve of Zn_{0.50}Sn_{0.50}O thin films for ethanol, (b) Comparison of sensitivity for different gas vapours

CHAPTER 6

DEVELOPMENT OF DATA ACQUISITION AND GAS SENSOR SYSTEM

6.1 INTRODUCTION

The idea of an artificial odour detection system is inspired from mammalian olfactory system which consists of nose, brain and neurons etc. With the progress in semiconductor metal oxide sensor technology, electronic devices and computational algorithms, the different basic units of the mammalian olfactory organ can be designed artificially. The sense of smell in mammals is stimulated only by gaseous molecules that come in the air. The odorant molecules stimulate the sensory nerve cells activating the protein molecules attached with it and produces the enzyme adenylate cyclise. This enzyme triggers the generation of action potential. The axons from all the receptor cells transmit the action potential to the brain as features. Brain collects all the features from individual receptor cell and stores then in the memory as odour. Upon receiving new features, brain starts to access memories, compare with the stored features and identify it if already there in memory. In the artificial olfactory system, receptor cells are replaced by an array of chemical sensors. The sensors generate analog electrical signals when the odour molecules react with the sensor surface. The olfactory neurons are represented by a data processing unit, whereas the brain is represented by odour pattern recognition system. Figure 6.1 displays the block diagram of human olfactory system and artificial odour detection system.

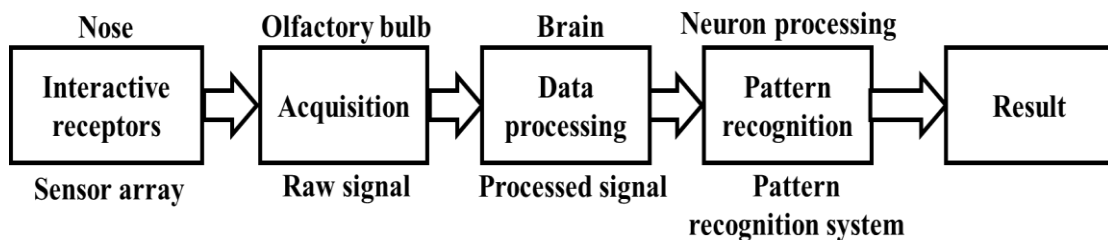


Figure 6.1: Comparison of mammalian and artificial olfactory system

6.2 DEVELOPMENT OF SENSOR ASSEMBLY AND DATA ACQUISITION SYSTEM

The prototype of an odour detection system requires a data acquisition system as well as a monitoring unit along with the setup of an array of gas sensors. The design and development of an experimental setup for real time data acquisition of different gases using an array of gas sensors is described in this section. This system mainly consists of metal oxide gas sensor array, measuring circuit, sensor temperature controller, microcontroller based data acquisition system.

6.2.1 Sensor array

The gas sensor array comprises of multiple metal oxide semiconductor gas sensors. In present study sensor array of three individual gas sensors was constructed. For electrical connections spring loaded connectors were used and mounted on heater substrate. Three separate wires were soldered to acquire data from three individual sensors.

6.2.2 Measuring circuit

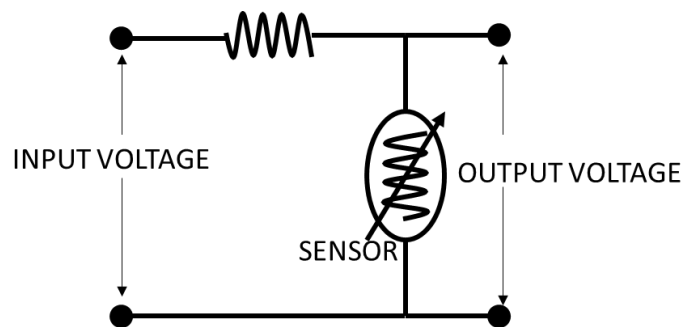


Figure 6.2: Gas sensing measurement circuit

In presence of gases resistance of sensor element varies, that resistance variation can be measured using standard potential divider circuit. In measuring circuit, sensor element forms one arm of potential divider and resistance of fixed value forms another arm of potential divider circuit. Schematic circuit diagram is shown in figure 6.2. A fixed voltage is applied across input voltage terminals of potential divider and varying sensor voltage can be acquired across sensor element using output voltage terminal.

Resistance of sensor element can be calculated using equation, where R_s = sensor resistance, R_c = constant resistance, V_o = output voltage, V_i = input voltage.

$$R_s = \left(\frac{V_o}{V_i - V_o} \right) \times R_c$$

6.2.3 Data acquisition system

The most important part of gas detection system is data acquisition system (DAS). DAS is a system which is used for acquisition of signals of physical parameters continuously for a certain period of time and keeps record of those acquired values for future use. A typical DAS consists of primary control and data processor, memory and clock for time stamping the acquired data. DAS can be built using commercially available microcontroller and by programming it in desired way using programming languages like C and C++. The use of microcontroller for DAS became popular because of its speed, energy efficiency, low cost and portability.

In present study, DAS is designed to acquire signals from three different sensors simultaneously by using well known open source microcontroller platform Arduino mega 2560. The Arduino mega 2560 is a microcontroller board based on microcontroller ATmega2560. It has 54 digital input/output pins (of which 15 can be used as PWM outputs), 16 analog inputs, 4 UARTs (hardware serial ports), a 16MHz crystal oscillator, USB connection, a power jack, an ICSP header and reset button. Figure 6.3(a) shows photograph of Arduino mega2560.

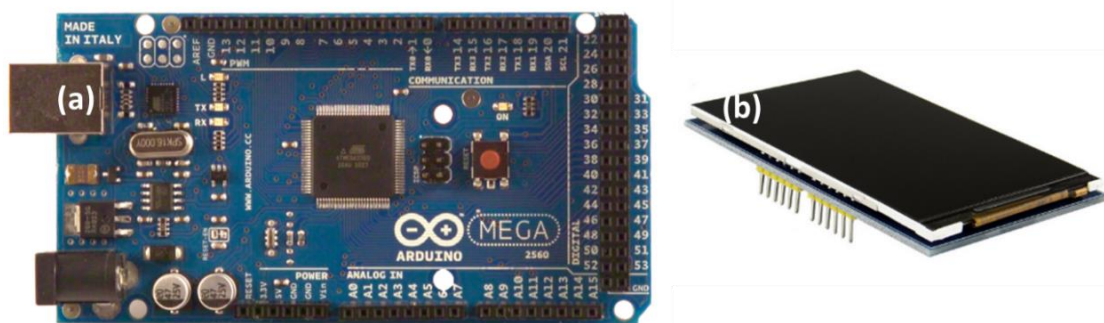


Figure 6.3: (a) Arduino mega, (b) LED display used in data acquisition system

In present scenario, voltage variation across sensor element is analog in nature. As most of the processes and calculations involved in DAS is digital in nature, analog signals from sensors must be converted into digital format before being used for processing. Analog voltage signals from sensor element can be converted into digital signal using analog to digital converter (ADC). Present study uses linear technology manufactured 24-bit resolution ADC named LTC2400. Three different LTC2400 were interfaced with Arduino mega2560 to acquire analog to digital converted signal form three different gas sensors. Acquired signals are processed and converted into resistance using equation.

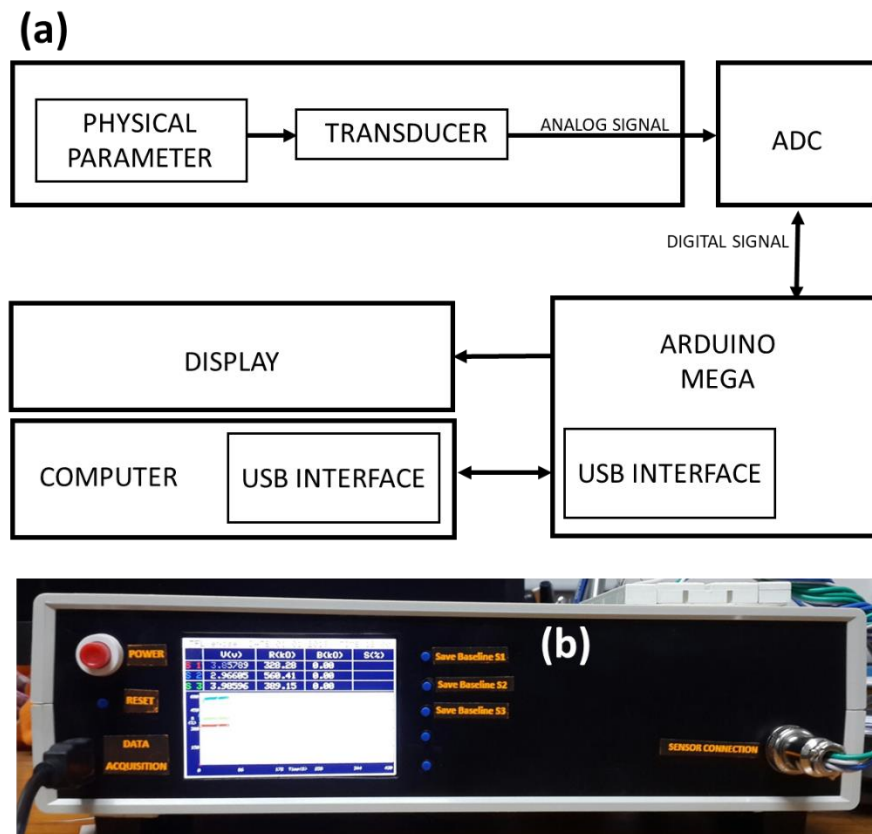


Figure 6.4: (a)Block diagram of data acquisition system, (b) Developed DAS

Arduino mega was also interfaced with LED display to show real time resistance value graphically. In present study, 3.2” LED display with resolution of 480X320 was used, image is shown in figure 6.3 (b). Complete block diagram of prepared DAS is shown in figure 6.4 (a). In block diagram physical parameter refers to change in gas concentration, which can be sensed using transducer (gas sensor). Analog

signal from transducer flows to ADC for digital conversion and acquired using Arduino mega. Photographs of constructed DAS is shown in figure 6.4 (b). Developed DAS also has capability to upload acquired data to personal computer using USB cable and can be saved in Microsoft excel format for future analysis as shown in figure 6.5 (a).

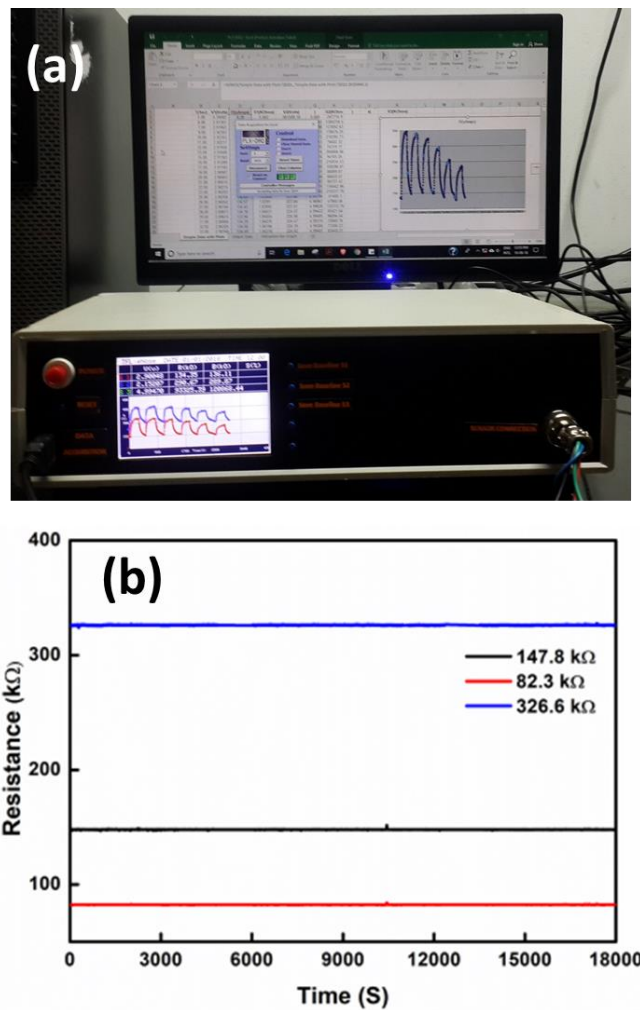


Figure 6.5: (a) Computer interfaced DAS, (b) Resistance value acquired using DAS

Developed DAS was subjected to testing and used to measure three constant resistances of different values 82.3kΩ, 147.8kΩ, 326.6kΩ. Resistance values were measured for 18000 seconds and 11000 samples of resistance were acquired using DAS. Acquired resistances are plotted against time and displayed in figure 6.5(b). Resistance values measured using DAS were almost comparable resistance measured using Keithley multimeter-2002 with minimal fluctuation over a long duration of time, which proves the stability of developed DAS. Further, DAS was tested by mounting

three different $\text{Cu}_{0.75}\text{Zn}_{0.25}\text{O}$ thin film sensors. Resistance transient of different $\text{Cu}_{0.75}\text{Zn}_{0.25}\text{O}$ thin films for different concentrations of ethanol, acetone and methanol using DAS is shown in figure 6.6. Multiple trials of calculated sensitivity for $\text{Cu}_{0.75}\text{Zn}_{0.25}\text{O}$ thin film sensors are tabulated in table 6.1.

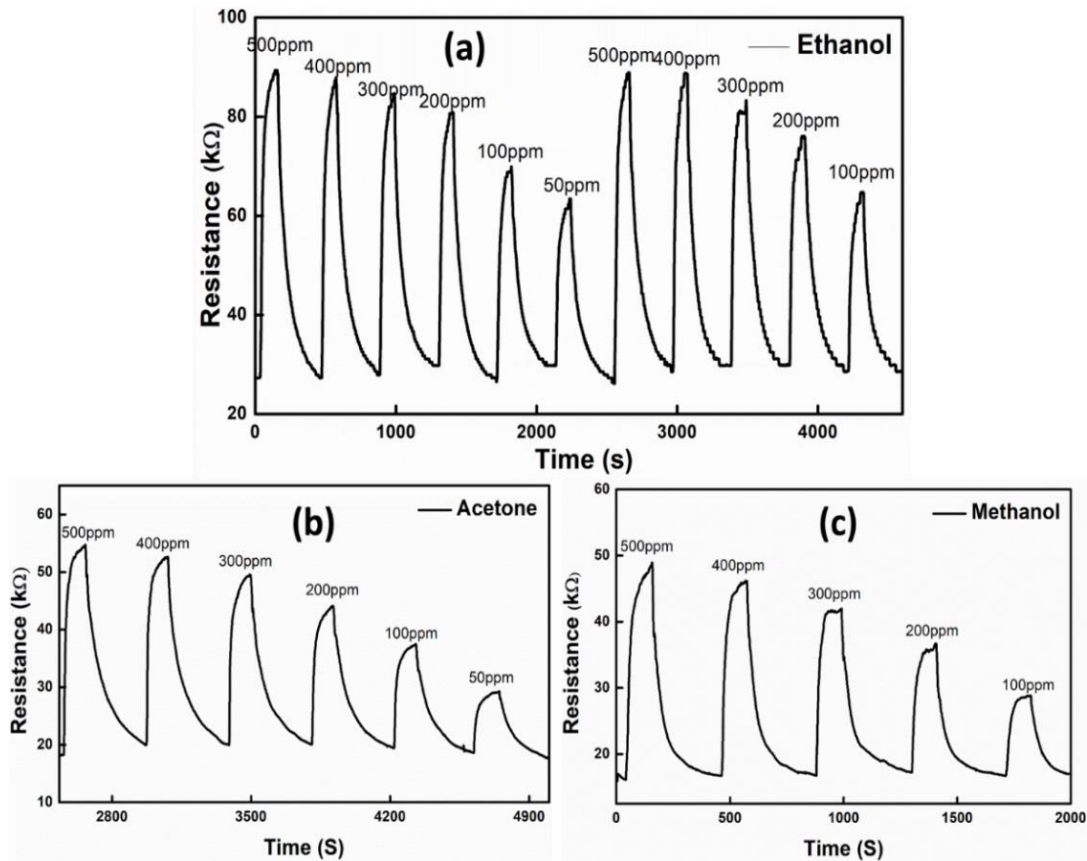


Figure 6.6: Resistance transient response of $\text{Cu}_{0.75}\text{Zn}_{0.25}\text{O}$ for (a) ethanol, (b) acetone and (c) methanol at 290°C

Table 6.1: Responsivity of $\text{Cu}_{0.75}\text{Zn}_{0.25}\text{O}$ thin films for ethanol, acetone and methanol

Concentration (ppm)	Sensitivity (%)					
	Ethanol		Acetone		Methanol	
	Trial-1	Trial-2	Trial-1	Trial-2	Trial-1	Trial-2
500	69	68	59	62	64	64
400	66	65	57	59	62	62
300	63	63	54	56	58	58
200	60	60	51	52	51	52
100	55	56	40	39	39	39

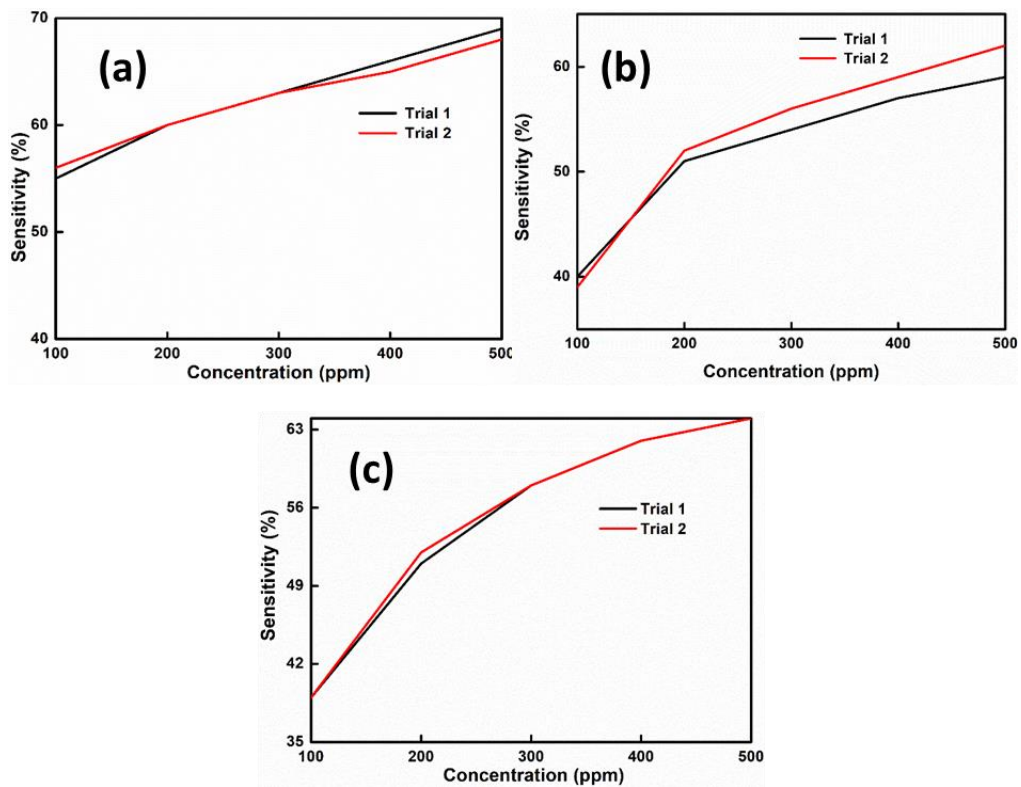


Figure 6.7: Calibration curve for (a) ethanol, (b) acetone and (c) methanol

6.3 DEVELOPMENT OF GAS SENSOR SYSTEM

Developed DAS can be easily modified into completely working gas sensor to estimate the concentration of ethanol, acetone and methanol in parts per million (ppm). To develop working gas sensor only one $\text{Cu}_{0.75}\text{Zn}_{0.25}\text{O}$ thin film sensor was used instead of three sensor array as in DAS. Graph of concentration against sensitivity can be seen in figure 6.7, called as calibration curve. Calibration curve for ethanol, acetone and methanol was saved in microcontroller Arduino mega to convert sensitivity into concentration in ppm. Gas to be sensed should be selected before starting the sensing experiment. After switching on the working sensor, selection window opens where sensing gas can be selected, photograph of selection window is shown in figure 6.8 (a). Resistance variation from sensor can be converted into sensitivity and subsequently sensitivity can be converted into concentration in ppm by using internally saved calibration curve, display showing concentration can be seen in figure 6.8 (b). Multiple trials of estimated gas concentration of ethanol, acetone and methanol in ppm using working gas sensor are tabulated in table 6.2, 6.3 and 6.4.

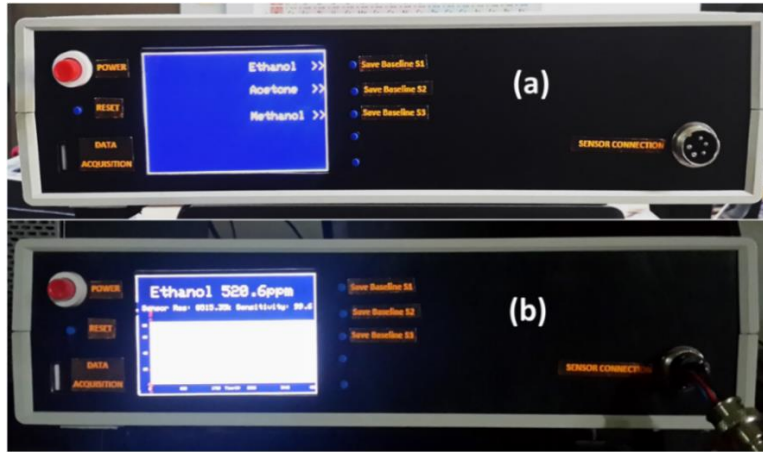


Figure 6.8: (a) Selection window, (b) Display showing concentration in ppm

Table 6.2: Estimated concentration of ethanol using developed gas sensor

Ethanol (ppm)		Estimated concentration (ppm)				
500	550	560	550	570	552	506
400	--	390	431	388	396	435
300	333	364	337	294	308	360
200	253	274	290	217	220	270
100	114	90	140	138	68	93

Table 6.3: Estimated concentration of acetone using developed gas sensor

Acetone (ppm)	Estimated concentration (ppm)		
500	508	547	528
400	424	363	415
300	351	291	334
200	237	209	--
100	116	70	147

Table 6.4: Estimated concentration of methanol using developed gas sensor

Methanol (ppm)	Estimated concentration (ppm)			
500	508	499	464	532
400	465	448	353	426
300	428	375	280	350
200	342	225	173	247
100	179	140	70	64

CHAPTER 7

SUMMARY AND CONCLUSIONS

7.1 INTRODUCTION

The objective of the present research work was to understand the sensing behavior of ZnO based metal oxide thin films. ZnO based thin films are known to exhibit good sensing property towards VOCs. An effective utilization of ZnO based metal oxides for sensor application can only be possible by improving its sensitivity by adding proper dopants or additives. Research work was carried out to optimize growth condition, to study the effect doping concentration and then for gas sensor application. Important conclusion drawn from present work are summarized below.

7.2 CONCLUSIONS

7.2.1 Preparation and characterization of doped ZnO thin films

Three different dopants for ZnO system were tried, Cadmium doped ZnO [$\text{Cd}_x\text{Zn}_{1-x}\text{O}$ (0-20 at. %)], indium doped ZnO [$\text{In}_x\text{Zn}_{1-x}\text{O}$ (0-5 at. %)], aluminum doped ZnO [$\text{Al}_x\text{Zn}_{1-x}\text{O}$ (0-5 at. %)] thin films were successfully deposited on glass substrate using spray pyrolysis technique. All the films crystallized in hexagonal wurtzite structure with orientation along (002), (101), (102), (103) directions. Systematic shift in the (002) peak, interplanar distance, lattice parameter a and c of ZnO proves the successful incorporation of dopants into ZnO lattice in case of Cd and In doping. For Al doping systematic change in lattice parameters were not observed. Here, divalent cadmium doping to ZnO was improves the crlystallinity of thin films, while trivalent dopant In and Al were decreasing the crystallinity of thin films. Preferred orientation along (002) plane was unaffected by Cd and Al doping, but with In doping preferred orientation was shifting to (101) direction. Hexagonal plate like structure of ZnO was changing to random granular structure with increase in doping concentration for all the dopants. Amount of cadmium in final Cd doped thin film was less as compared to initial precursor material. Amount of dopants in case of Al and In doping remained almost same in final thin films. For cadmium and indium doping, optical absorption edge and band gap of the films were red shifted with increase in the

doping concentration. For 20 at.% Cd doping highest reduction in band gap was observed, which was reaching 2.83eV. For all concentration of aluminum doping band gap and absorption edge remained almost constant. $Cd_xZn_{1-x}O$ thin films with 10 at. % Cd doping showed good electrical conductivity. For electrical application of $In_xZn_{1-x}O$ and $Al_xZn_{1-x}O$ thin films, 3 at. % is optimal doping concentration. Highest electrical conductivity was achieved for 10 at. % Cd doping as compared to other dopants. At optimal doping concentration all the thin films showed ~80% transmittance, so all these doped thin films can be used for transparent conducting electrode application.

Table 7.1: List of different criteria to choose transparent conducting material

Sample name	Criteria for choosing transparent conducting material			
	Transparency	Conductivity	Non toxicity	Low cost
$Cd_xZn_{1-x}O$	✓	✓		✓
$In_xZn_{1-x}O$	✓	✓	✓	
$Al_xZn_{1-x}O$	✓	✓	✓	✓
$Cu_xZn_{1-x}O$		✓	✓	✓
$Zn_xSn_{1-x}O$	✓	✓	✓	✓

7.2.2 Gas sensing applications of doped ZnO thin films

Doping of ZnO with other impurity material improves its sensing ability towards detection of VOCs such as acetone, ethanol and methanol. $Cd_xZn_{1-x}O$ thin films were highly sensitive with 50% sensitivity towards 1 ppm of ethanol and 40% sensitivity towards 10ppm of methanol. $In_xZn_{1-x}O$ thin films were capable of detecting 25ppm of ethanol with 30% sensitivity. $Al_xZn_{1-x}O$ thin films were highly sensitive for 10 ppm of acetone and ethanol with ~20% and ~30% sensitivity. Compared to In and Al doping, in terms of sensitivity, Cd proved to be efficient dopant to detect VOCs and were selective and highly sensitive to ethanol vapors. As compared to $Cd_xZn_{1-x}O$, $In_xZn_{1-x}O$ and $Al_xZn_{1-x}O$ thin films showed very less response and recovery time, which can be used as fast response sensors. As compared to $In_xZn_{1-x}O$, $Cd_xZn_{1-x}O$ and $Al_xZn_{1-x}O$ thin films are cost effective and can be used to produce low cost high sensitive gas sensor.

Table 7.2: List of different criteria to choose different gas sensor

Sample name	Criteria for choosing gas sensor			
	Sensitivity	Response and recovery time	Non toxicity	Low cost
$Cd_xZn_{1-x}O$	✓			✓
$In_xZn_{1-x}O$	✓	✓	✓	
$Al_xZn_{1-x}O$	✓	✓	✓	✓
$Cu_xZn_{1-x}O$	✓	✓	✓	✓
$Zn_xSn_{1-x}O$			✓	

7.2.3 Synthesis, characterization and gas sensing properties of mixed oxides

Copper-Zinc-Oxide [$Cu_{1-x}Zn_xO$ ($0 \leq x \leq 1$)] Zinc-Tin-Oxide [$Zn_xSn_{1-x}O$ ($0 \leq x \leq 1$)] thin films were successfully developed using spray pyrolysis technique for VOC sensor application. $Cu_{1-x}Zn_xO$ thin films showed very poor crystallinity, which may increase the sensitivity towards different gases. $Cu_xZn_{1-x}O$ thin films formed composite thin films with two different peaks for monoclinic CuO and hexagonal ZnO with granular nanostructures. Initial precursor materials were present in final thin films with proper stoichiometry. $Cu_{1-x}Zn_xO$ composite thin films exhibited significant improvement in its sensing behavior because of formation of CuO-ZnO heterostructure. $Cu_{0.75}Zn_{0.25}O$ thin films showed good sensing property towards VOCs such as acetone, ethanol and methanol. $Cu_{1-x}Zn_xO$ thin films were selective towards ethanol and capable of detecting 1ppm of ethanol. $Cu_{1-x}Zn_xO$ thin films were showing sensitivity for different VOCs at lower temperature range of 270°C-290°C as compared to doped ZnO thin films, so these sensors are energy efficient. $Cu_{1-x}Zn_xO$ thin films are nature friendly and low cost, so these thin films can be efficiently used in field of gas sensor.

$Zn_xSn_{1-x}O$ thin films showed stable amorphous nature with granular morphology. Good conductivity of 104S/m with ~80% transmittance was observed for $Zn_{0.50}Sn_{0.50}O$ thin films. As compared to all other dopants, highest conductivity was achieved for $Zn_xSn_{1-x}O$ thin films. $Zn_xSn_{1-x}O$ thin films showed good conductivity along with transmittance; hence it can be used as transparent conducting

electrodes. $Zn_xSn_{1-x}O$ thin films are very poor sensitive towards VOCs as compared to $Cu_xZn_{1-x}O$ thin films, which were capable of sensing 250 ppm of ethanol.

Use of low cost material and industrially applicable spray pyrolysis technique for production of $Cd_xZn_{1-x}O$, $Al_xZn_{1-x}O$ and $Cu_{1-x}Zn_xO$ thin films with high sensitivity makes them potential candidate for VOC sensor application. Table 7.1 and Table 7.2 compares different selection criteria required to select good transparent conductor material and sensor material.

7.2.4 Development of data acquisition system and gas sensor system

Lab fabricated data acquisition system using microcontroller was cost effective and efficiently acquiring data from multiple sensors at a time. Developed system will be helpful for future electronic nose application. Developed gas sensor system to detect acetone, ethanol and methanol was also working efficiently, which can be useful to develop hand held gas sensor.

7.3 SCOPE FOR THE FUTURE WORK

Improving selectivity of metal oxide gas is very important task to fabricate a stable sensor. This can be achieved by applying pattern recognition algorithms during development of device or by adding proper additives during synthesis of sensor materials. Detailed study on development of pattern recognition algorithms such as principal component analysis and artificial neural network will be helpful for device application of gas sensors. Coating sensor surface with hydrophobic material can reduce effect of humidity on sensing property. Further, device can be miniaturized to make it energy efficient, which can be useful for commercial application.

REFERENCES

- Alamdari, S., Tafreshi, M. J., and Ghamsari, M. S. (2017). "The effects of indium precursors on the structural, optical and electrical properties of nanostructured thin ZnO films." *Mater. Lett.*, 197, 94–97.
- Bagnall, D. M., Chen, Y. F., Zhu, Z., Yao, T., Koyama, S., Shen, M. Y., and Goto, T. (1997). "Optically pumped lasing of ZnO at room temperature." *Appl. Phys. Lett.*, 70(17), 2230–2232.
- Bao, D., Gu, H., and Kuang, A. (1998). "Sol-gel-derived c-axis oriented ZnO thin films." *Thin Solid Films*, 312(10), 37–39.
- Bari, M. A., Kindzierski, W. B., Wheeler, A. J., Héroux, M. È., and Wallace, L. A. (2015). "Source apportionment of indoor and outdoor volatile organic compounds at homes in Edmonton, Canada." *Build. Environ.*, 90, 114–124.
- Bashir, A., Wöbkenberg, P. H., Smith, J., Ball, J. M., Adamopoulos, G., Bradley, D. D. C., and Anthopoulos, T. D. (2009). "High-performance zinc oxide transistors and circuits fabricated by spray pyrolysis in ambient atmosphere." *Adv. Mater.*, 21(21), 2226–2231.
- Bharath, S. P., Bangera, K. V., and Shivakumar, G. K. (2017). "Properties of Cd_xZn_{1-x}O thin films and their enhanced gas sensing performance." *J. Alloys Compd.*, 720, 39–46.
- Bi, D., Boschloo, G., Schwarzmüller, S., Yang, L., Johansson, E. M. J., and Hagfeldt, A. (2013). "Efficient and stable CH₃NH₃PbI₃-sensitized ZnO nanorod array solid-state solar cells." *Nanoscale*, 5(23), 11686–91.
- Bian, H., Ma, S., Sun, A., Xu, X., Yang, G., Yan, S., Gao, J., Zhang, Z., and Zhu, H. (2016). "Improvement of acetone gas sensing performance of ZnO nanoparticles." *J. Alloys Compd.*, 658, 629–635.
- Borse, R. Y., & Salunke, V. T. (2010). "Synthesis and characterization of nanostructured ZnO thick film gas sensors prepared by screen printing method". *Sensors & Transducers*, 9, 161.

Bossche, M. Van Den, Rose, N. T., Franz, S., and Wekker, J. De. (2017). "Sensors and Actuators B: Chemical Potential of a low-cost gas sensor for atmospheric methane monitoring." *Sensors Actuators B. Chem.*, 238(2), 501–509.

Brattain, B. W. H., and Bardeent, J. (1952). "The Bell System Surface Properties of Germanium." *Am. Teleph. Telegr. Co.*, 32, 1–41.

Chin, H. S., Chao, L. S., and Wu, C. C. (2016). "Crystal, optical, and electrical characteristics of transparent conducting gallium-doped zinc oxide films deposited on flexible polyethylene naphthalate substrates using radio frequency magnetron sputtering." *Mater. Res. Bull.*, 79, 90–96.

Cho, S. Y., Yoo, H. W., Kim, J. Y., Jung, W. Bin, Jin, M. L., Kim, J. S., Jeon, H. J., and Jung, H. T. (2016). "High-resolution p-type metal oxide semiconductor nanowire array as an ultrasensitive sensor for volatile organic compounds." *Nano Lett.*, 16(7), 4508–4515.

Fan, H., and Jia, X. (2011). "Selective detection of acetone and gasoline by temperature modulation in zinc oxide nanosheets sensors." *Solid State Ionics*, Proceedings of the 17th International Conference on Solid State Ionics, 192(1), 688–692.

Ferro, R., Rodríguez, J. A., and Bertrand, P. (2008). "Peculiarities of nitrogen dioxide detection with sprayed undoped and indium-doped zinc oxide thin films." *Thin Solid Films*, 516(8), 2225–2230.

Forleo, A., Francioso, L., Capone, S., Siciliano, P., Lommens, P., and Hens, Z. (2010). "Synthesis and gas sensing properties of ZnO quantum dots." *Sensors Actuators B Chem.*, 146(1), 111–115.

Gao, W., Emaminejad, S., Yin, H., Nyein, Y., Challa, S., Chen, K., Peck, A., Fahad, H. M., Ota, H., Shiraki, H., Kiriya, D., Lien, D., and Brooks, G. A. (2016). "Fully integrated wearable sensor arrays for multiplexed in situ perspiration analysis." *Nature*, 529(7587), 509–514.

Ghosh, A., Kumari, N., Tewari, S., and Bhattacharjee, A. (2015). "Structural, electrical and optical studies on ruthenium doped ZnO pellets for device

applications.” *Mater. Sci. Eng. B Solid-State Mater. Adv. Technol.*, 196, 7–14.

Ghosh, A., Schneller, T., Waser, R., and Majumder, S. B. (2017). “Sensors and Actuators B: Chemical Understanding on the selective carbon monoxide sensing characteristics of copper oxide-zinc oxide composite thin films.” *Sensors Actuators B Chem.*, 253, 685–696.

Gong, H., Hu, J. Q., Wang, J. H., Ong, C. H., and Zhu, F. R. (2006). “Nanocrystalline Cu-doped ZnO thin film gas sensor for CO.” *Sensors Actuators B Chem.*, 115(1), 247–251.

Han, N., Wu, X., Zhang, D., Shen, G., Liu, H., and Chen, Y. (2011). “CdO activated Sn-doped ZnO for highly sensitive, selective and stable formaldehyde sensor.” *Sensors Actuators, B Chem.*, 152(2), 324–329.

Hastir, A., Kohli, N., and Chand, R. (2016). “Temperature dependent selective and sensitive terbium doped ZnO nanostructures.” *Sensors Actuators B Chem.*, 231, 110–119.

Hemmati, S., Anaraki Firooz, A., Khodadadi, A. A., and Mortazavi, Y. (2011). “Nanostructured SnO₂-ZnO sensors: Highly sensitive and selective to ethanol.” *Sensors Actuators, B Chem.*, 160(1), 1298–1303.

Heiland, G. (1954). "Zum Einfluß von adsorbiertem Sauerstoff auf die elektrische Leitfähigkeit von Zinkoxydkristallen". *Zeitschrift für Physik*, 138(3-4), 459-464.

Järvinen, T., Lorite, G. S., Rautio, A. R., Juhász, K. L., Kukovecz, Á., Kónya, Z., Kordas, K., and Toth, G. (2017). “Portable cyber-physical system for indoor and outdoor gas sensing.” *Sensors Actuators, B Chem.*, 252, 983–990.

Jing, Z., and Zhan, J. (2008). “Fabrication and gas-sensing properties of porous ZnO nanoplates.” *Adv. Mater.*, 20(23), 4547–4551.

Katoch, A., Choi, S., Kim, J., Lee, J. H., Lee, J., and Kim, S. S. (2015). “Sensors and Actuators B: Chemical Importance of the nanograin size on the H₂S-sensing properties of ZnO – CuO composite nanofibers.” *Sensors Actuators B Chem.*, 214, 111–116.

Khasim, S., and Al-Hartomy, O. A. (2014). "Fabrication and gas sensitivity in heterostructures of ortho-chloropolyaniline–ZnO nanocomposites." *RSC Adv.*, 4(75), 39844.

Kim, M. S., Yim, K. G., Kim, S., Nam, G., Lee, D. Y., Kim, J. S., Kim, J. S., and Leem, J. Y. (2012). "Growth and characterization of indium-doped zinc oxide thin films prepared by sol-gel method." *Acta Phys. Pol. A*, 217–220.

Kim, S., Kim, C., Na, J., Oh, E., Jeong, C., and Lim, S. (2015). "Improvement in electrical properties of sol-gel-derived In-doped ZnO thin film by electron beam treatment." *J. Sol-Gel Sci. Technol.*, 74(3), 790–799.

Li, F., Gao, X., Wang, R., Zhang, T., and Lu, G. (2017). "Study on TiO₂-SnO₂ core-shell heterostructure nanofibers with different work function and its application in gas sensor." *Sensors Actuators, B Chem.*, 248, 812–819.

Ma, X., Chen, P., Zhang, R., and Yang, D. (2011). "Optical properties of sputtered hexagonal CdZnO films with band gap energies from 1.8 to 3.3 eV." *J. Alloys Compd.*, 509(23), 6599–6602.

Neri, G. (2015). "First fifty years of chemoresistive gas sensors". *Chemosensors*, 3(1), 1-20.

Öztürk, S., Kösemen, A., Kösemen, Z. A., Kiliç, N., Öztürk, Z. Z., and Penza, M. (2016). "Electrochemically growth of Pd doped ZnO nanorods on QCM for room temperature VOC sensors." *Sensors Actuators, B Chem.*, 222, 280–289.

Park, S., Kim, S., Kheel, H., Keun, S., Jin, C., and Lee, C. (2016). "Enhanced H₂ S gas sensing performance of networked CuO-ZnO composite nanoparticle sensor." *Mater. Res. Bull.*, 82, 130–135.

Pati, S., Banerji, P., and Majumder, S. B. (2015). "Properties of indium doped nanocrystalline ZnO thin films and their enhanced gas sensing performance." *RSC Adv.*, 5(75), 61230–61238.

Qin, N., Xiang, Q., Zhao, H., Zhang, J., and Xu, J. (2014b). "Evolution of ZnO microstructures from hexagonal disk to prismoid, prism and pyramid and their crystal

- facet-dependent gas sensing properties.” *CrystEngComm*, 16(30), 7062–7073.
- Raghu, P., Srinatha, N., Naveen, C. S., Mahesh, H. M., and Angadi, B. (2017). “Investigation on the effect of Al concentration on the structural , optical and electrical properties of spin coated Al : ZnO thin fi lms.” *J. Alloys Compd.*, 694, 68–75.
- Rambu, A. P., Ursu, L., Iftimie, N., Nica, V., Dobromir, M., and Iacomi, F. (2013). “Study on Ni-doped ZnO films as gas sensors.” *Appl. Surf. Sci.*, 280, 598–604.
- Rao, G. S. T., and Tarakarama Rao, D. (1999). “Gas sensitivity of ZnO based thick film sensor to NH₃ at room temperature.” *Sensors Actuators B Chem.*, 55(2–3), 166–169.
- Santhosh, T. C. M., Bangera, K. V, and Shivakumar, G. K. (2017). “Band gap engineering of mixed Cd(1–x)Zn(x)Se thin films.” *J. Alloys Compd.*, 703, 40–44.
- Seiyama, T., Kato, A., Fujiishi, K., and Nagatani, M. (1962). “A New Detector for Gaseous Components Using Semiconductive Thin Films.” *Anal. Chem.*, 34(11), 1502–1503.
- Shaver, P. J. (1967). “Aativated tungsten oxide gas detectors.” *Appl. Phys. Lett.*, 11(8), 255–257.
- Shinde, S. D., Patil, G. E., Kajale, D. D., Gaikwad, V. B., and Jain, G. H. (2012). “Synthesis of ZnO nanorods by spray pyrolysis for H₂S gas sensor.” *J. Alloys Compd.*, 528, 109–114.
- Shinde, S. S., Shinde, P. S., Bhosale, C. H., and Rajpure, K. Y. (2008). “Optoelectronic properties of sprayed transparent and conducting indium doped zinc oxide thin films.” *J. Phys. D. Appl. Phys.*, 41(10).
- Shinde, V. R., Gujar, T. P., and Lokhande, C. D. (2007). “Enhanced response of porous ZnO nanobeads towards LPG: Effect of Pd sensitization.” *Sensors Actuators, B Chem.*, 123(2), 701–706.
- Su, X., Jia, Y., Liu, X., Wang, J., Xu, J., He, X., Fu, C., and Liu, S. (2014). “Preparation, dielectric property and infrared emissivity of Fe-doped ZnO powder by

coprecipitation method at various reaction time.” *Ceram. Int.*, 40(4), 5307–5311.

Taguchi, I. N., Jarvis, P. E. L., and Geoffrey, A. E. (1971). “United States Patent (72).”

Tseng, M.-C., Wu, D.-S., Chen, C.-L., Lee, H.-Y., Lin, Y.-C., and Horng, R.-H. (2016). “Performance comparison of p-side-up thin-film AlGaInP light emitting diodes with aluminum-doped zinc oxide and indium tin oxide transparent conductive layers.” *Opt. Mater. Express*, 6(4), 1349.

Tsubota, T., Ohtaki, M., Eguchi, K., and Arai, H. (1997). “Thermoelectric properties of Al-doped ZnO as a promising oxide material for high-temperature thermoelectric conversion.” *J. Mater. Chem.*, 7(1), 85–90.

Vijayalakshmi, S., Venkataraj, S., and Jayavel, R. (2008). “Characterization of cadmium doped zinc oxide (Cd: ZZZnO) thin films prepared by spray pyrolysis method.” *J. Phys. D. Appl. Phys.*, 41(24).

Vuong, N. M., Chinh, N. D., Huy, B. T., & Lee, Y. I. (2016). "CuO-decorated ZnO hierarchical nanostructures as efficient and established sensing materials for H₂S gas sensors". *Scientific reports*, 6(1), 1-13.

Wang, C., Cui, X., Liu, J., Zhou, X., Cheng, X., Sun, P., Hu, X., Li, X., Zheng, J., and Lu, G. (2016a). “Design of Superior Ethanol Gas Sensor Based on Al-Doped NiO Nanorod-Flowers.” *ACS Sensors*, 1(2), 131–136.

Wang, Z., Tian, Z., Han, D., and Gu, F. (2016b). “Highly Sensitive and Selective Ethanol Sensor Fabricated with In-Doped 3DOM ZnO.” *ACS Appl. Mater. Interfaces*, 8(8), 5466–5474.

Xie, J., Cao, Y., Jia, D., Li, Y., and Wang, Y. (2016). “Solid-state synthesis of Y-doped ZnO nanoparticles with selective-detection gas-sensing performance.” *Ceram. Int.*, 42(1), 90–96.

Xing, R., Xu, L., Song, J., Zhou, C., Li, Q., Liu, D., and Song, H. W. (2015). “Preparation and gas sensing properties of In₂O₃/Au nanorods for detection of volatile organic compounds in exhaled breath.” *Sci. Rep.*, 5(1), 1–14.

Yu, M. R., Suyambrakasam, G., Wu, R. J., and Chavali, M. (2012). "Performance evaluation of ZnO-CuO hetero junction solid state room temperature ethanol sensor." *Mater. Res. Bull.*, 47(7), 1713–1718.

Zhai, Y. J., Li, J. H., Fang, X., Chen, X. Y., Fang, F., Chu, X. Y., Wei, Z. P., and Wang, X. H. (2014). "Preparation of cadmium-doped zinc oxide nanoflowers with enhanced photocatalytic activity." *Mater. Sci. Semicond. Process.*, 26(1), 225–230.

Zhang, B., Fu, W., Meng, X., Ruan, A., Su, P., and Yang, H. (2018). "Applied Surface Science Synthesis of actinomorphic flower-like SnO₂ nanorods decorated with CuO nanoparticles and their improved isopropanol sensing properties." *Appl. Surf. Sci.*, 456(June), 586–593.

Zhang, D., Liu, J., Jiang, C., Liu, A., and Xia, B. (2017). "Quantitative detection of formaldehyde and ammonia gas via metal oxide-modified graphene-based sensor array combining with neural network model." *Sensors Actuators, B Chem.*, 240, 55–65.

Zhang, G., and Xie, C. (2015). "A novel method in the gas identification by using WO₃ gas sensor based on the temperature-programmed technique." *Sensors Actuators, B Chem.*, 206, 220–229.

Zhang, J., Wang, S., Xu, M., Wang, Y., Zhu, B., Zhang, S., & Wu, S. (2009). "Hierarchically porous ZnO architectures for gas sensor application." *Crystal Growth and Design*, 9(8), 3532-3537.

LIST OF PUBLICATIONS

PUBLICATIONS IN INTERNATIONAL JOURNALS

1. **Bharath, S. P.**, Kasturi V. Bangera, and G. K. Shivakumar. "Properties of $Cd_xZn_{1-x}O$ thin films and their enhanced gas sensing performance." Journal of Alloys and Compounds 720 (2017): 39-46.
2. **Bharath, S. P.**, Kasturi V. Bangera, and G. K. Shivakumar. "Effect of cadmium incorporation on the properties of zinc oxide thin films." Applied Nanoscience 8.1-2 (2018): 187-193.
3. Navya, K., **Bharath, S. P.**, Bangera, K. V., & Shivakumar, G. K. (2018). Effect of indium content on the characteristics of indium tin oxide thin films. Materials Research Express, 5(9), 096410.
4. **Bharath, S. P.**, Kasturi V. Bangera, and G. K. Shivakumar. "Enhanced gas sensing properties of indium doped ZnO thin films." Superlattices and Microstructures 124 (2018): 72-78.
5. **Bharath, S. P.**, Kasturi V. Bangera, and G. K. Shivakumar. "Synthesis and characterization of $Cu_{1-x}Zn_xO$ composite thin films for sensor application." Accepted in Ceramic international

CONFERENCE PROCEEDINGS

1. Preethi, M. S., **S. P. Bharath**, and Kasturi V. Bangera. "Spray deposited gallium doped tin oxide thinfilm for acetone sensor application." AIP Conference Proceedings. Vol. 1943. No. 1. AIP Publishing, 2018.

Bharath SP

Curriculum Vitae

Contact Thin film lab

Information Department of Physics
National Institute of Technology Karnataka, Surathkal
Mangalore – 575025
Ph:8095030008
pbharathbhat@gmail.com

Education

December 2014 - **National Institute of Technology Karnataka, Surathkal**
Present Ph.D., Physics (pursuing) (CGPA: 8.33)
ZnO based thin films for sensor application

July 2011- **Kuvempu University, Shimoga**
June 2013 M. Tech. (Nanoscience and Nanotechnology) (69%)

July 2009- **Kuvempu University, Shimoga**
June 2011 M.Sc. (Electronics) (76%)

Exams Qualified

NET – 2013 and SET – 2013

Publications

- 1. Bharath, S. P.**, Kasturi V. Bangera, and G. K. Shivakumar. "Properties of $Cd_xZn_{1-x}O$ thin films and their enhanced gas sensing performance." *Journal of Alloys and Compounds* 720 (2017): 39-46.
- 2. Bharath, S. P.**, Kasturi V. Bangera, and G. K. Shivakumar. "Effect of cadmium incorporation on the properties of zinc oxide thin films." *Applied Nanoscience* 8.1-2 (2018): 187-193.
- 3. Navya, K., Bharath, S. P.**, Bangera, K. V., & Shivakumar, G. K. (2018). Effect of indium content on the characteristics of indium tin oxide thin films. *Materials Research Express*, 5(9), 096410.

4. **Bharath, S. P.**, Kasturi V. Bangera, and G. K. Shivakumar. "Enhanced gas sensing properties of indium doped ZnO thin films." *Superlattices and Microstructures* 124 (2018): 72-78.
5. **Bharath, S. P.**, Kasturi V. Bangera, and G. K. Shivakumar. "Synthesis and characterization of $\text{Cu}_{1-x}\text{Zn}_x\text{O}$ composite thin films for sensor application." Accepted in *Ceramic international*
6. Preethi, M. S., **S. P. Bharath**, and Kasturi V. Bangera. "Spray deposited gallium doped tin oxide thinfilm for acetone sensor application." *AIP Conference Proceedings*. Vol. 1943. No. 1. AIP Publishing, 2018.
7. **Bharath, S. P.**, Manjanna, J., Javeed, A., & Yallappa, S. (2015). Multi-walled carbon nanotube-coated cotton fabric for possible energy storage devices. *Bulletin of materials science*, 38(1), 169-172.

**Papers presented
in conference**

1. Preethi, M. S., **S. P. Bharath**, and Kasturi V. Bangera, "Growth and Characterization of spray deposited Gallium Doped SnO₂ Thin Films" presented in national conference on "Condensed Matter Physics and Application-2015", held at Manipal Institute of Technology
2. Preethi, M. S., **S. P. Bharath**, and Kasturi V. Bangera. "Spray deposited gallium doped tin oxide thinfilm for acetone sensor application." presented in international conference on "International Conference on Design, Materials & Manufacture", held at National Institute of Technology Karnataka

**Conference and
workshop
attended**

1. International Conference on Design, Materials & Manufacture, NITK
2. International Conference on Thin Films, New Delhi